BACTERIAL THERMOTAXIS BY SPEED MODULATION

by

Mahmut Demir

B. S. in Physics, Bilkent University, Ankara, 2005

M. S. in Physics, University of Pittsburgh, 2007

Submitted to the Graduate Faculty of

The Kenneth P. Dietrich School of Arts and Sciences in partial fulfillment

of the requirements for the degree of

Ph.D. in Physics

University of Pittsburgh

2013

UNIVERSITY OF PITTSBURGH

THE KENNETH P. DIETRICH SCHOOL OF ARTS AND SCIENCES

This dissertation was presented

by

Mahmut Demir

It was defended on

September 6, 2013

and approved by

Ayres Freitas, Ph.D., Assistant Professor

David Jasnow, Ph.D., Professor

Hanna Salman, Ph.D., Assistant Professor

James Faeder, Ph.D., Associate Professor

Jeremy Levy, Ph.D., Professor

Xiao-lun Wu, Ph.D., Professor

Dissertation Advisor: Hanna Salman, Ph.D., Assistant Professor

BACTERIAL THERMOTAXIS BY SPEED MODULATION

Mahmut Demir, PhD

University of Pittsburgh, 2013

One of the most important factors that affects bacterial migration and is sensitive to thermal changes is the bacterial swimming speed controlled by the rotation of the flagellar motors. In the natural habitats of bacteria, gradients often extend over relatively long distances such that their steepness is too small for bacteria to detect. We studied the bacterial behavior in such thermal gradients and found that they migrate along shallow thermal gradients due to a change in their swimming speed resulting from the effect of temperature on the intracellular pH. When nutrients are scarce the bacteria's intracellular pH and consequently the swimming speed decreases with increasing temperature, which causes them to drift towards the warm end of the gradient. However, when serine is added to the medium at concentrations >300μM, the intracellular pH increases causing the swimming speed to increase continuously with increasing temperature, and the bacteria to drift towards the cold end of the gradient. This directional migration is not a result of bacterial thermotaxis in the classical sense, because the steepness of the gradients is below the sensing threshold of bacteria. Nevertheless, our results show that the directional switch requires the presence of the bacterial sensing receptors which seem to be involved in regulating the intracellular pH. Additionally, it is also important to understand how thermal fluctuations and rate of thermal changes experienced by bacteria during their excursion in natural environments affect their run speed. To this end we have studied the dynamics of the bacterial flagellar motor's speed in response to thermal fluctuations by tethering bacteria to a glass surface through their flagella. Our results show that under heavy load the response of the

motor to fast linear thermal changes is instantaneous. However, when subjected to thermal fluctuations with varying frequency, they exhibit a resonant response to specific frequencies reflecting the complex internal dynamics of the motor.

TABLE OF CONTENTS

LIST OF TABLES

LIST OF FIGURES

LIST OF APPENDIX FIGURES

LIST OF EQUATIONS

PREFACE

To my parents Melahat and Ahmet.

Rahmetli babama ve canım anama armağan olsun.

1.0 INTRODUCTION

Temperature variations modulate and drive many physical, chemical and biological processes. For example, phase transitions from solid to liquid and from paramagnetic to ferromagnetic phases (1) are temperature dependent. The tectonic plate movements are driven by thermal convection caused by the temperature gradient below the earth crust due to the magma layer under it (2–5). Enzymatic activity also depends on temperature (6). In addition, heat is an important driving energy source of micron size molecules inside the cell, which govern the function of living organisms. Therefore, almost all living organisms have developed mechanisms of sensing and responding to temperature changes. Although the response strategies of organisms to temperature changes vary significantly, their outcome is maximizing the benefit and minimizing the harm of the temperature changes to the organism.

Many multi-cellular complex organisms, such as humans, are able to regulate their body temperature in response to temperature changes and maintain an optimal temperature around 37 °C. Other organisms such as the golden-mantled ground squirrels (Spermophilus lateralis) hibernate when their body temperature drops below 18 °C, which causes a significant decrease in their biosynthetic activities (7, 8). Another common strategy of responding to temperature changes often exhibited by birds is migration. Most of the birds migrate in the winter to warmer places (9). Migration towards warmth is a common strategy among many simpler organisms as well. Drosophila is another example that exhibits migration towards optimal temperature (i.e.

thermotaxis) directed by a temperature activated ion (10). Similarly, C. elegans migrate towards the cultivation temperature (i.e. the temperature at which they are grown) when subjected to a temperature gradient (11).

In the case of microorganisms thermotaxis is the only strategy they have to cope with thermal changes, and it has been observed in many different microorganisms. It has been shown for example, that white blood cells, leukocytes, migrate to warmer temperatures in vitro (12). Thermotaxis is not only a strategy for microorganisms to avoid unfavorable temperatures but also a method to find certain locations. It has been suggested for example, that mammalian sperm cells navigate towards the egg guided by ovulation-dependent temperature difference within the female genital tract (13). Bacteria as well, sense temperature differences and follow thermal gradients towards their favorable temperature (14, 15), which could help them colonize certain regions, form biofilms, and infect host cells or tissues.

During his postdoctoral training in Munich, Germany, Theodor Escherich isolated the bacterium coli, later called as after him, *Escherichia coli* (*E. coli*), from infant stool and presented his findings to the Society for Morphology and Physiology on 14 July 1885 (16). This was the first time that *E. coli* was introduced to the academic society. Since then, *E. coli* has become a standard model system for studies in different disciplines and is commonly used by many scientists from various disciplines from biology and bacteriology to physics, mathematics and engineering. The vast knowledge acquired about *E. coli* thus far makes it an excellent model system for our study and in this work *E. coli* bacteria are used as the model organism in order to study the effect of temperature on the behavior of the bacteria individually and at the population level.

E. coli has a signal transduction system which senses both chemical and thermal cues, and responds by altering its swimming pattern in order to bias motion in the direction of better conditions. This sensory system has been studied intensively and its structural elements and their functional properties are well elucidated and will be described in details in the following subsections.

However, temperature unlike chemicals cannot be considered as an input signal affecting only the sensing apparatus of the bacteria. It affects all biochemical activity in the cell including the switching rate and rotational speed of the bacterial rotary motor, which controls the swimming pattern and speed of the cell, and can be viewed as the output channel of the bacterial signal transduction system. Consequently, the effect of temperature on the motor can be considered as an additional input signal, which can influence the bacterial behavior in a temperature gradient. Therefore it is important to understand and characterize these effects and their consequences to the bacterial behavior. This is the focus of my thesis.

1.1 SCIENTIFIC BACKGROUND

1.1.1 Escherichia coli and their signal transduction system

E. coli is an enteric bacteria species which is 2μm in length and 1μm in diameter and can be considered as a cylindrical micron size rod having hemispherical caps (Figure 1.1). It has 4-6 10 μm long flagella (17) each of which is attached at its base to a bi-directional rotary motor embedded in the cell wall (18, 19). The bacteria move through their environment by rotating

their flagella which propel the bacterial cell body forward in space. It is important to note here that due to its size and speed, the motion of *E. coli* bacteria is classified as motion in the low Reynolds number regime (i.e. $\Re \sim 10^{-4}$) (20). In this regime viscous forces dominate inertial forces eventually creating an over-damped environment for the bacteria. Thus, if all flagellar motors rotate in counter clockwise direction simultaneously (CCW), when viewed from the end of the flagellum or behind the cell, they form a single helical bundle, and only then the bacterium is propelled in an arbitrary direction is space with a typical speed of 20-30 μm/sec. This motion of the bacterium is called a "run".

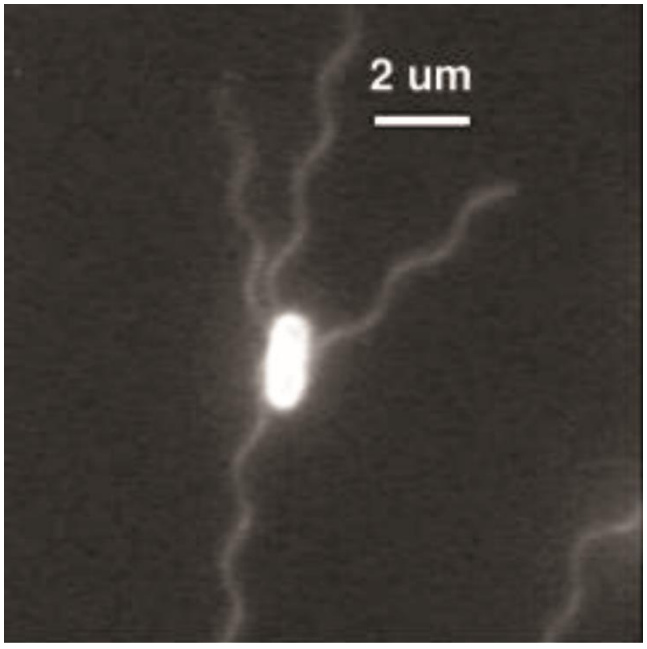

Figure 1.1: Fluorescently labeled Escherichia coli bacterium

Oregon Green 514 labeled E. coli cells were immobilized and illuminated with mercury lamp. Reproduced from Turner et al. (21)

When one or more motors change their rotational direction to clockwise (CW), the flagella attached to the switched motor leave the bundle disturbing the force balance on the

bacterium. This process causes the bacterium to make an erratic motion called a "tumble" (22), after which the bacterium chooses a new run direction which is on average 62º with respect to the previous direction (23). Therefore, bacteria swim in sequential intervals of runs and tumbles. In an environment having sufficient food and appropriate temperature a bacterium runs for ~1 second, and then tumbles for ~0.1 second.

E. coli is equipped with five types of receptors that are responsible for sensing chemicals and temperature. These receptors are the input channels through which environmental signals are received. Each receptor detects different chemicals such as: Tsr (mainly serine and glycine) (24), Tar (mainly aspartate) (25), Tap (mainly dipeptides) (26), Trg (mainly galactose) (27), and Aer (oxygen) (28). Tsr, Tar, Tap and Trg are trans-membrane proteins whereas Aer is a cytoplasmic receptor bound to the inner membrane (29). Tsr and Tar are highly abundant receptors expressed in several thousand copies, whereas Tap, Trg and Aer are less abundant, found at few hundred copies only in the cell (30). Receptors are not scattered on the cell wall, they are clustered at the poles (31). It was also shown that not only the receptors but all other chemotaxis proteins, detailed later, are also clustered at the cell's poles (32–35). This implies that the signal transduction system operates at the cell poles in a small volume fraction which as a result might increase the sensitivity (22) and the efficiency of the system.

In addition to the receptors and the motors representing the input and output channels respectively, the signal transduction system of the bacteria encompasses a processing unit (Figure 1.2), which receives the signals through the receptors and generates an output through the motor. This processing unit consists of the kinase CheA, the response regulator CheY, the methylation and demethylation enzymes CheR and CheB respectively, and the phosphatase CheZ. The kinase CheA is attached to the receptor's clusters with an adapter protein CheW (36,

37) and auto-phosphorylates and transfers phosphate groups to CheY and CheB (38–40). When phosphorylated, CheY (CheY-P) binds to the flagellar motor and causes it to switch its rotational direction from CCW to CW (41, 42). CheY-P also interacts with CheZ which dephosphorylates CheY-P and regulates the concentration of CheY-P in the cell (42, 43).

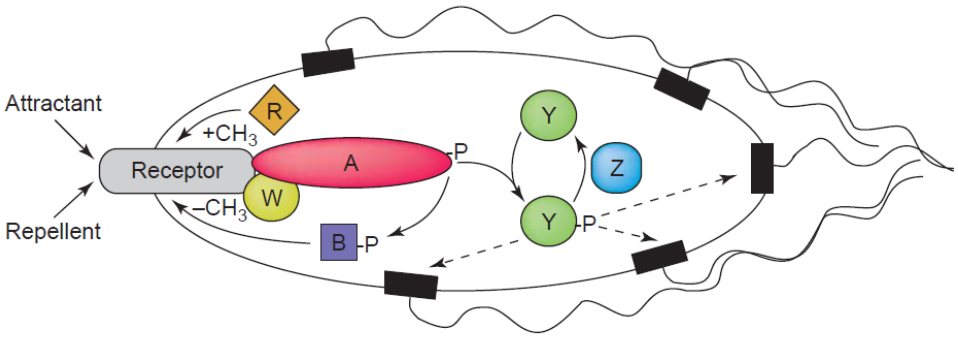

Figure 1.2: Signal transduction protein network

Signals are received by Methyl Accepting Chemotaxis Proteins (MCP). An attractant ligand binds to the receptor and decreases the activity of Kinase CheA which is attached to the MCP's by a coupling protein CheW. Decreased kinase activity decreases phosphorylation of CheY. CheY is responsible for binding to the rotary motor to change rotation from CCW to CW to induce tumbling. Concentration of phosphorylated CheY decreases and results in decrease of tumbling frequency. CheZ enhances the de-phosphorylated of CheY-P and decreases the probability of tumbling. In short, attractant bound to the receptor increases the run length of the bacteria such that bacteria will swim in the direction of increasing chemical concentration in a biased random walk. Meanwhile, CheR adds methyl groups to the receptors to increase sensitivity of the sensors to the chemicals, and CheB works in the opposite direction to remove methyl groups from the receptor to decrease sensitivity of the receptors. CheB and CheR work in cooperation to reset the sensitivity of the receptors allowing the cell to adapt changes in chemical concentrations. Adapted from Sourjik et al. 2004, Trends in Microbiology (44).

The methylase CheR and methylesterase CheB work in antagonist directions to methylate and de-methylate the receptors in order to reset their sensing threshold and the level of CheA activity and therefore allow the system to adapt to the new chemical (thermal) environmental conditions. CheR adds methyl groups to the (45, 46) receptors which increases their sensitivity to

ligands whereas phosphorylated CheB (CheB-P) removes methyl groups from them (47, 48) and decreases their sensitivity.

The mechanism by which the signal transduction system allows bacteria to perform chemotaxis is as follows. When a repellent binds to a receptor, the receptor exhibits a conformational change (49). This conformational change leads to an increased activity of the kinase CheA which in turn increases the concentration of CheY-P. The increased concentration of CheY-P causes an increase in the bacterial tumbling rate and a decrease in the run length. As a result, an increase in the concentration of a repellent (a decrease in the concentration of an attractant) causes shorter runs with increased tumbling rate, whereas a decrease in the concentration of a repellent (an increase in the concentration of an attractant) causes longer runs with decreased tumbling rate. Consequently, in a gradient of repellents (attractants) bacteria drift down (up) the gradient by performing what is known as “biased random walk”, which increase the duration of their runs in the favorable direction and shorten their runs in the opposite direction along the gradient (23).

By changing their run time and tumbling frequency bacteria can bias their random walk in response to changes in the environment. However, the run time of the bacteria does not exceed 10 seconds because of the physical limitations. Due to rotational diffusion, the swimming direction of the cell drifts by about 90 degrees in 10 seconds (50). On the other hand if the run time is shorter than about a second the bacterium cannot propel itself far enough to overcome the diffusion and cannot make measurements of the nutrient amount for comparison.

In addition to sensing chemicals, there is clear evidence that the signal transduction network described above is responsible for sensing and processing thermal signals as well (51, 52). In a series of articles Yasuo Imae and his colleagues have elucidated the role of receptors in

temperature sensing. Initially, Maeda et al. observed in 1976 that the tumbling frequency of bacteria increased with a rapid decrease of temperature and a sudden increase of temperature suppressed the tumbling temporarily (14). That particular experiment was the first well documented observation supporting E. coli's thermotaxis ability. They also subjected bacterial populations to a linear temperature gradient between 17 ºC and 39 ºC along 1 cm, $\left(\sim\frac{20^{\circ}C}{cm}\right)$, and observed that 2 hours after turning on the gradient the bacteria accumulated where the temperature was about 30 ºC. That band moved slowly to colder temperatures probably due to a metabolically created oxygen gradient. They also showed that swimming speed of bacteria depends on temperature, and that the bacteria have a peak steady state tumbling frequency at around 34 ºC.

Two years later in 1978 Maeda et al. reported that a Tsr mutant did not respond to the temperature decrease indicating that it would be the main receptor responsible for temperature sensing (51). They observed that L-serine at concentrations as low as 100 µM inhibits temperature sensing via increasing the methylation level of the receptors.

A later, seemingly contradicting yet elaborate, work was reported by Mizuno et al. in 1984. This time they observed that Tsr mutants showed the same but weaker thermoresponse as wild type such that they exhibited smooth swimming upon temperature increase and tumbled when temperature decreased suddenly (53). When mutants were adapted to Tar specific attractants such as aspartate, glutamate, methyl-DL-aspartate or maltose, the temperature response was switched from warm seeking to cold seeking. They observed that temperature decrease causes decreased methylation of Tar receptor proteins; furthermore low methylated Tsr and Tar produce smooth swimming signal whereas high methylation inhibits Tsr sensing ability and switches Tar response as temperature increases.

In 1988, Lee et al. showed that serine binding deficient Tsr mutants were not altered in their thermosensing ability (54), but rather the ability of serine to inactivate Tsr thermoreceptor function was altered. In another study, thermosensing ability of the two low abundance receptors Trg and Tap were elucidated by the Imae group in 1991 by over expressing them in an all receptors deleted strain. Nara et al. (55) showed that Trg functioned as warm sensor whereas Tap was a cold sensor. In 1996, they reported that Tar functions as a three state thermoreceptor such that it can be a null, warm, and cold sensor depending on covalent modifications of the methylations sites (56).

However, by modifying the methylation sites of Tar with alanine Nishiyama et al. later reported that the negative charge at the methylation sites is one factor that determines the thermosensing phenotypes (57). In a following study in 1999, they replaced methyl-accepting glutamyl residues of the receptors by non-methylatable aspartyl residues in order to examine the effect of methylation level of Tar on thermotaxis. They observed that methylation of a single site is sufficient to convert the thermosensing response of Tar from warm seeking to cold seeking in the presence of aspartate (58).

The Imae group later studied the effect of the Tar methylation by genetic mutations of the receptor and they were able to demonstrate that the inversion of thermosensing ability could be done artificially without presence of aspartate by permanently methylating the receptors via genetic modifications (59). They presented evidence that, relative movements of methylation sites on different parts of the receptor driven by conformational changes caused by binding of aspartate might play crucial role in temperature sensing. The oxygen receptor, Aer, of E. coli was also shown by Nishiyama et al. in 2010 to function as a warm seeking thermoreceptor. (52).

They suggested that, since Aer is a receptor lacking the periplasmic part, the thermosensing property of receptors is a general attribution of their highly conserved cytoplasmic domain.

More recently, Paster et al. studied the response of bacteria to a thermal impulse by measuring the CCW rotational bias of tethered bacteria in response to fast thermal changes and as a function of the background temperature. They reported that the response function (defined as the CCW bias) of the bacteria to changes of ~3°C/100ms from a background temperature less than 31°C has a similar time course, the same directionality and biphasic character as the chemotaxis response. Above 31 ºC some cells inverted their response and the fraction of inverted response increased with increasing temperature with a sharp increase at 37 ºC. These results indicate that cells are warm seeking below 37 ºC and cold seeking at higher temperatures (60).

This switch in the bacterial temperature preference was shown by Salman et al. to depend on the ratio of the two most abundant receptors Tar/Tsr (61), which was also found to change with the growth conditions of the bacteria.

In summary, the role of each receptor in sensing temperature changes was elucidated in the past and it is known how each receptor responds when the temperature is increased or decreased at a rate which bacteria can sense. It is also known how the chemical content of the environment alters the temperature sensing ability of the bacteria by changing the methylation state of the receptors. However, quantitative studies of bacterial thermotaxis under conditions where the temperature gradient is below the sensing threshold of the bacteria are still lacking, and it is not obvious how bacteria would behave in such conditions based on the results obtained from previous observations. In this thesis we focus on the behavior of bacteria in shallow temperature gradients and aim to understand and characterize the effect of temperature variations

on bacterial motility, in particular on the bacterial flagellar motor, and over longer time scales (i.e. hrs.).

1.1.2 Bacterial Flagellar Motor

The Bacterial Flagellar Motor (BFM) is one of the largest protein complexes in the bacterium comprising 13 structural proteins and an additional 25 proteins for expression and assembly (62) (Figure 1.3). Each motor is typically 45 nm wide (63) and attached to a flagellum which is on average about 10 μm long with a width of 20 nm made of 11 helical filaments which are assembled in alternating short and long forms (64–70).

The main structure of the BFM presented in Figure 1.3 was revealed by electron microscopy, particularly by cryo-EM, which was combined with biochemical and genetic studies to determine where proteins are located and what would be their function in the motor (71–73). The main components of the motor are a membrane spanning rotor and several stator complexes anchored to the peptidoglycan layer.

The rotor is attached to the flagellum with a flexible hook and they all rotate together with respect to the cell wall. The hook is so flexible that it works as a universal joint that allows several flagella from motors all around the cell to rotate together as a single bundle. There are two bushings, one in the outer lipopolysaccharide layer (L ring) and one in the peptidoglycan layer (P ring), between the rotor and the cell wall which hold the core of the motor (i.e. the rod) stable in the cell and let it rotate freely. Nevertheless it is not known if the rotor rotates with respect to stationary L and P rings or with L and P rings with respect to the cell wall.

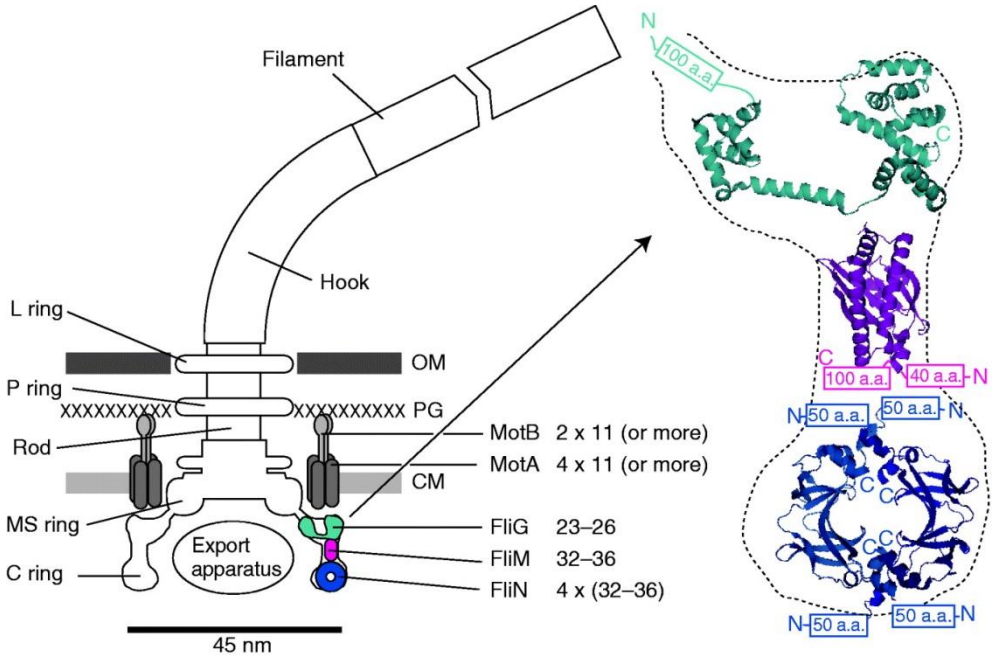

Figure 1.3: Bacterial Flagellar Motor

BFM schematic view. Proteins composing the motor and their location as well as the copy number of the torque generators are presented. Rotor is composed of the L, P, MS, C rings and the rod. L and P rings function as bearings. MS and C rings are the parts involved in torque generation and switching. Stators are complexes of MotA and MotB proteins. They are anchored to peptidoglycan layer through MotB and torque is generated via electrostatic interactions between stators and rotor upon proton translocation. On the right the proteins of torque generation on C ring are shown in detail. The figure is reproduced from Sowa et al. (62)

The hook is connected to the membrane and supramembranous (MS) ring, which is the first part to be assembled in the motor (74, 75), located in the cytoplasm and which consists of 26 copies of FliF proteins (76–78). The cytoplasmic face of the MS ring is attached to the cytoplasmic (C) ring consisting of FliG (23-26 copies), FliM (32-36 copies) and FliN (4x(32-36) copies) proteins. FliG was thought to be the site for force generation (71, 79, 80) and FliM and FliN were thought to control the motor direction via an interaction with CheY-P. Inside the C ring there is an export apparatus that pumps proteins needed to make the hook and filament (81).

The stators are protein complexes consisting of MotA (4x11 copies) and MotB (2x11 copies) subunits (82). Stator complexes anchor to the peptidoglycan cell wall by MotB proteins, while MotA proteins span the cytoplasmic membrane forming channels for proton translocation (83–85). The cytoplasmic domain of MotA contains two charged residues that interact with five charged residues on FliG to generate torque (86–89). The mechanism of the force generation is thought to be such that, the protonmotive driven proton flux causes conformational changes in MotA, including movements of the charged residues on MotA that interact electrostatically with FliG subunits on the C ring. These interactions create forces that pull FliG subunits towards anchored stator complexes resulting in a torque that rotates the rotor with respect to stators. One interesting property of the stators is that, they are not permanently incorporated in the motor, rather they are motile and diffuse in and out of the motor with time scales of minutes, which is observed via fluorescence recovery after photobleaching experiments (90).

The BFM under natural conditions switches direction from CCW to CW stochastically every second under the control of the signal transduction network described in the previous subsection (22). It has been shown that reversal of a single motor is enough to make the flagellar filament leave the bundle and cause a tumble, and the switching of more motors increases the reorientation angle (21).

The rotational nature of the BFM was observed more than 40 years ago by tethering cells to a glass surface through their flagella, causing them to rotate at a maximum rate of 20 Hz (18, 19). The speed of the BFM was measured in two different ways; by tethering the cell to a glass surface through a single shortened flagellum and recording the body's rotation (91, 92) or by fixing the cell to the glass surface and attaching a micron size bead to broken flagella and recording the rotational rate of the bead (93–99). In addition, the rotational speed of the BFM

was measured in free swimming bacteria by fluorescently labeling flagella and recording the rotational rate of both, flagella and cell body. This measurement revealed that, on average, a bacterium swimming at ~30 μm/s has its flagellar bundle rotating at 131 Hz, and the cell body at 23 Hz, indicating that the BFM rotates at 154 Hz (100).

The BFM converts chemical energy to mechanical work. Energy is supplied by the proton motive force (PMF) which is a result of the electric potential and pH differences across the membrane as shown in Eqn. 1 (101).

$$\Delta p = \Delta\psi - 2.3\left(\frac{RT}{F}\right)\Delta pH \qquad \textbf{Eqn. 1}$$

Which is derived from the Gibbs free energy (102) change when one mol of hydrogen ions pass through the membrane from outside to inside under the electrochemical gradient created by the cell. Here $\Delta\psi$ is the membrane potential difference ($\Delta\psi = \psi_{in} - \psi_{out}$), R and F are the gas and Faraday constants, respectively, T is the temperature, and ΔpH is the pH difference across the membrane ($\Delta pH = pH_{in} - pH_{out}$). This potential energy drives protons across the membrane through the flagellar-motor's force-generating units and generates torque.

The BFM is a stepper motor (96). This has been demonstrated recently by attaching small beads to the hooks of immobilized bacteria consisting of Na^+ driven chimeric motors (103), in which the stators were expressed in low numbers and sodium motive force was reduced by lowering the external sodium concentration in order to decrease the rotational speed, and thus allowing steps, with periodicity of 26 steps per revolution, to be detected. Note that 26 steps per cycle is consistent with the periodicity of the FliG proteins in the C ring.

The BFM is a tightly coupled motor where the proton flux through MotA/B complexes is strictly proportional to the rotation (104) and the system operates near thermodynamic

equilibrium. Since the system is over-damped, a motor rotating at 150 Hz and 26 steps per revolution will have a waiting time of about $\frac{10^6 \mu s}{(150 \times 26)} \approx 250 \mu s$ between two steps assuming instantaneous power strokes, and that time will be enough for viscous forces to damp the motion and stop it immediately within a microsecond (105). Therefore, for each revolution the work done equals the energy dissipated, that is: $2\pi\tau = 2\pi f\omega = ne\Delta p$, where τ is the torque generated, f is the frictional drag coefficient on the flagellar bundle, ω is the rotational speed, n is the number of protons passing through the motor per revolution, e is electron charge, and Δp is the proton motive force described in Eqn. 1. In this regime of low Reynolds numbers, conventional conservation of energy does not apply, i.e. $\frac{1}{2} I\omega^2 = E_k \neq ne\Delta p$, since the kinetic energy created by the force generating units of the motor is instantaneously dissipated by the viscous forces.

One of the significant properties of rotary motors is the torque-speed curve which describes the motor's torque generation capacity at different operating conditions. Measurements of the BFM rotational rate by varying load on the flagellum show that the torque is constant up to a specific "knee" speed, after which it decreases linearly as seen in Figure 1.4 (106). In the plateau, speed is limited mechanically by the load (62) and the speed in the high-speed regime is limited by factors affecting the proton transition rates such as temperature (107) and the mass of the proton ions in the medium (93). Free swimming bacteria experience a drag force on their flagella that causes the motor to rotate close to the knee speed, which interestingly corresponds to the maximum power output of the motor (62).

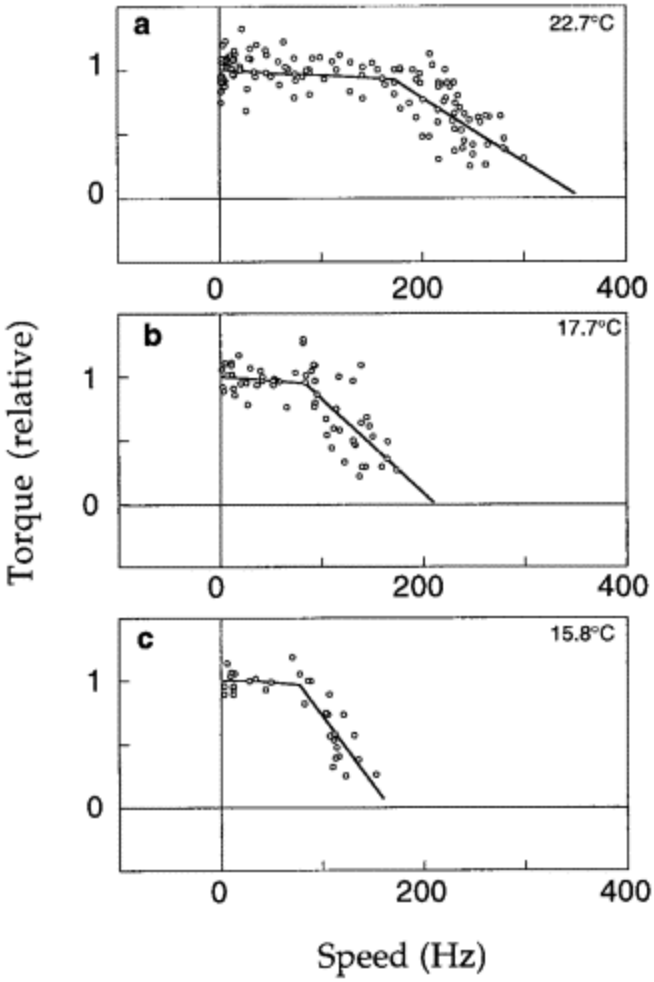

Figure 1.4: Torques speed relation of BFM

Reproduced from Chen et al. Biophys. J. 2000 (106). They immobilized an E. coli strain whose motors rotate exclusively CCW and attached small beads (~0.3μm) to broken flagella. They varied the load on the motor by changing concentration of the Ficoll in the medium and measured the speed of the BFM under that load. The knee frequency of the motor decreases with decreasing temperature.

In summary, extensive studies have been previously performed on the BFM, which aimed to understand the structure of its mechanical components, the way it is assembled, the nature of the torque generation, and the mechanism of switching. However, as a mechanical machine, the BFM has a dynamical range of response to environmental changes and driving factors. This dynamical range defines the limits of the bacterial response to environmental changes, i.e.

chemical content of the environment and/or temperature of the surroundings. Therefore, it is important to study the response of the BFM to rapid changes in the environment, which is another aim of this thesis.

2.0 MATERIALS AND METHODS

In this section, the experimental methods implemented throughout this study and the materials in terms of chemicals, bacterial strains and vectors are explained in detail, and the sources where we obtained them are listed. The designs of the experimental apparatuses are presented as well.

2.1 MICROCHANNEL FABRICATION

2.1.1 Mask preparation

Masks for micro-channel fabrication were designed with Corel Draw (Corel Corporation, Ottawa, Canada) software. The mask presented in Figure 2.1 was used for all studies of bacterial behavior in linear shallow temperature gradient experiments, as well as, in sharp temperature gradients. In order to prevent the collapsing of the PDMS channels 200 μm diameter poles were placed at the center of the channel with 1 mm distance in between. The ends of the two channels at the top and bottom were bent at 45° to allow side loading of the temperature sensitive dye (used for measuring the temperature before every experiment) and prevent its mixing with the bacterial culture. This mask was printed at high resolution (1200dpi) on transparencies and used as for imprinting the structure in photoresist material.

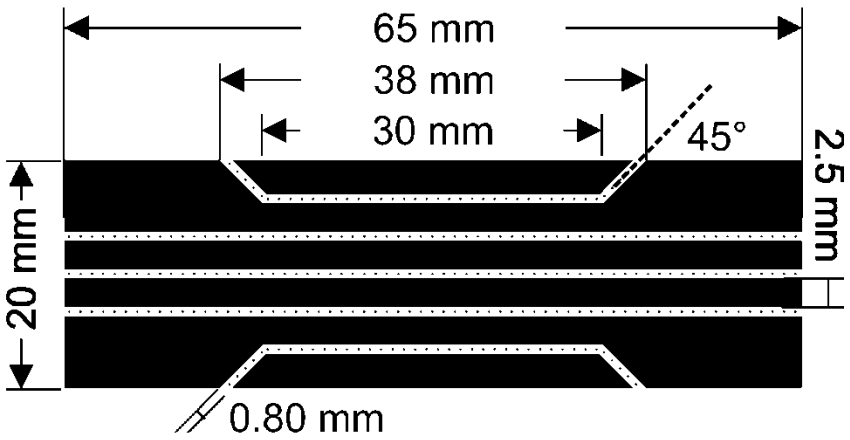

Figure 2.1: Linear temperature gradient mask

2.1.2 Photoresist coating, exposure and development

The microchannels were prepared by utilizing the lift-off micro-technology. All processes were carried out in near dark room to avoid unintended exposure of the photoresist material to ambient light. Glass microscope slides (25x75x1mm, Fisher Scientific) were coated with a ~20 µm thick layer of negative photoresist material (SU-8 10, Micro-Chem). This was accomplished by covering the microscope slide with ~3 ml of the photoresist material and spinning it at 1500 rpm for 20 seconds following acceleration from rest in 10 seconds. The coating was followed by two steps of baking. The slide was first soft-baked for 2 minutes at 65 °C, and then hard-baked for 5 minutes at 95 °C. Using a mercury lamp (Mercury Short Arc, 50W, Osram), the coated slides covered with the mask described above were then exposed to UV light for 2.5 minutes. Following the light exposure, the slides were developed in SU-8 Developer (Microchem) to remove excess photoresist, rinsed with isopropanol, and air dried.

The slides with the imprinted photoresist pattern were then used as templates for the microchannels fabrication with Polydimethylsiloxane (PDMS).

2.1.3 Channel fabrication in PDMS and attachment to the glass slide

PDMS was prepared by mixing the silicone elastomer base and silicon elastomer curing agent (Dow Corning, Sylgard 184 Silicone Elastomer) at a 9:1 ratio (w/w) and mixed vigorously for 5 minutes. Total weight of the mixture was kept at 20 grams in order to ensure similar sample thicknesses in all experiments. A slide with the imprinted pattern was placed in a 100 mm diameter petri dish with the pattern facing up. The liquid PDMS mixture was poured onto the slide template and spread carefully in order to cover the whole slide. Air bubbles in the mixture were removed by placing the petri dish in a vacuum chamber for 30-45 minutes. Following the removal of air bubbles, the PDMS was cured at 60-100 °C for 1-2 hours or at room temperature for two days. The resulting PDMS structure was clear and perfect for microscopy use. In addition, the porous nature of PDMS ensured the continuous diffusion of oxygen into the channels and thus extending the lifetime of bacteria in our samples (108–110).

To form the channels, the PDMS was peeled off the photoresist template and plasma-cleaned with a clean microscope glass slide for 30s in order to make both surfaces hydrophilic. Following the plasma treatment, the PDMS was adhered to the microscope slide such that the channels are formed between the two (Figure 2.2).

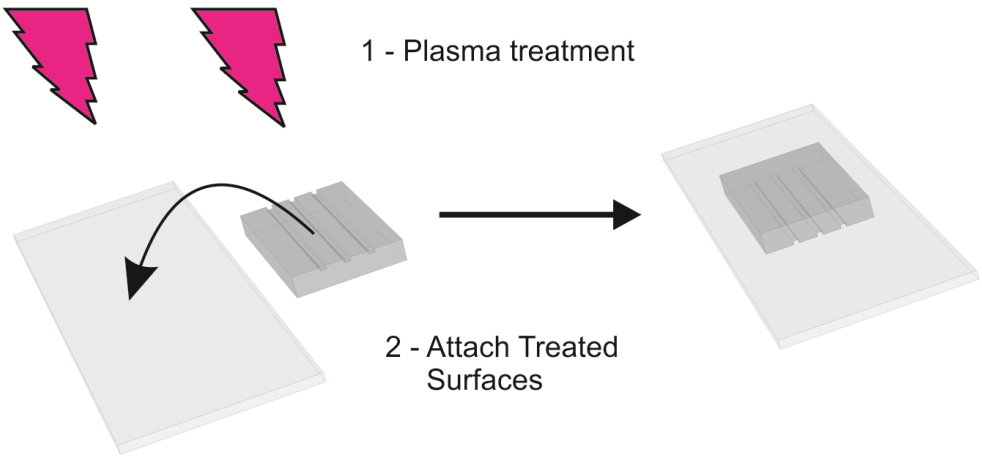

Figure 2.2: Glass slide and PDMS plasma treatment

Glass slide and micro-channel engraved PDMS pieces were treated under air plasma for 30 seconds and then treated surfaces were adhered against each other, leaving the micro-channels in between, in order to seal them permanently.

2.2 TEMPERATURE GRADIENT APPARATUSES

2.2.1 Linear temperature gradient apparatus

To study the behavior of bacteria in a shallow temperature gradient, we have designed, manufactured, and assembled an apparatus that allows us to apply a linear temperature gradient that extends over 10mm distance on the micro-channels described in the previous section. The designs of all parts were carried out using a 3D CAD program, IronCAD (IronCAD LLC, Atlanta, GA) and the apparatus was manufactured in the Department of Physics and Astronomy Machine Shop (for further details see Appendix A).

As presented in Figure 2.3 (Figure A.1, Table 5.1) the device consisted of one heat sink, two Peltier devices separated with a plastic insulation layer, two copper plates attached to the

Peltier devices, and one plastic base. The heat sink was made of aluminum and had a zigzag shaped channel for water circulation. The temperature of the heat sink water was kept at 30 °C with a refrigerating bath circulator (Jeio Tech Inc. Des Plaines, IL USA, RW-1025G).

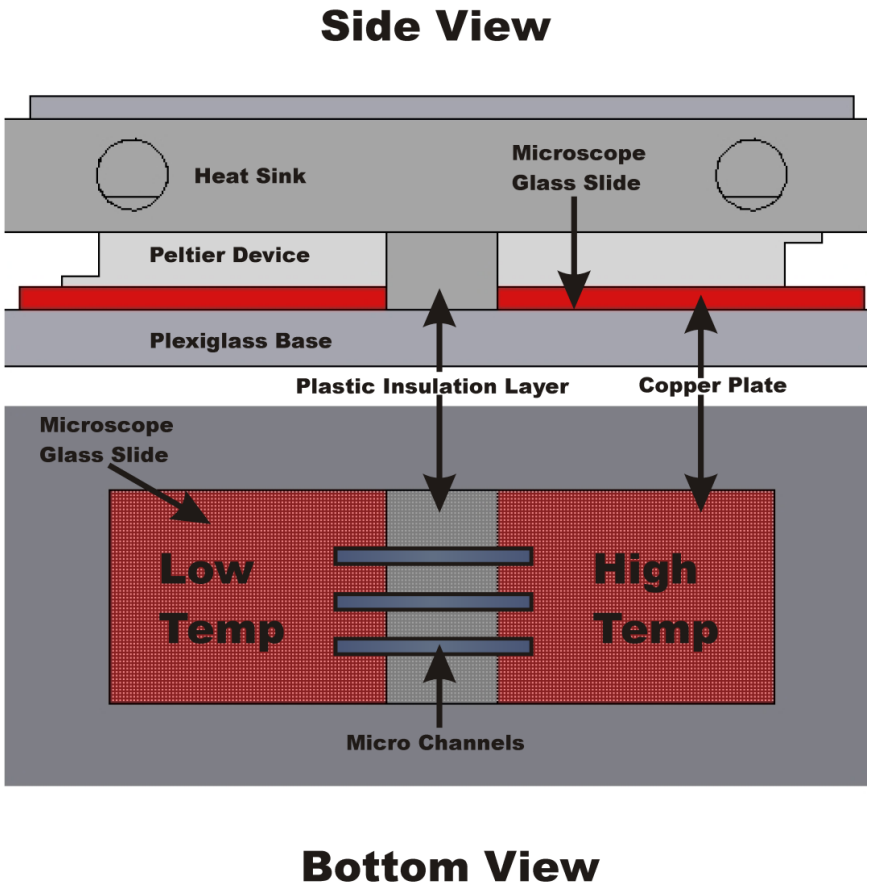

Figure 2.3: Linear temperature gradient device

Two Peltier devices, 10mm apart, were attached to a microscope slide via thin copper plates on one side and to a heat sink on the other side. The heat sink was simply composed of an aluminum plate through which water was circulated by a water bath to maintain its temperature. The PDMS channels were attached to the other side of the microscope slide and all the exposed spaces of the slide were then covered with Plexiglas for better thermal isolation. All contacts were made using thermal grease.

The two Peltier devices (Custom Thermoelectric Inc., Bishopville, MD, USA, 12711-5L31-03CK) and the plastic insulation layer in between were attached permanently to the heat

sink from one side. The other side of the Peltier devices were attached permanently to thin copper plates with silver based epoxy glue (Arctic silver, Arctic Silver Inc., Visalia, CA USA) to ensure good and uniform thermal contacts between the glass slide and Peltier devices.

To avoid bad thermal conduction due to surface roughness and maintain better contact between the copper plates and the microscope slide we applied a thin layer of thermal grease (GC Electronics, Type Z9 heat sink compound, Rockford, IL, USA) right before each experiment.

The microscope glass slide was placed into the slot of a plastic base, with the PDMS channels facing downwards, and attached to the rest of the apparatus through screws at both ends. The complete setup was mounted on an inverted microscope and the bacterial behavior was observed and recorder by Epifluorescence microscopy.

2.2.2 Sharp temperature gradient apparatus

In order to create a sharp temperature gradient over a distance of ~100 μm we focused an infrared laser (λ=1480 nm) into the sample through a 20X objective (Zeiss 20X, 0.40 LD Acroplan). To control the background temperature of the environment a device was designed, manufactured and assembled as was done for the linear temperature gradient apparatus. The apparatus depicted in Figure 2.4 was designed using the same 3D drawing program (IronCAD (IronCAD LLC, Atlanta, GA)), machined and assembled at the facilities of the University of Pittsburgh.

As presented in Figure 2.4 (Figure A.6, Table 5.2) the device consisted of two heat sinks, two Peltier devices, one copper plate attached to the two Peltier devices with a large through hole at the center to allow the laser to reach the sample, and one plastic base. The background

temperature was controlled via the two Peltier devices. The heat sinks on the other side of the Peltier devices were used to stabilize the devices' temperature. The contacts between the heat sinks, the Peltier devices, and copper plate were made permanent to ensure a more stable device using silver based epoxy glue, which also guaranteed good thermal contacts between the different components.

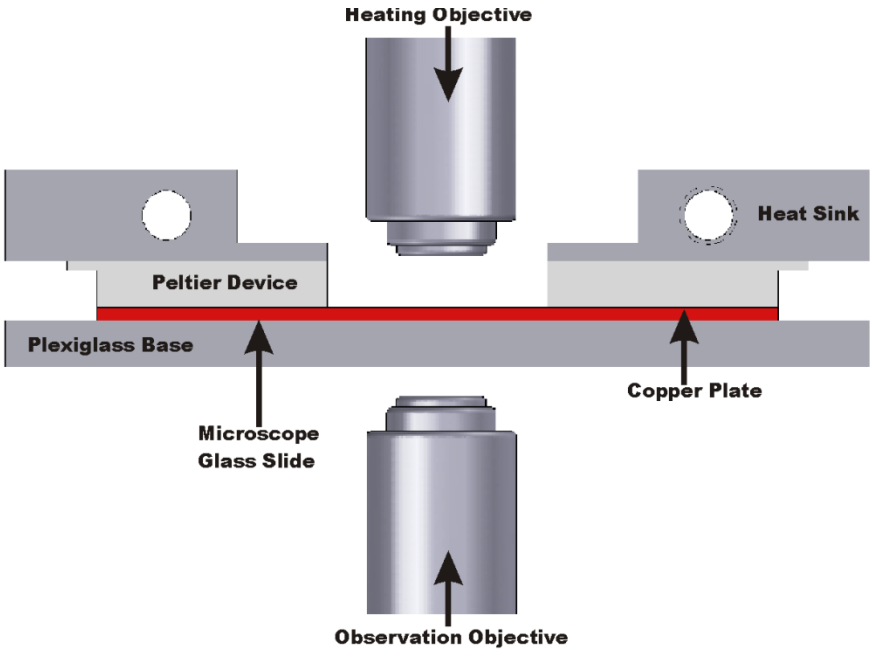

Figure 2.4: Sharp temperature gradient apparatus

Two Peltier devices were attached to a microscope slide via a thin copper plate on one side and to heat sinks on the other side. The copper plate had a circular opening in the middle in order to apply a sharp temperature gradient via focusing an infrared laser from top. The heat sink was an aluminum plate with a through hole in which water was circulated by a water bath to maintain its temperature. The PDMS channels were attached to the other side of the microscope slide and all the exposed spaces of the slide were then covered with Plexiglas for better thermal isolation. All contacts were made using thermal grease

Observations using this device were carried out as before via Epifluorescence microscopy using an inverted microscope onto which the complete setup could be mounted. The temperature of the copper plate was continuously measured by inserting a thermocouple (Stamford, CT USA,

5TC-GG-T-24-36) into the center of the copper plate from the side and monitored with thermocouple temperature readers (Omega Stamford, CT USA, Dpi32) to ensure constant background temperature during experiments (For more details see Appendix A).

2.2.3 Calibration of the apparatuses

The temperature gradient apparatuses were calibrated using the temperature sensitive dye BCECF (111). The fluorescence of BCECF decreases with increasing temperature in an almost linear fashion. As stated previously the temperature of the linear gradient apparatus as well as the temperature of the uniform temperature apparatus were continuously measured via a thermocouple embedded in the copper plate. However there is some temperature difference between the microchannels and copper plate due to heat dissipation through the glass slide and the PDMS containing the bacterial sample. Two calibration curves were generated: one for the relation between the measured copper temperature and the temperature at the bottom surface of the microscope slide, and a second for the relation between the relative fluorescence of the BCECF and the temperature.

The first calibration curve was generated by inserting a second thermocouple between the bottom surface of the slide and the PDMS attached to it and measuring the temperature of that surface as a function of the temperature of the copper plate. The results are presented in Figure 2.5 and Table 2.1.

As stated earlier, BCECF fluorescence decreases as temperature increases. By measuring the percentage of fluorescence decrease one can estimate how much the temperature has increased relative to an initial specific value. We have generated one standard curve for this purpose.

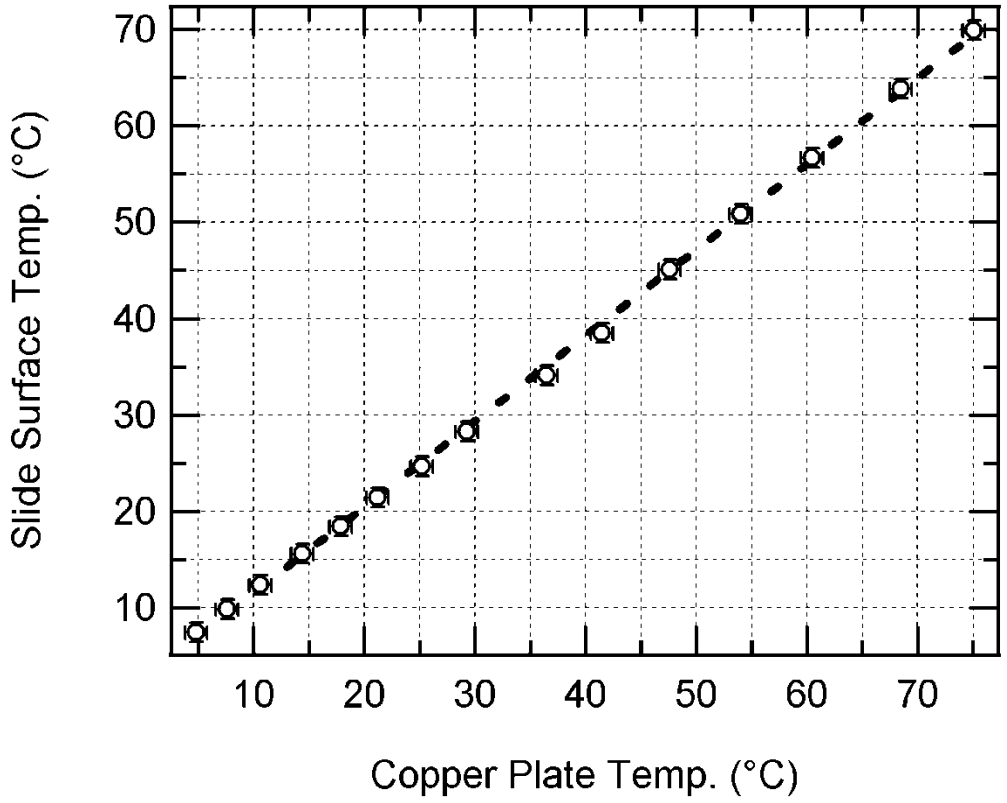

Figure 2.5: Calibration curve for copper plate temperature and actual temperature

The calibration curve for the temperature of the copper plate and the temperature of the bottom surface of the microscope glass slide where bacterial sample is attached. Empty circles are measured values, error bars represent one degree measurement error and dashed line is linear fit to the data. The linear relation is expressed as: $\boldsymbol{Actual\ Temp. = 2.67 + 0.89 \times Copper\ Temp.}$

BCECF at 200 μM was loaded into the PDMS-Slide micro-channels and the sample was mounted on the linear temperature gradient apparatus. The PDMS was carefully attached at the center of the copper plate beneath one of the Peltier devices and the temperature of the sample was controlled by the Peltier device. The sample was initially cooled down to 7.5 °C and the temperature was then increased gradually by changing the current. After the temperature stabilized (~2 minutes after the power is changed) three fluorescence images of the dye were

acquired consecutively. The dye was imaged using a mercury lamp with an excitation bandpass filter (450-490 nm) (Carl Zeiss filter set 09), and an emission longpass filter (515 nm). In addition, the light intensity was reduced to 10% with a neutral density filter (Thorlabs Inc. ND2) in order to avoid fast bleaching. Images were acquired using a CCD camera (ProgRes MF) with an exposure of 500 ms.

Table 2.1: Temperature apparatus calibration values

Copper Temp (°C)	Actual Temp (°C)	Fluorescence (a. u.)	Relative Fluorescence % (w.r.t 20°C)
7.5	9.3	155.21	104.07
8.5	10.2	155.06	103.97
10.0	11.6	154.35	103.49
12.0	13.3	154.08	103.31
14.0	15.1	152.43	102.21
16.0	16.9	151.75	101.75
17.8	18.5	150.42	100.86
20.0	20.4	148.42	99.52
22.0	22.2	148.81	99.78
24.0	24.0	147.60	98.97
26.0	25.8	146.03	97.92
28.0	27.5	144.50	96.89
31.0	30.2	142.32	95.42
32.0	31.1	141.28	94.73
34.0	32.9	140.05	93.91
36.0	34.7	138.12	92.61
38.2	36.6	136.78	91.71
40.0	38.2	135.45	90.82
42.0	40.0	133.51	89.52
44.0	41.8	132.33	88.73
46.0	43.5	130.02	87.18
48.0	45.3	128.46	86.14
50.0	47.1	126.79	85.01
52.0	48.9	124.90	83.75
54.0	50.7	123.57	82.85
57.0	53.3	121.72	81.61
57.5	53.8	119.62	80.21
60.0	56.0	119.07	79.84
65.0	60.4	116.59	78.17
67.0	62.2	114.76	76.95
71.0	65.8	112.43	75.38

The mean values of the BCECF images were calculated using ImageJ "measure" module. Water in the microchannels was imaged under the same experimental conditions in order to estimate the background fluorescence of the system. This background was subtracted from the dye raw fluorescence values. The resulting fluorescence values were then used to estimate the standard curve for the BCECF fluorescence as a function of temperature. The BCECF dye's fluorescence at 20°C was used as a reference point, and the relative fluorescence of the dye with respect to 20 °C was calculated to be a reference for future measurements. In Table 2.1 the dye fluorescence values (see also Figure 2.6A) and the relative fluorescence values with respect to 20 °C (see also Figure 2.6B) are presented. Although the standard error estimated from different measurements is relatively high the data obtained in each measurement is smooth, therefore the mean fluorescence is smooth. Since we calculate the relative fluorescence change and convert that change into temperature changes the error in the standard curve does not affect our temperature estimation. This error represents the variation between different measurements of the same quantity following the same trend, not the standard deviation of a group of measurements with fluctuating data and different trends. This error estimation method is used for all of the measurements in the thesis.

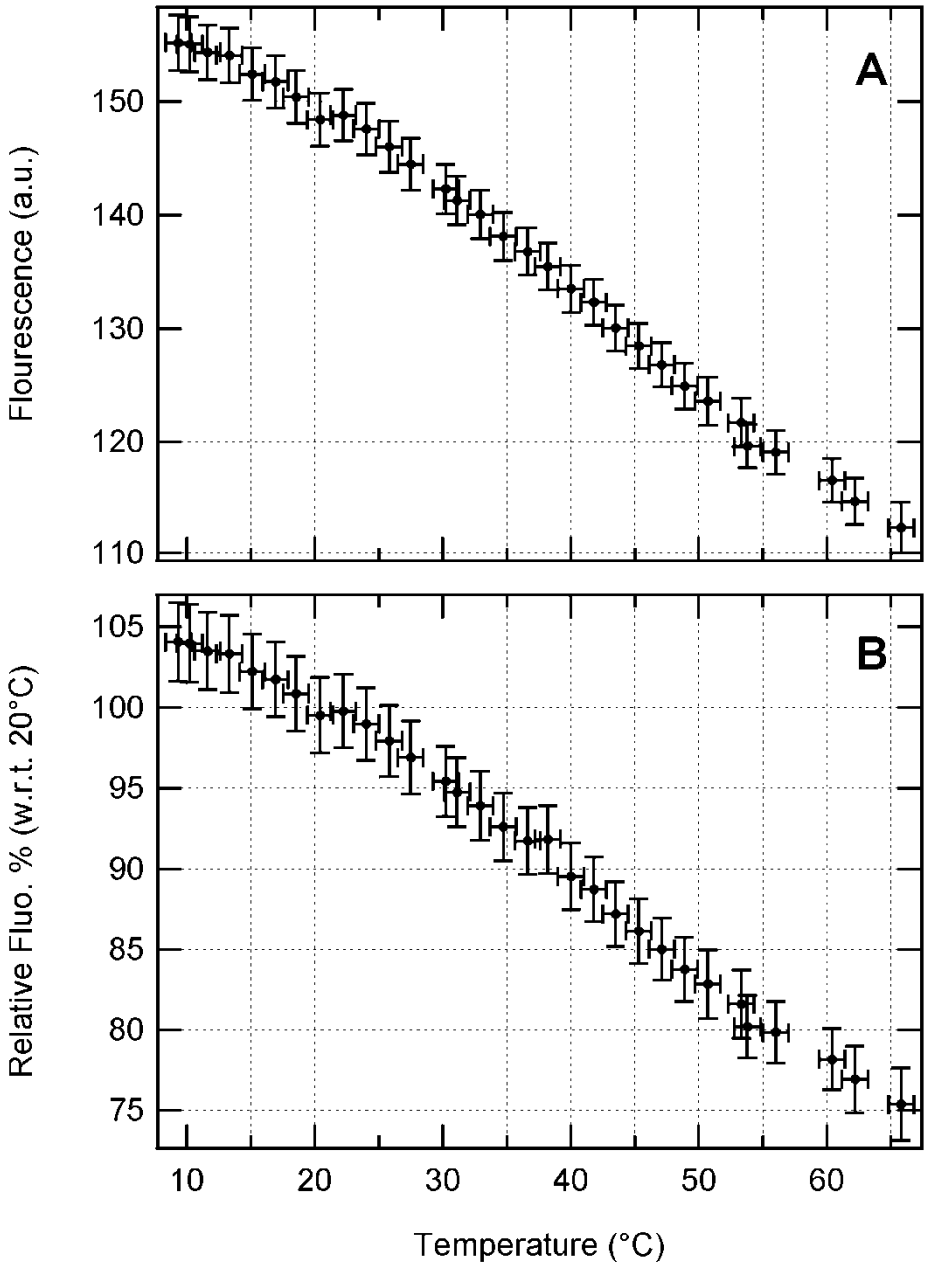

Figure 2.6: BCECF dye calibration standard curves

(A) Background subtracted fluorescence values of BCECF dye pictured under 10% mercury lamp exposure with a CCD camera for 500 ms, and (B) relative fluorescence w.r.t. 20 °C. Error bars of temperature indicate one degree measurement error, and y-error bars are standard error of the mean.

Calibration of the linear temperature gradient apparatus was done by inserting BCECF in the microchannels and acquiring fluorescence images of the dye at several locations separated by 1mm along the channel before and after the gradient was turned on. The change in the fluorescence intensity after the gradient was applied relative to the intensity before was, used to estimate the temperature at each location along the channel. The estimated temperature, before and after the gradient was turned on, obtained from the dye fluorescence measurements are presented in Figure 2.7.

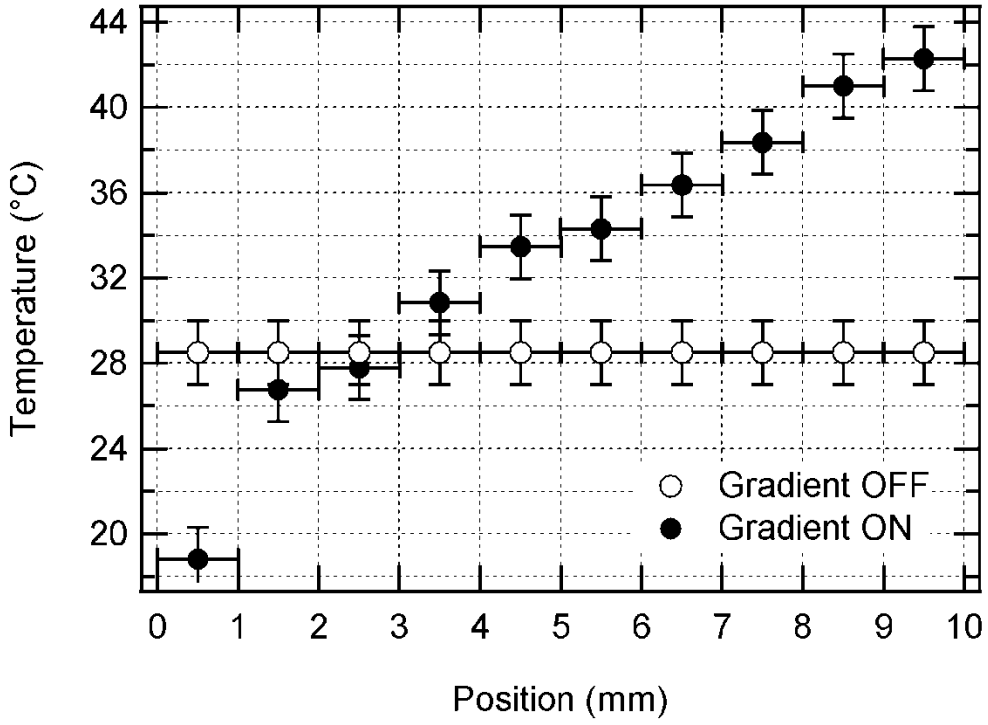

Figure 2.7: Linear gradient apparatus calibration curves

Temperature along the linear temperature gradient apparatus is calibrated and calculated using BCECF in microchannels. Temperature in the microchannels is ~28.5 °C when gradient is turned off (open circles). The water in the heat sink temperature is set to 30 °C. Temperature along the apparatus when gradient is turned on has a linear shape (filled circles).

Similarly, the temperature profile of the gradient applied by focusing an infrared laser was also estimated from the changes in the fluorescence intensity of the BCECF dye. The shape of the temperature profile of IR laser heated area resembles a 2D-Gaussian, where the center has the maximum temperature, which then decays exponentially as a function of distance away from the center. A typical image of IR laser heated BCECF dye and the fitted Gaussian profile are presented in Figure 2.8 A and B respectively. The discrepancy between the data and the fit arises from the heat diffusion in the sample, which causes a small deviation from the Gaussian profile. However, this does not influence our measurements, since we are interested in the temperature at the center of the heated spot only.

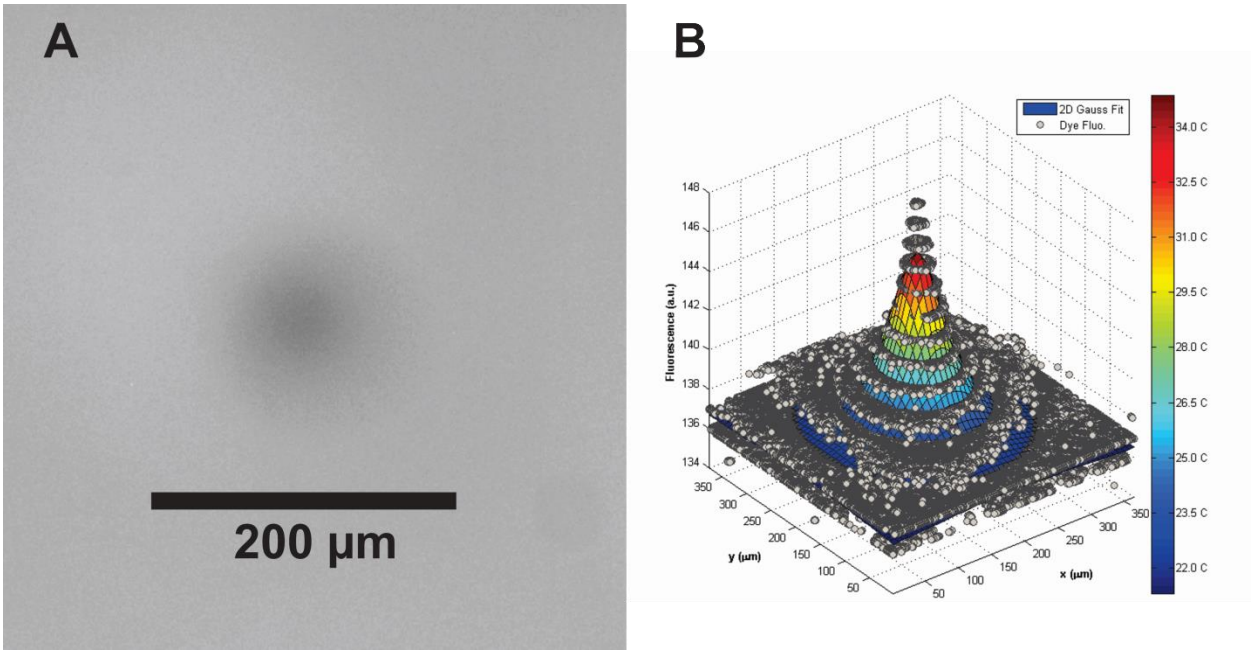

Figure 2.8: IR laser heated BCECF dye and Gaussian fit

A. Temperature sensitive dye BCECF at 200 µM is loaded in micro-channel engraved PDMS-Glass piece and fluorescence of the dye was imaged as described in the text. Fluorescence intensity decreases with increasing temperature which is seen at the center of the image. B. Surface plot of the dye intensity and 2D Gaussian fit to the surface. Color scale indicates the corresponding temperature created by the focused laser.

2.3 BACTERIAL CULTURE PREPARATION AND HANDLING

2.3.1 Chemicals

Several chemicals were used to grow bacterial cultures and measure different physical quantities throughout the experiments, such as membrane potential of the cell and intra and extracellular pH. The chemicals used in this study and the companies that they were purchased from are listed in Table 2.2.

Table 2.2: Chemicals list

Chemical	Source	Chemical	Source
all trans-Retinal	Sigma-Aldrich Co.	Luria Broth	Sigma-Aldrich Co.
Ampicillin	Sigma-Aldrich Co.	M9 Salts	MP Biomedical, LLC.
Arabinose	Sigma-Aldrich Co.	$MgSO_4$	Sigma-Aldrich Co.
Bacto Agar	Becton Dickinson	Monobasic K_2HPO_4	EMD Chemicals.
BCECF	Molecular Probes, Inc.	NaCl	Fisher Scientific
Boric Acid	Fisher Scientific	Nigericin	Sigma-Aldrich Co.
$CaCl_2$	Sigma-Aldrich Co.	PDMS	Dow Corning Co.
Casamino Acids	MP Biomedical, LLC.	Pipes	Sigma-Aldrich Co.
CCCP	Sigma-Aldrich Co.	Potassium Chloride	Sigma-Aldrich Co.
Chloramphenicol	Sigma-Aldrich Co.	Sodium Benzoate	Sigma-Aldrich Co.
Dibasic KH_2PO_4	EMD Chemicals.	Sodium Lactate	Sigma-Aldrich Co.
DiSC3(5)	Anaspec	Sodium Phosphate	Fisher Scientific
D-Serine	Sigma-Aldrich Co.	Sodium Salycilate	Sigma-Aldrich Co.
EDTA	Lonza Group Ltd.	TMRM	Invitrogen
Glucose	MP Biomedical, LLC.	Tris	BIO-RAD
Glycerol	EMD Chemicals.	Ultrapure Agarose	Invitrogen
IPTG	Fisher Scientific	Valinomycin	Sigma-Aldrich Co.
L-Aspartate	Sigma-Aldrich Co.	α-methyl-DL-Aspartate	Sigma-Aldrich Co.
L-Methionine	Sigma-Aldrich Co.	α-methyl-DL-Serine	Sigma-Aldrich Co.
L-Serine	Sigma-Aldrich Co.		

2.3.2 Bacterial culture preparation

Several strains of *Escherichia coli* were used in the experiments throughout this study. In addition, plasmids carrying fluorescent protein genes were transferred into the strains for different experiments. The list of strains, plasmids, and their sources are presented in Table 2.3.

Table 2.3: Strains and plasmids

Strain/Plasmid	Genome	Resistance/Induction	Source
RP437	Wild type for Chemotaxis	Streptomycin	Leibler
HCB317	Δtsr	Streptomycin	Berg
RP2361	Δtar	Streptomycin	Parkinson
UU2612	Δ(tsr, tar, tap, trg, aer)	Streptomycin	Parkinson
VH1	Δ(cheR cheB cheY cheZ) Δ(tsr, tar, tap, trg, aer)	Streptomycin	Sourjik
pZA3R-YFP	Yellow Fluorescent Protein	Chloramphenicol	Salman
PZA1R-YFP	Yellow Fluorescent Protein	Ampicillin	This Work
pBAD TOPO GPR D97N	PROPS	Ampicillin / Arabinose (requires retinal)	Cohen

Bacterial cultures used in the experiments, unless otherwise stated, were initiated from a frozen glycerol stock stored at -80°C, and grown in M9CG (111) (M9 minimal medium supplemented with 1g/L Casamino acids and 4g/L glucose) with the appropriate antibiotics in order to prevent contamination and ensure the purity of the grown culture, at 30 °C while shaking at 240 rounds per minute (rpm). The growth was monitored by measuring the optical density of the culture at 600 nm (OD_{600}) with a spectrophotometer (Biophotometer plus, eppendorf).When the culture reached an OD_{600} of 0.1, the bacteria were centrifuged at 10,000 rpm for 5 minutes, the supernatant was discarded, and the bacteria were washed once in motility buffer (MB: 10mM potassium phosphate, 0.1mM EDTA, 10mM sodium lactate, 1μM L-methionine, pH=7.0). Motility buffer was then used to resuspend the bacteria, always

maintaining the same final concentration of OD_{600}=0.3. Samples were incubated at room temperature for 30 min before starting experiments. Amino acids or other chemicals were then added to the required concentration prior to the measurement. The bacteria were labeled by insertion of the plasmid pZA3R-YFP, which constitutively expresses YFP, for the purpose of observation via fluorescence microscopy.

For the purpose of plasmid DNA extraction, bacteria were grown in Luria Broth (LB) at 37 °C while shaking at 240 rpm until OD_{600} of ~1.5. DNA extraction was carried out using DNA extraction kit (Plasmid Midi Kit, Qiagen) and following the manufacturer's protocols.

To determine the cell concentration in units of #/cm^3, we have generated a calibration curve representing the number of cells per cm^3 as a function of OD_{600}. The number of cells per cm^3 for each OD_{600} was measured by taking a known volume of bacterial culture, plating it onto an agar plate at several dilutions, and incubating at 37°C over night. The next day, images of the plates containing the colonies were acquired and the colonies on each plate were counted. The number of colonies on the plate represents the number of cells in the original sample. These measurements were used to estimate the cell density as a function of OD_{600} as depicted in Figure 2.9.

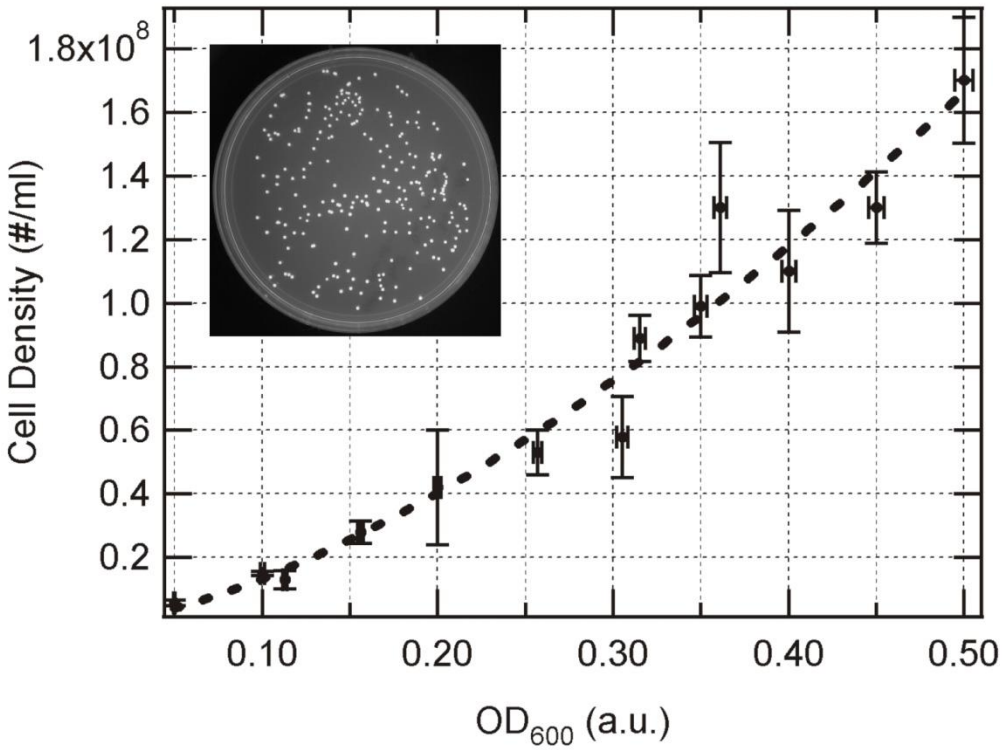

Figure 2.9: Cell density vs. OD

The number of cells in a cubic centimeter (milliliter) is estimated by plating bacterial cultural at different OD_{600}'s and counting the number of colonies on the plate (inset).

2.4 MEASUREMENTS AND IMAGING

2.4.1 Measurements of bacterial swimming speed and concentration profile in a gradient

After resuspending the bacteria in motility buffer with the required concentration of amino acids, they were immediately transferred into the thin channels microfabricated in PDMS described earlier (15). The channels were sealed on both ends immediately after filling them by epoxy glue. The temperature of the sample was set using a Peltier device attached to the

microscope slide. Movies of swimming bacteria were acquired at the various conditions by fluorescence microscopy with a 20X objective. 20 seconds videos were recorded at a rate of 5 fps by a CCD camera (ProgRes MF, Jenoptik). Swimming trajectories were analyzed using ImageJ Particle Tracker plugin (112, 113) and custom MATLAB scripts (The Mathworks, Natick, MA). The speed was then calculated from these trajectories by simply calculating the average distance traveled by the bacteria between consecutive frames. Each measurement was repeated at least two times and each measurement yielded a few thousand trajectories for analyses.

To measure distribution of bacterial concentration in the temperature gradient, images of the fluorescent bacteria were acquired at different locations along the gradient using a 10X objective. The Number of bacteria at each location was counted using ImageJ particle analyzer module and used to calculate the bacteria's concentration at that location.

2.4.2 pH measurements

The change in the bacterial intracellular pH was measured by means of measuring the fluorescence intensity of YFP, which is pH sensitive as has been demonstrated previously (114). YFP expressing cells were grown from a frozen stock in 50 mL M9CG medium at 30^{o}C, while shaking at 240 rpm. When the culture reached an OD_{600} of ~0.1, cells were harvested, washed in motility buffer via centrifugation at 10000 rpm for 5 minutes, and resuspended at a final OD_{600} ~0.3 in motility buffer. Samples were incubated at room temperature for 30 minutes.

50µl of the bacterial cultures were then transferred into a 96 well Eppendorf RT-PCR plate. Nutrients and chemicals whose effect on pH would be tested were added afterwards. The plate was sealed from top with a clear thin plastic cover. The fluorescence intensity of the YFP in

the culture was measured using a real-time PCR machine (eppendorf). After mounting the plate into the RT-PCR, the temperature was set to 18 °C and the bacteria were incubated at that temperature for 2 minutes before starting the fluorescence measurements.

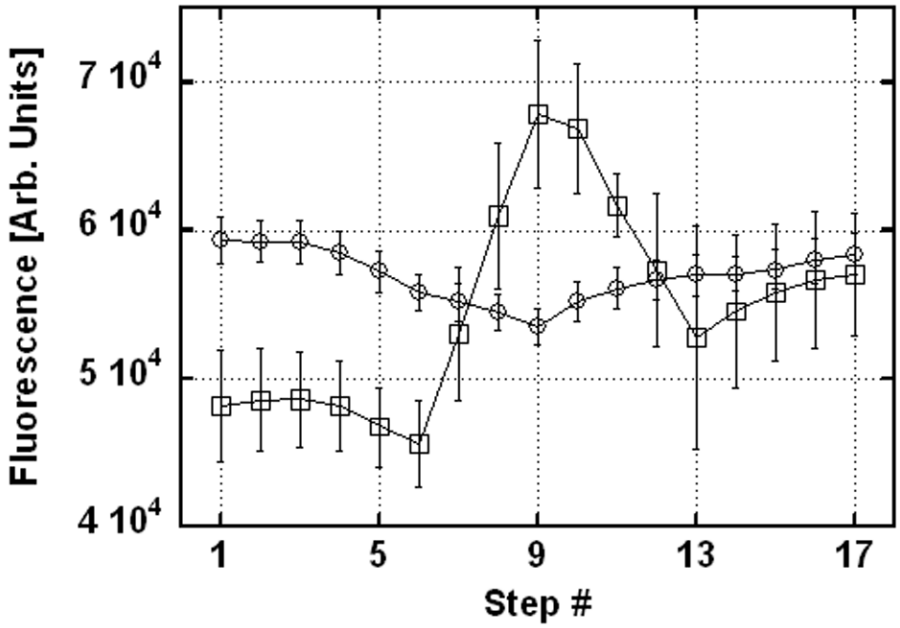

Figure 2.10: Measurement of the YFP fluorescence intensity

The fluorescence intensity of YFP measured as a function of temperature in bacteria incubated in motility buffer (circles), and in motility buffer with 600μM serine (squares). The temperature of each step in order is: 18, 21, 24, 27, 30, 33, 35, 37, 39, 37, 35, 33, 30, 27, 24, 21, and 18°C. Increasing the temperature is known to reduce the pH of the medium. And as can been seen in the graph, the YFP fluorescence intensity inside the bacteria decreases as well when serine is absent from the surrounding medium, which implies that the intracellular pH decreases as well with increasing temperature. However, when serine is added to the medium, the YFP fluorescence intensity increases with the increasing temperature above 30°, indicating that the intracellular pH is increasing.

The bacterial samples were excited at 470nm and their fluorescence intensity was measured at 520 nm. The temperature values set for measurements were 18 °C, 21 °C, 24 °C, 27 °C, 30 °C, 33 °C, 35 °C, 37 °C, 39 °C, 37 °C, 35 °C, 33 °C, 30 °C, 27 °C, 24 °C, 21 °C, and 18

°C. At each temperature 10 measurements were taken with 11 seconds intervals. The last four stable measurements of each set were averaged to get the fluorescence of the well at the measurement temperature (Figure 2.10).

The fluorescence intensity of each sample at each temperature measured as the temperature increased was then averaged with the corresponding measurement for the same temperature acquired as the temperature decreased in order to eliminate effects arising from the temperature change's directionality. But, since there could be a variation in the number of cells in each sample, the average fluorescence intensities were then normalized by the intensity of the sample at 18°C, and the normalized values were averaged between the different samples measured at the same conditions. The relative fluorescence values of several wells (3-12 wells) having the same experimental conditions were averaged to estimate the sample's mean and standard deviation. Experiments were repeated at least three times with cultures grown on different days.

The reason we chose to normalize the fluorescence measurements by the intensity at 18°C is that the speed of the bacteria at that temperature does not change with the serine concentration. This indicates that the internal pH changes with the serine concentration in a similar fashion to the external pH, maintaining the same difference. However, the external pH does not change with addition of serine (Figure 3.11 inset). Therefore, we assumed that the intracellular pH does not change as well at 18°C. The normalized values thus, represent the change in the YFP fluorescence relative to the same fluorescence intensity. Note that the medium used in all the measurements does not support the growth of bacteria and the measurement time is too short to cause any damage to the bacteria. This can be also seen in the reverse measurements, where similar results were obtained as in the forward measurements.

In order to convert YFP fluorescence values to pH, a calibration curve for pH as a function of YFP fluorescence was generated. YFP expressing cells were grown from frozen stock in 50 mL M9CG medium at 30^{o}C, while shaking at 240 rpm. When the culture reached an OD_{600nm} of ~0.1, cells were harvested, washed in motility buffer via centrifugation at 10000 rpm for 5 minutes, and resuspended at a final OD_{600nm} ~0.25 in motility buffer having various pH values between 5.6 and 8.5. The final cell concentration was carefully kept the same for the different buffers to eliminate variation due to cell density.

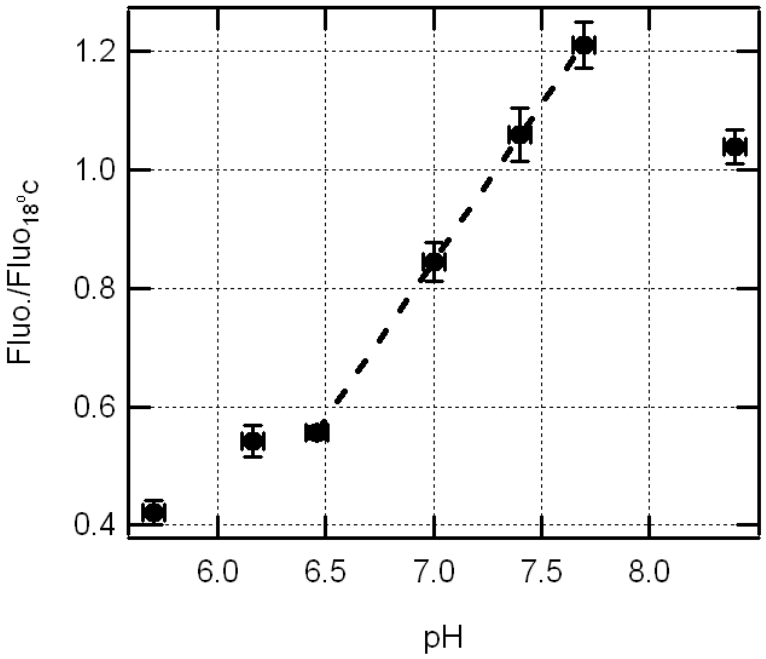

Figure 2.11: YFP Fluorescence vs. pH calibration curve

The fluorescence intensity of YFP was measured at 18 °C as a function of pH as described in the text above. All measurements were then normalized by the fluorescence intensity at pH=7.25 (the measured value of the intracellular pH at 18 °C) as a reference point. All of our fluorescence measurements were in the range covered by the dashed line. Therefore, we used a linear fit depicted by the dashed line to estimate the pH from the fluorescence measurements as explained in the text above.

Sodium benzoate was added to the buffers at a final concentration of 20mM to set the cells' internal pH equal to the external pH (114). The culture's YFP fluorescence was measured using eppendorf realplex RT-PCR while maintaining the temperature at 18^{o}C. The final fluorescence intensity of YFP in each buffer was determined by averaging 12 different samples, each measured 30 times.

Using the calibration curve, presented in Figure 2.11, we estimated the internal pH of RP437 cells in the motility buffer at the same temperature as a reference point. Our results show that the internal pH under these conditions is 7.25 (± 0.07).

The fluorescence measurements for the different temperatures were normalized by the intensity at 18°C. To convert fluorescence values to pH at different temperatures, the fluorescence intensities were first normalized by the intensity at 18^{o}C, which we know should have a pH of 7.25, and the normalized values were then converted to pH values using the calibration curve in Figure 2.11.

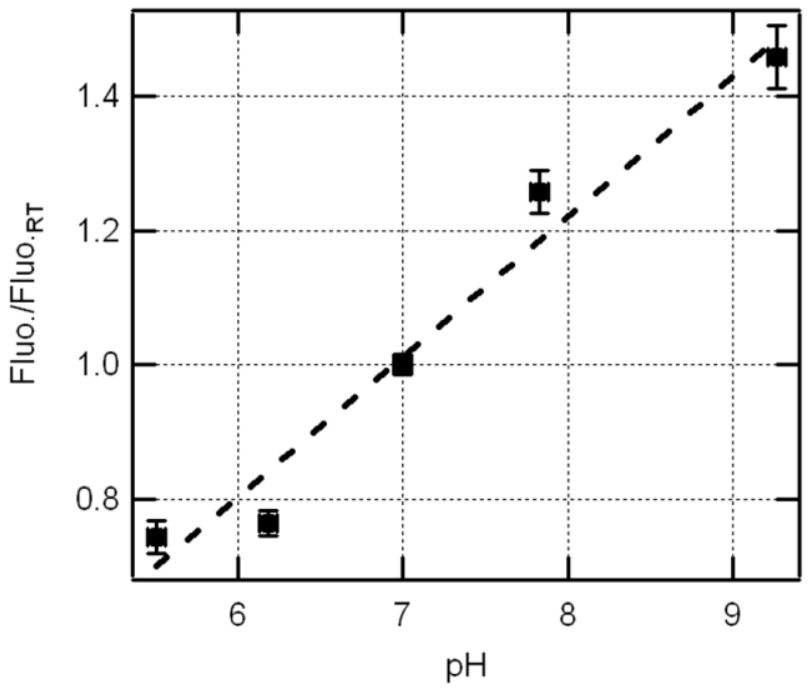

Figure 2.12: BCECF calibration curve

The pH sensitive dye BCECF was suspended in motility buffer at different pH values as indicated by the x-axis, and its fluorescence intensity was measured as a function of the buffer's pH.

The change in the medium's pH was measured using the BCECF dye, whose fluorescence increases with increasing pH. BCECF dye was dissolved in motility buffer with different pH values, and its fluorescence was measured in a similar fashion to the YFP as described above. Also here, the fluorescence intensity of the dye was normalized by its value at 23°C as a reference point. The calibration curve of the dye is presented in Figure 2.12.

2.4.3 Serine uptake measurements

Serine uptake by bacteria was measured following the protocol described by Udenfriend et al. (115). This method measures the amount of free aminoacids in the medium. By measuring

the change in the amino acids concentration we were able to determine the rate at which bacteria uptake amino acids from the environment.

Bacteria were grown, as described in subsection 2.3.2, from frozen stock (-80 °C) in fresh M9CG medium at 30 °C while shaking at 240 rpm. When the OD_{600} reached ~0.1 bacteria were harvested via centrifugation at room temperature at 10000 rpm for five minutes and the supernatant was discarded. The bacterial pellet was washed twice with motility buffer by resuspension and centrifugation, and finally resuspended in motility buffer at OD_{600} ~0.2. The sample was then incubated at room temperature for 30 minutes, and serine was added to a final concentration of 600 μM.

In order to measure the amount of serine remaining in the medium, one ml sample was collected every 20 minutes after the addition of serine. The samples were then centrifuged at 13000 rpm for five minutes, the supernatant was carefully collected without disturbing the bacterial pellet, and filtered through a 0.22 μm size filter (Millipore) in order to remove any remaining bacteria. The collected media were mixed with sodium-borate (200 mM boric acid mixed with NaOH to adjust pH to 9) at 1:20 v/v ratio. The resulting mixture was then mixed with 15% Fluorescamine (Sigma-Aldrich) (w/v) in acetone at a 2:1 v/v ratio. The fluorescamine interacts with amine groups within a second and yields a stable fluorescent derivative (116). The fluorescence intensity of the stained amino acid mixtures was measured using a microplate reader by exciting the sample at 390 nm and measuring the emission at 475 nm.

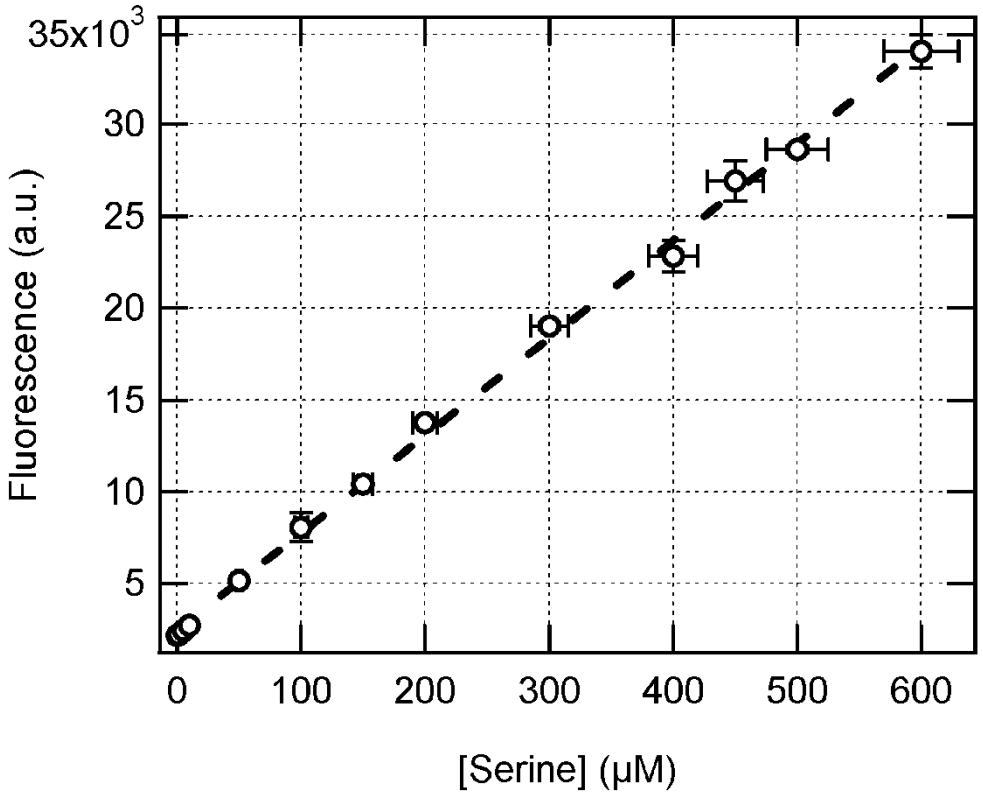

Figure 2.13: Fluorescamine fluorescence calibration curve

The fluorescence intensity of Fluorascamine was measured as a function of serine concentration as described in the text above. Average fluorescence values from several measurements were used to construct the presented calibration curve. Therefore, we used a linear fit depicted by the dashed line to estimate the amount of serine in the bacterial suspensions from the fluorescence measurements as explained in the text above.

In order to convert fluorescence values into concentration of serine a calibration curve was produced following the protocol described above. The fluorescence intensity of stained mixtures increases linearly with the increasing amount of serine present in the medium as shown in Figure 2.13.

2.4.4 Membrane potential measurements

The membrane potential of *E coli* was measured using a mutated green-absorbing proteorhodopsin (GPR) developed by the group of Dr. Adam Cohen at Harvard University. GPR is a light driven proton pump of marine bacteria which translocate protons upon green light absorption. The mutated form, GPR^{D97N} named by its developers Proteorhodopsin Optical Proton Sensor (PROPS), was shown to have membrane-potential dependent fluorescence intensity (117).

For our purposes, PROPS was expressed in bacteria using the pBAD plasmid obtained from Dr. Cohen's Laboratory and following their protocol; Wild type *Escherichia coli* RP437 expressing PROPS were grown in 50 mL of LB medium at 30^{o}C while shaking at 240 rpm to early log-phase (OD_{600nm} = 0.3 – 0.4). Arabinose and all-*trans* retinal were then added to the culture to a final concentration of 1.3mM and 5µM respectively. Arabinose is the inducer for the plasmid and retinal is necessary for PROPS to be fluorescent. The culture was further grown in the dark for 3-4 hr. Cells were then washed with 10mM Potassium Phosphate buffer (pH 7) by centrifugation at 4 ^{o}C, 10000 rpm, for 5 minutes, resuspended in 3 ml of the testing buffer, and incubated on ice for ~30 minutes.

Prior to the measurement, nigericin was added to the culture to a final concentration of 1 µM in order to eliminate the effect of the pH (118) by inducing an H^{+}/K^{+} exchange (119), and cells were incubated for at least 7 minutes at each temperature to allow them to reach steady state. At the end of each run, Carbonyl Cyanide 3-ChloroPhenylhydrazone **(**CCCP) was added to the mix at a final concentration of 50 µM to set the membrane potential to zero, by eliminating the proton gradient across the membrane, (120, 121) as a reference point. Spectroscopic measurements of PROPS were carried out using Tecan Infinite M200 microplate reader. The

cells were excited at 570 nm and the fluorescence emission was scanned between 630 and 780 nm. Maximum emission was observed at 718 nm (±6 nm) and was used to estimate the membrane potential following the calibration curve described below.

The fluorescence intensity of PROPS as a function of the membrane potential was calibrated following the protocol of (120, 122) (Figure 2.14). The fluorescence emission of PROPS (expressed in RP437) was measured for different known membrane potentials. The membrane potential was determined as follows: Cells were incubated in 10mM potassium phosphate buffer, pH=7.0, with varying concentration of sodium and potassium while maintaining the total ionic concentration constant, i.e. $[Na^+]$ + $[K^+]$ = 300mM. Valinomycin, a potassium-selective ionophore, was added to the solution to a final concentration of 5 µM, which sets the membrane potential equal to the potassium Nernst potential (120), determined by:

$$\frac{[K^+]_{\text{in}}}{[K^+]_{\text{out}}} = \exp\left(\frac{-\text{F}\Delta\psi}{\text{RT}}\right) \qquad \textbf{Eqn. 2}$$

where F is Faraday constant, $\Delta\psi$ is the membrane potential, R is the gas constant, and T is the temperature in degrees Kelvin.

Fluorescence measurements were carried out at 30^{o}C. Also here, nigericin was added to the cultures to eliminate effect of transmembrane pH gradient (118) on PROPS fluorescence, and CCCP was added at the end of the measurement to collapse the membrane potential (120) and provide a reference point for all the measurements.

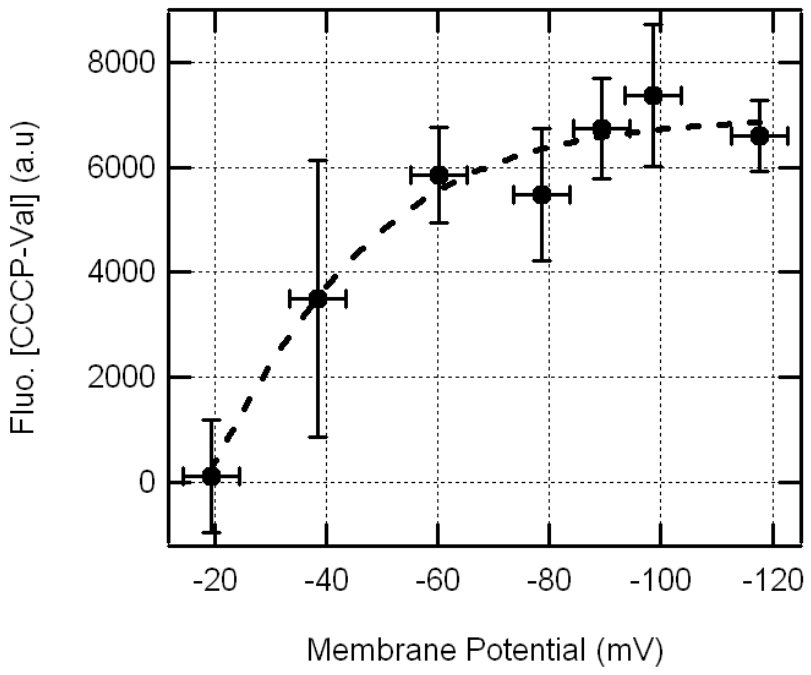

Figure 2.14: Membrane potential calibration curve

The Fluorescence intensity of PROPS as a function of the membrane potential. The membrane potential was set using the potassium ion gradient and valinomycin as described in the text above.

2.4.5 Tethering and rapid temperature modulation

Studying the effect of gradient steepness and thermal fluctuations on the bacterial swimming speed in a spatial temperature gradient is a challenging task due to the difficulty of controlling the swimming direction of bacteria in space. To overcome this problem, we used an experimental setup that allows us to change the temperature in a well-controlled manner while following the rotational speed of the flagellar motors one at a time. Using the infrared laser apparatus described earlier in subsection 2.2.2, we changed almost linearly the surrounding temperature of a bacterium fixed in space by tethering to a glass slide and measured its rotational speed as a function of time and temperature.

To avoid the effects of changing the rotational direction in response to thermal changes, we used the mutant strain whose motors rotate continuously in one direction only. That mutant strain of *E. coli* bacteria VH1 (Δ(cheR cheB cheY cheZ) Δtsr Δ(tar tap) Δtrg Δaer) (123)), expressing yellow fluorescent protein (YFP) constitutively were grown at 30°C in 5 mL M9CG while shaking at 240 rpm until early exponential phase (OD_{600}=0.1). Cells were centrifuged at 10,000 rpm for 5 minutes and resuspended in 2 mL tethering buffer (10 mM Potassium Phosphate, 0.1 mM EDTA, 67 mM Sodium Chloride, 1 μM L-methionine, and 50 mM glycerol, pH=7) (60). The harvested cells were then sheared by gently passing them 33 times through a PS#24 gauge syringe, and incubated at room temperature for 30 minutes. The bacteria were loaded into channels formed by a microscope glass slide and a cover slip separated by two parafilm straps and left at room temperature for 10 minutes to allow the tethering of bacteria to the surface. The channels were then flushed gently with one mL tethering buffer to remove unattached cells, and the ends of the channel were sealed with epoxy glue.

The surrounding temperature of each bacterium was then changed by focusing an infrared laser (λ=1480 nm) into the sample using a 20X objective (Zeiss 20X, 0.40 LD Acroplan). The temperature was changed by changing the laser power through the applied current controlled with a custom written LabVIEW software (National Instruments Corporation, Austin TX), which allowed us to modulate the temperature as desired (Figure 2.15). At the beginning and end of each experiment the speed of the bacteria at room temperature was recorded for 10 second in order to determine the change in speed due to damage that might have occurred to the cell as a result of the fluorescence imaging. The temperature of the heated region surrounding the tethered bacteria was measured using the temperature sensitive dye BCECF.

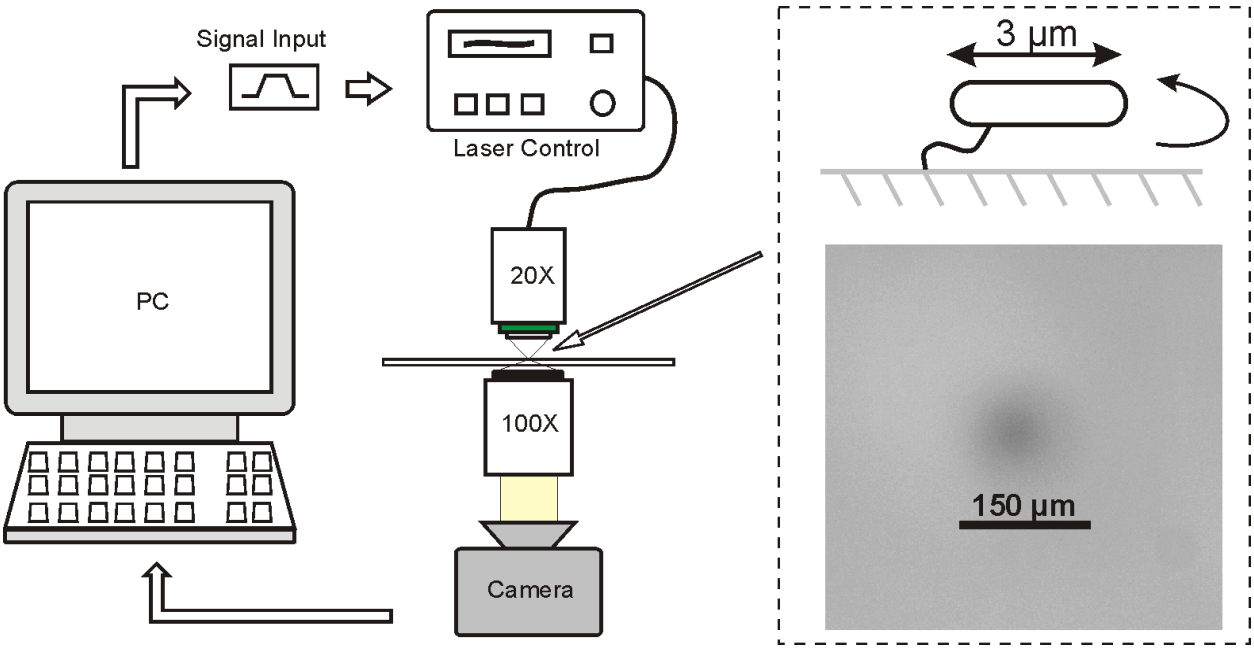

Figure 2.15: Temporal sharp gradient setup

Heating was applied by focusing an infrared laser (λ=1480 nm) through a 20X objective into the sample, and the temperature was changed by changing the laser power through the applied current using a custom written LabVIEW (National Instruments Corporation, Austin TX) program. The rotation of tethered bacteria (depicted in the dashed panel) was observed with 100X objective via fluorescence microscopy, and movies were recorded using a CCD camera (Jenoptik, ProgRes MF) at a rate of 20 fps. The sample temperature around the tethered bacteria was measured using the temperature sensitive dye BCECF, whose fluorescence decreased with increasing temperature as can be seen in the bottom frame of the dashed panel.

Rotating tethered cells were observed in fluorescence mode using a Zeiss Axiovert 40 CFL inverted microscope with 100X microscope objective (Zeiss 100X, 1.3 EC Plan-NEOFLUAR). Movies of the rotation were recorded with a CCD camera (Jenoptik, ProgRes MF) at a rate of 20 fps. The cell's center of mass in each frame was extracted by ImageJ particle analyzer, and the angular velocity between each consecutive frames of the cell's rotation was calculated from the cell's center of mass and the center of rotation using custom scripts written in MATLAB (The Mathworks, Natick, MA). The speed of each bacterium was corrected to account

for any decrease caused by the mercury lamp used for fluorescence imaging, by fitting a line to the 10 second stable ends of each measurement and subtracting the linear decrease from the data, and the data from all bacteria measured were then averaged together.

3.0 BACTERIA IN SHALLOW TEMPERATURE GRADIENTS

Microorganisms such as bacteria sense thermal changes in their environment, and respond by changing their swimming pattern to facilitate their migration towards their favored region (22, 28, 124–129). As detailed earlier, the five receptor species of *E. coli* bacteria are able to sense temperature (14, 15, 51–58, 60, 61, 130). The response of each receptor to thermal changes is different and depends on the methylation state of the receptor, determined by the concentration of the different attractants and repellents in the surrounding medium (51–58).

The reaction of the receptors to thermal changes facilitates the bacteria's migration in temperature gradients towards their favored temperature. In short, when swimming in a thermal gradient, bacteria continuously detect changes in temperature (60, 131) . If they sense an improvement in the environmental conditions along their swimming trajectory, they respond by extending their swim in that direction (132, 133), a process known as thermotaxis. This response occurs almost instantaneously over time scales as short as seconds (134, 135).

But since thermal cues are processed through the same signal transduction network as chemicals, the concentration of different attractants in the cell's surrounding can alter its response to temperature changes by increasing the receptors' methylation state (51, 53, 56–58). For example, at serine concentrations as high as 600μM, bacteria do not respond to temperature changes (Figure 3.1C), whereas without nutrients in the medium bacteria always go to the high temperature (Figure 3.1A).

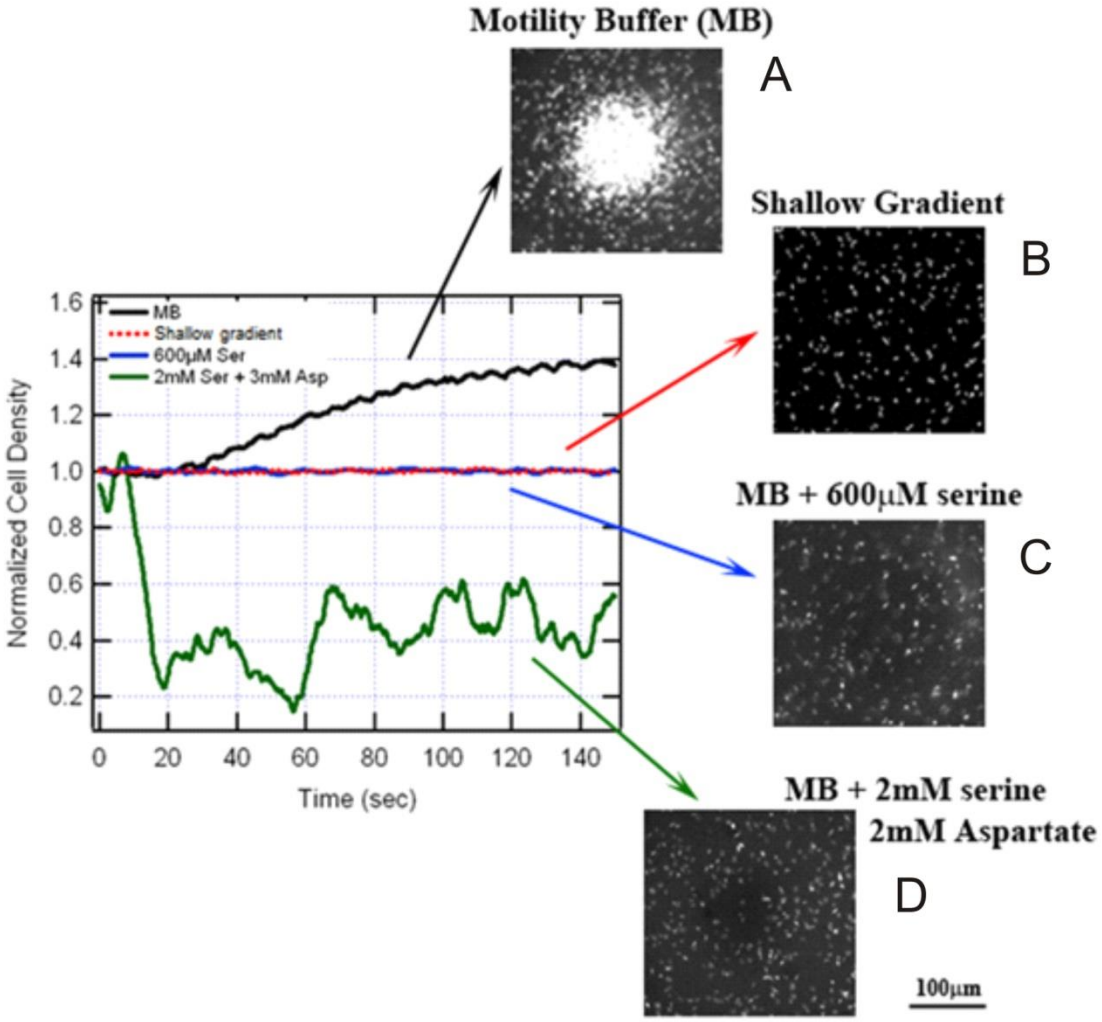

Figure 3.1: The effect of the chemical environment and the steepness of the gradient on the response of the bacteria to a temperature gradient

The temperature gradient was applied by focusing an infrared laser (λ=1480nm) into the bacterial sample (for details see (61)). The background temperature was the room temperature (~24°C), and the center spot was heated by the laser to a temperature of ~27°C in the image labeled "shallow gradient" (making the gradient ~0.02°C/μm), and ~34°C in all other images. The graph depicts the fluorescence intensity at the center of the heated spot measured as a function of time and normalized by the initial intensity for all the experiments described. In motility buffer the bacteria accumulate in the heated spot. In a shallow temperature gradient and in a sharp gradient with 600μM serine added to the medium, no response is detected. When 2mM serine and 3mM aspartate are added to the medium, the bacteria escape from the heated region.

On the other hand, when serine concentration is increased to 2mM, and aspartate is added to a concentration of 3mM, the bacteria escape from the heated region towards lower temperature (Figure 3.1D). However, bacterial sensing and responding through this signal transduction pathway in general is limited, i.e. bacteria are not able to sense or respond to changes, either chemical (124) or thermal, below a certain threshold. In the case of temperature for example, when bacteria are exposed to a temperature gradient with steepness less than 0.02°C/μm that extends over short distances (~100μm), no response or directed migration is observed (Figure 3.1B). Such shallow gradients are frequently found in nature, albeit they often extend over much longer distances. When encountering such conditions, the response mechanism described above will not drive bacteria towards their favored environment.

The main difference between these two scenarios, i.e. short and long shallow gradients, is the distance over which the gradient extends. In the first scenario, the difference in temperature between the two extremes of the gradient is too small to cause any significant change in the cellular processes. On the other hand, when the gradient extends over long distances of the order of magnitude of ~10mm, the difference in temperature that bacteria experience along the gradient is as high as 20°C. This can in turn cause a significant change in many cellular processes.

Since bacteria have a temperature sensing threshold such that the signal transduction mechanism is not able to detect and respond to temperature changes in the environment below a certain threshold, one could predict that bacteria would not show directed migration in shallow temperature gradients. However, previous studies showed that bacteria in shallow temperature gradients actually exhibited thermotaxis and accumulated in the gradient. For instance, Maeda et al. in 1976 (14) and Salman et al. in 2006 (15) showed that WT *E. coli* accumulate around their

favored temperature, 35–37 °C in motility buffer and M9CG medium respectively. The former experiment was done in a channel impermeable to oxygen, therefore oxygen gradient formed by bacterial oxygen consumption would have involved aerotaxis in the process of accumulation. The latter experiment was conducted in PDMS, permeable to oxygen, and aerotaxis was eliminated. However, in this case, temperature dependent consumption of other nutrients available in the testing medium could produce a nutrient gradient, which in turn can lead to the observed accumulation.

When we repeated the same experiment in motility buffer, we surprisingly observed that bacteria accumulated at the highest temperature even though that temperature is harmful to them. This result implies that the chemical environment affects the migration of bacteria in shallow temperature gradients as well as sharp gradients. But the fact that the bacteria migrate to the extreme of the gradient and do not accumulate around 37°C as predicted by previous studies, indicate that this migration is not controlled by the signal transduction network. To test this hypothesis we tested a mutant of RP437 bacteria with all sensors deleted (UU2612 (136)). Since all the receptors are deleted, chemical and thermal signals received through the receptors cannot affect the motor switching (i.e. tumbling rate) and therefore cannot control the swimming pattern of the bacteria or their migration's direction. The UU2612 bacteria were tested in motility buffer under linear temperature gradient and found that they move up the gradient (Figure 3.2). This observation shows that bacteria can actually migrate in shallow temperature gradients without the aid of their signal transduction network.

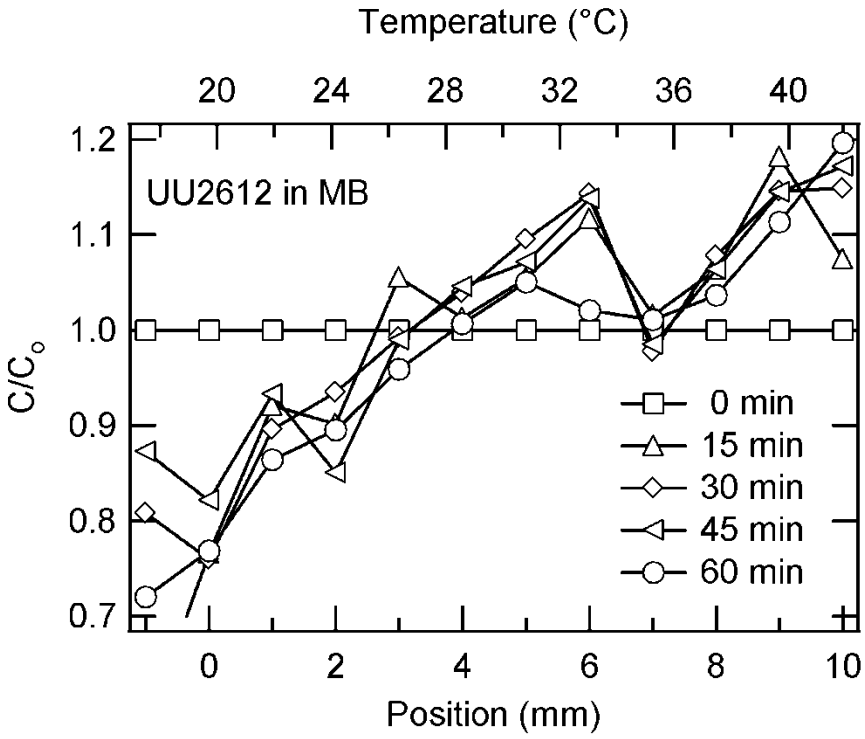

Figure 3.2: Accumulation of UU2612 in MB under shallow temperature gradient

The concentration profiles of the mutant bacteria UU2612, whose receptors are deleted, in the motility buffer measured at different times after applying the temperature gradient. The concentrations were measured as explained in Materials and Methods (section 2.0). All measurements were normalized by the initial concentration at each location.

Thus far, we have shown that in a shallow temperature gradient with steepness below the bacteria's sensing threshold, *E. coli* bacteria still exhibit a directed migration that occurs over timescales as long as tens of minutes. We also showed that the bacterial migration in such shallow temperature gradients is affected by the chemical environment. The direction of the bacterial migration and their favored environment, however, cannot be attributed to their chemo- and thermotaxis system in the classical sense as explained previously, because bacteria lacking all of their methyl accepting receptors also exhibit directed migration under such conditions (Figure 3.2).

In order to understand these results, we note first that temperature and chemicals influence the cellular behavior in other regards. Temperature changes the rate of enzymatic activity (137–139), biochemical reactions (140–144), proteins' conformation (145–149) and binding affinity (150–152), as well as the viscosity (153, 154) and pH of the environment (155, 156). Certain chemicals can also affect the rate of enzymatic activity (if they are sources of energy), and can change the environment's pH. In addition, the rotation of the bacterial flagellar motors is driven by the flux of protons across the membrane (62, 66, 157). To maintain this flux, the cell needs to sustain a pH difference between the interior and exterior of the cell, which in turn requires energy (158, 159). Therefore, it is expected that the speed of bacteria would be affected by all factors that influence the pH or cellular metabolism, including temperature and chemicals.

To understand how the change in the bacterial swimming speed can lead to an accumulation in shallow temperature gradients where temperature sensing is negligible, we consider the bacteria as simple random walkers whose run time and speed depend on temperature, but the rate of tumbling does not depend on the swimming direction which would imply temperature sensing. Schnitzer et al. theoretically analyzed such random walks in one dimension. They assumed that during instantaneous tumbles, half of the random walkers switch their direction at a rate α and they have speed υ. Defining the right and left moving particles as $R(x,t)$ and $L(x,t)$, flow of particles can be expressed as:

$$\frac{\partial R}{\partial t} = -\frac{\partial (vR)}{\partial x} - \frac{\alpha R}{2} + \frac{\alpha L}{2} \qquad \textbf{Eqn. 3}$$

$$\frac{\partial L}{\partial t} = \frac{\partial (vL)}{\partial x} + \frac{\alpha R}{2} - \frac{\alpha L}{2} \qquad \textbf{Eqn. 4}$$

Adding and subtracting Eqn. 3 and Eqn. 4 yields:

$$\frac{\partial \rho}{\partial t} = -\frac{\partial (v\sigma)}{\partial x} = -\frac{\partial J}{\partial x} \qquad \textbf{Eqn. 5}$$

$$\frac{\partial \sigma}{\partial t} = -\frac{\partial (v\rho)}{\partial x} - \alpha\sigma \qquad \textbf{Eqn. 6}$$

where $\rho = R + L$ is the local density of particles, and $\sigma = R - L$ is defined as $v\sigma = J$, where $J \equiv$ particle flux. In the case when both $v(x)$ and $\alpha(x)$ have spatial dependence and $v(x)/\alpha(x)$ is not constant, Eqn. 5 and Eqn. 6 cannot be described in terms of a generalized Fick's law and a $D(x)$, since the effects of $v(x)$ and $\alpha(x)$ cannot be described by one single parameter as $D(x)$. Nevertheless, under these conditions, analysis of such systems in one dimension revealed that the steady-state concentration profile of the random walkers is inverse proportional to their speed profile (160, 161), i.e.

$$\rho(x) = \rho_o \frac{\nu_o}{\nu(x)} \qquad \textbf{Eqn. 7}$$

In this equation $\rho(x)$ and $\nu(x)$ are the density and the speed of the random walkers as a function of position$x$, whereas ρ_o and ν_0 are the density and speed at a reference point respectively. This suggests that it is possible that the bacterial distribution observed in shallow temperature gradient is due to the effect of temperature on the swimming speed of the bacteria.

To test this hypothesis, we measured, by image-recording, the bacteria's swimming speed as a function of temperature. In addition, since we also observed an effect of the chemical environment, we tested the effect of one chemical, for simplicity, on the bacterial swimming speed and their behavior in a shallow temperature gradient. Our chemical of choice was serine due to the fact that serine is known to be one of few amino acids that allow *E. coli* to maintain its motility under anaerobic conditions (113, 162) and has been shown to change the swimming speed of *E. coli* (163). In addition serine is a strong attractant that is sensed by the most abundant chemoreceptor Tsr (61, 164), and it is known to be a rich source of carbon.

Our findings, detailed in the following three subsections, show that bacteria migrate along shallow thermal gradients due to a change in their swimming speed resulting from the effect of temperature on the intracellular pH, which also depends on the chemical environment. When nutrients are scarce in the environment, the bacterium's intracellular pH decreases with increasing temperature. As a result, the swimming speed of the bacteria decreases with increasing temperature, which causes them to slowly (i.e. compared to active sensing and responding) drift toward the warm end of the thermal gradient. However, when serine is added to the medium at concentrations >300 mM, the intracellular pH increases causing the swimming speed to increase continuously with increasing temperature, and the bacteria to drift toward the cold end of the temperature gradient. This directional migration is not a result of bacterial thermotaxis in the classical sense, because the steepness of the gradients applied is below the sensing threshold of bacteria (Figure 3.1D). Nevertheless, our results show that the directional switch requires the presence of the bacterial sensing receptors. This seems to be due to the involvement of the receptors in regulating the intracellular pH which will be discussed later. In addition, our measurements of the effects of temperature and serine on the swimming speed reveal a previously undetected feature. We find that the speed is a two-state function of serine concentration and the difference between the two states increases with increasing temperature. We are able to describe these results using a simple phenomenological model that separates between thermal and chemical effects.

These findings are the first experimental results that suggest an alternate thermotaxis method to the classical signal transduction pathway. They also reveal the importance of the physical environment effects on cellular processes in controlling the behavior of microorganisms. Finally, the detected change in the intracellular pH, which is seemingly

regulated, at least in part, by the chemical- and heat-sensing receptors, could have significant consequences to the field of cellular biology due to the importance of pH in regulating many cellular and molecular processes.

3.1 THE BEHAVIOR OF BACTERIA IN A SHALLOW TEMPERATURE GRADIENT

We have studied the behavior of the wild-type *E. coli* bacteria RP437 in a simple chemical environment (MB) without any nutrients added, under a shallow temperature gradient between ~22 °C and ~43 °C extending over a distance of 10 mm as described in Materials and Methods (section 2.0). Under such conditions the steepness of the gradient is 0.002 °C/μm. We found that the bacteria accumulate at the warm end (Figure 3.3A). However, when serine is added to the medium, the direction of bacterial migration in the temperature gradient is inverted. At serine concentrations higher than 300μM, the bacteria accumulated at the cold end of the gradient (Figure 3.3B-C). This response shift is not due to the change in the methylation state of the receptors, since at serine concentrations of ~300 - 600μM, bacteria lose their ability to sense temperature changes (Figure 3.1C).

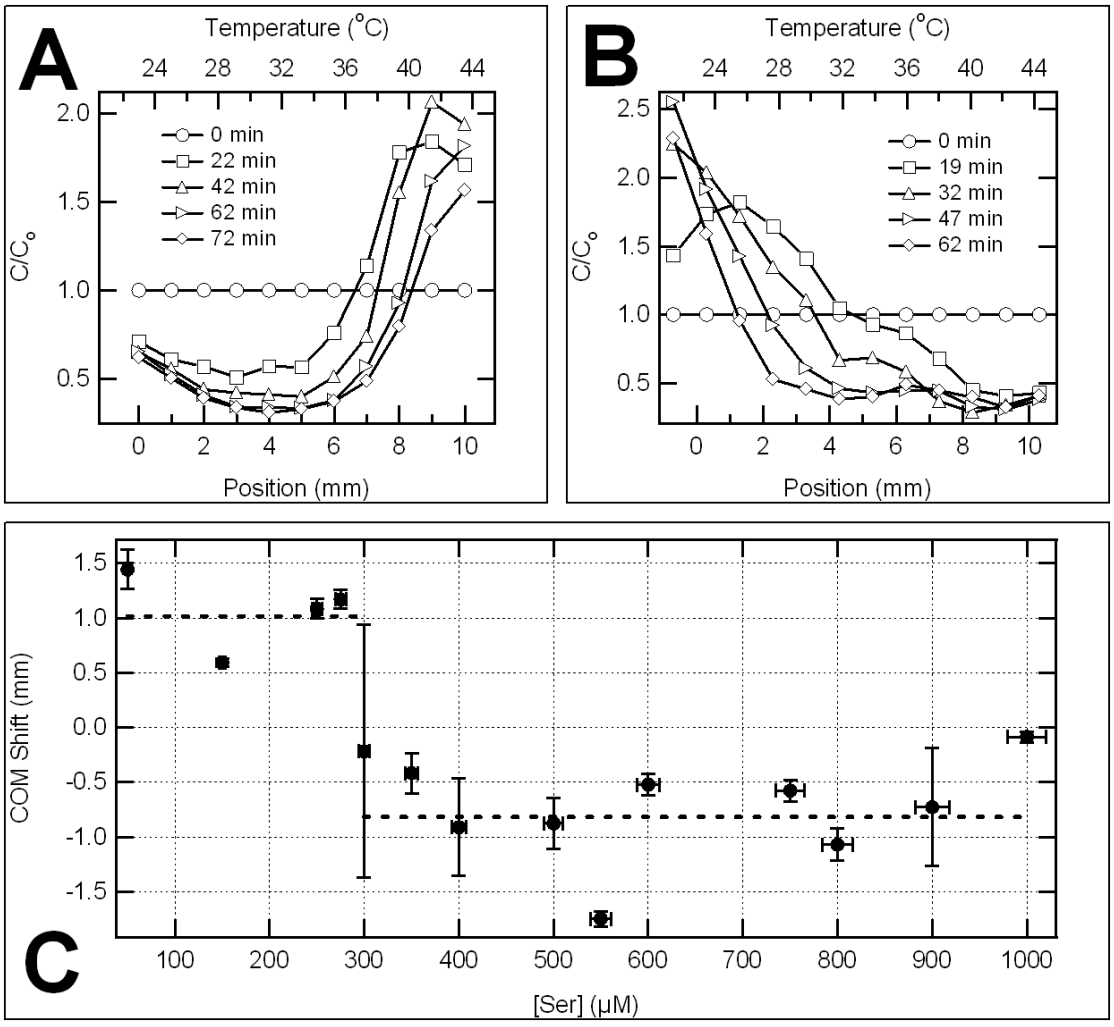

Figure 3.3: The effect of serine concentration on the direction of bacterial migration in a shallow temperature gradient

Examples of concentration profiles of the bacteria, without serine added to the medium (A) and with 600μM serine (B) measured at different times after applying the temperature gradient. The concentrations were measured as explained in Materials and Methods (section 2.0). All measurements were normalized by the initial concentration at each location to allow better comparison of different experiments. (C) The shift of the bacterial population's center of mass (COM) as a function of serine concentration calculated after ~ 45 minutes from applying the temperature gradient. A positive shift indicates migration to the right (higher temperature), whereas a negative shift indicates migration to the left (lower temperature). Each point on the graph is the average of at least three different experiments, and the error bars represent the standard deviation between experiments. Note that the error bar of the 300μM measurement is very large. That is due to the fact that some of the experiments exhibited a shift towards higher temperature while in other experiments the bacteria migrated towards lower temperature.

In addition, when the non-metabolizable form of serine (α-methyl-DL-serine) is added to the medium, the response is not altered and bacteria accumulated at the hot end of the gradient (Figure 3.4).

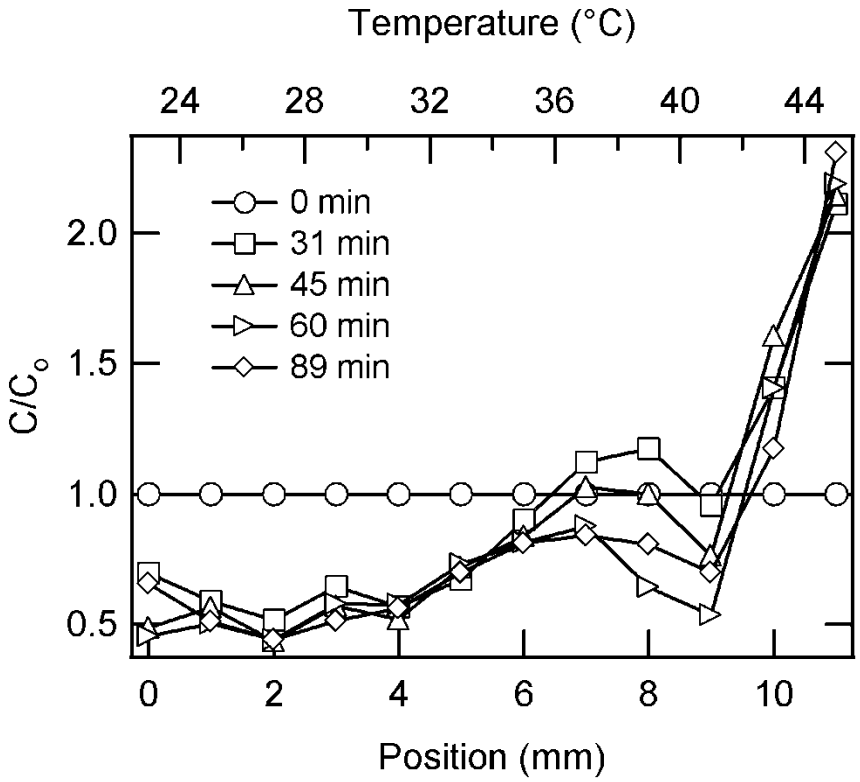

Figure 3.4: The effect of non-metabolizable serine (α-methyl-DL-serine) on bacterial migration in a shallow temperature gradient

The concentration profiles of the wild type bacteria RP437 in the motility buffer with 600 μM α-methyl-DL-serine, a non-metabolizable form of serine, measured at different times after applying the temperature gradient. The concentrations were measured as explained in Materials and Methods (section 2.0). All measurements were normalized by the initial concentration at each location.

To understand this phenomenon, we recall that if considered as simple random walkers, with position-dependent speed and run time, the steady-state distribution of the bacteria in the gradient will be inverse proportional to their swimming speed as described in Eqn. 7.

To test this hypothesis, we measured the bacterial swimming speed as a function of serine concentration in the medium at different background temperatures as described in Materials and Methods (section 2.0).

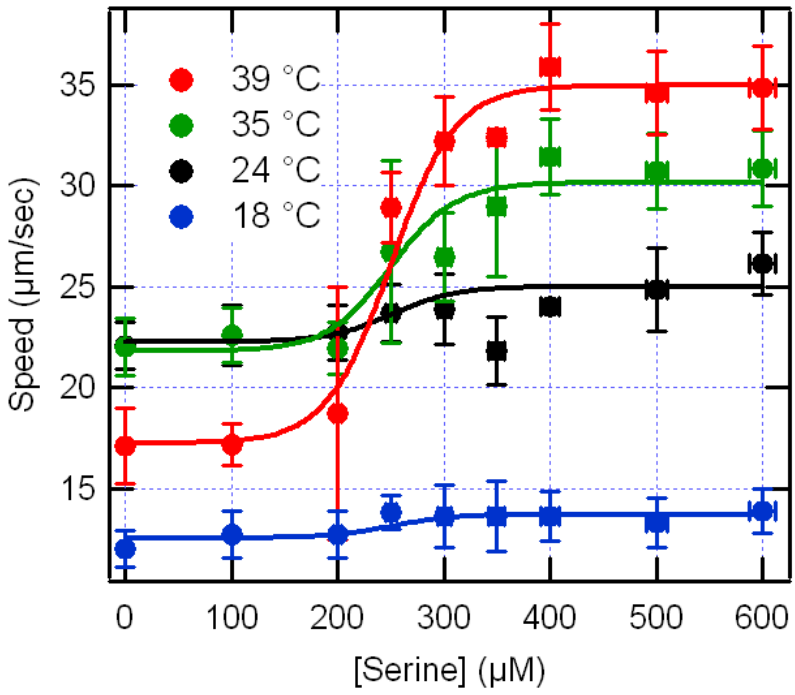

Figure 3.5: The effects of serine concentration and temperature on the bacterial swimming speed.

The swimming speed of bacteria as a function of serine concentration for different temperatures as indicated in the legend. Note that the increase in the speed occurs around the same serine concentration for all temperatures. The lines depict the function: $v(T,S) = v_{min}(T) + \frac{v_{max}(T)-v_{min}(T)}{1+\exp\left[-\frac{(S-S_H)}{S_o}\right]}$ with $S_H \approx 250mM$, $S_o \approx 30mM$, and $v_{min}(T)$ and $v_{max}(T)$ are temperature dependent functions that represent the speed of the bacteria at low and high serine concentration respectively.

Our results, presented in Figure 3.5, show that the bacterial swimming speed exhibits a sharp increase as a function of the serine concentration for all temperatures. The increase in the speed occurs always at ~250μM serine and can be described to a very good approximation by a sigmoidal function:

$$v(T,S) = v_{min}(T) + \frac{v_{max}(T) - v_{min}(T)}{1 + exp\left[-\frac{S - S_H}{S_o}\right]} \qquad \textbf{Eqn. 8}$$

where $v_{min}(T)$ and $v_{max}(T)$ are temperature-dependent functions that describe the speed of the bacteria asymptotically at low and high serine concentrations, respectively.

Fitting this equation to our experimental data results in the values for S_H and S_0 as 250 ±33 mM and 30 ±11 mM respectively. Even though S_H and S_0 are assumed to be independent of temperature, the speeds of the different modes, i.e. $v_{min}(T)$ for low serine concentration and $v_{max}(T)$ for high serine concentration, are functions of temperature (Figure 3.6). At high serine concentrations the speed increases continuously with increasing temperature, whereas at low concentration the speed increases initially with the increasing temperature but decreases when the temperature increases above ~30°C. It has been reported that addition of serine to the motility medium increases the speed of the bacteria at room temperature (163).

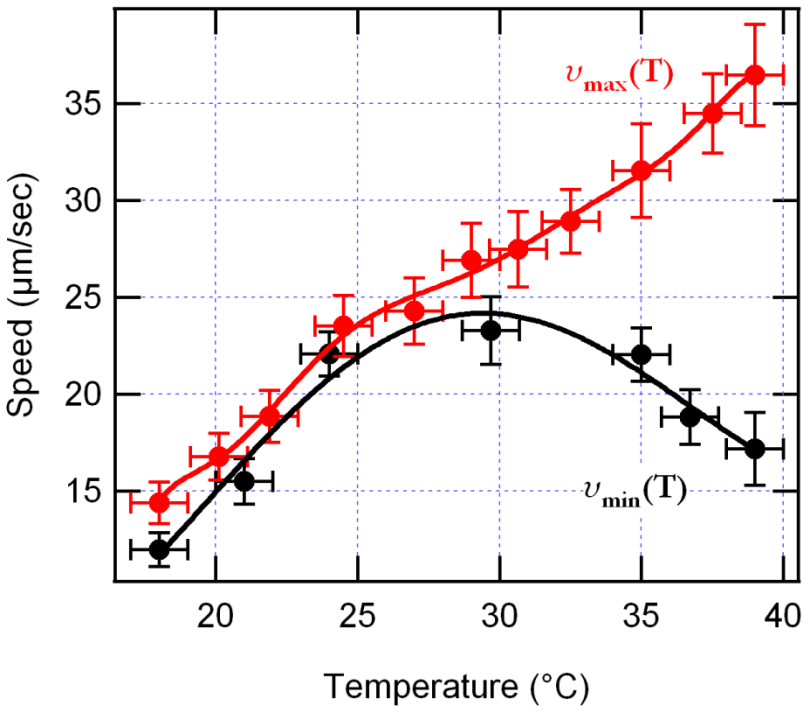

Figure 3.6: The speed of bacteria as a function of temperature

The speed of bacteria is presented as a function of temperature in motility buffer and with 600μM serine. Each point in these graphs was calculated from few thousands trajectories acquired in at least two different experiments. $\nu_{min}(T)$ was calculated by averaging the speed measured at 0 and 100μM serine, whereas $\nu_{max}(T)$ was calculated by averaging the speed measured at 400, 500 and 600μM serine.

This increase is not due to widening of the speed distribution, which would indicate an increase in the speed of a fraction of the population but rather a shift in the distribution (Figure 3.7), which suggests that the rotational speed of all flagellar motors increases with the serine concentration.

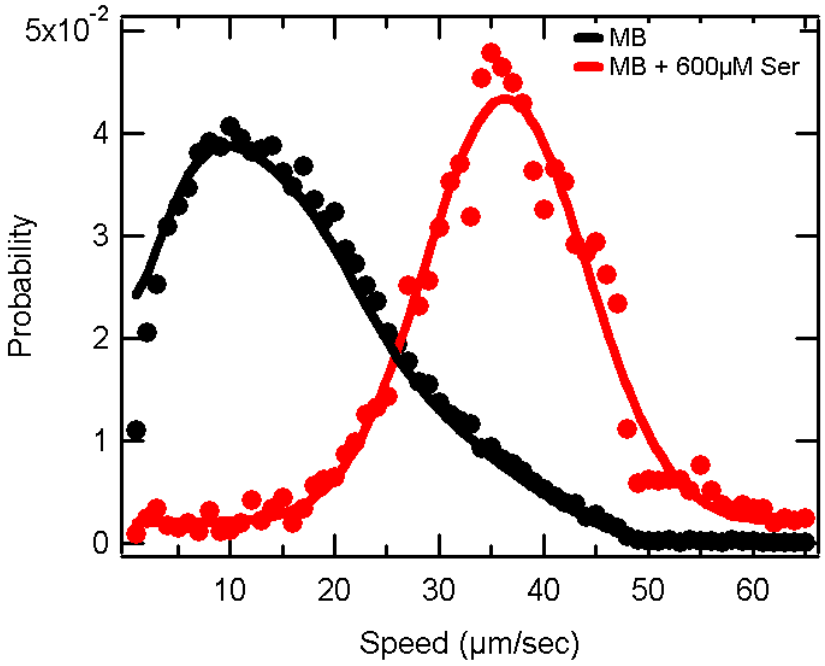

Figure 3.7: Speed distribution of bacteria with and without serine

The black line describes the probability distribution of bacterial speed measured in motility buffer without serine, whereas the red line depicts the probability distribution measured in the presence of 600μM serine. The points are values obtained from experiments at 39 ºC.

The model given by Eqn. 7 implies that the density profile of the bacteria reflects their inverse speed profile (Figure 3.8) and suggests a linear relation between bacterial density along the gradient and the inverse of their speed as a function of location. Indeed, our results show that the bacterial density along the gradient is linearly proportional to the bacterial inverse speed (Figure 3.9). This linear relation between the inverse speed profile and the concentration profiles suggests that the effect of temperature on the bacterial swimming speed could indeed be the driving mechanism of bacterial thermotaxis in shallow temperature gradients, where the steepness of the gradient is lower than the sensitivity threshold of the bacteria.

There is some discrepancy, however, between the model and the experimental data. The slope of the linear fit (m_{exp}~3.5, average of MB and serine) to the data presented in Figure 3.9 is

higher than what the model predicts (m_{model}=1), and the y-intercept is negative instead of being zero. This discrepancy could be attributed in part to the fact that in our experiments the bacteria are not uniform, but rather they exhibit a wide variability in motility and swimming speed. In addition, our experimental system is not completely closed. The channels, in which the bacteria reside, extend 2-3 millimeters beyond the end of the gradient at both ends, where the temperature is uniform and constant.

As a result, bacteria that reach either end of the gradient get trapped in that region due to a severe slowing down at cold temperature or death at high temperature, and thus can be considered as if they are no longer part of the system.

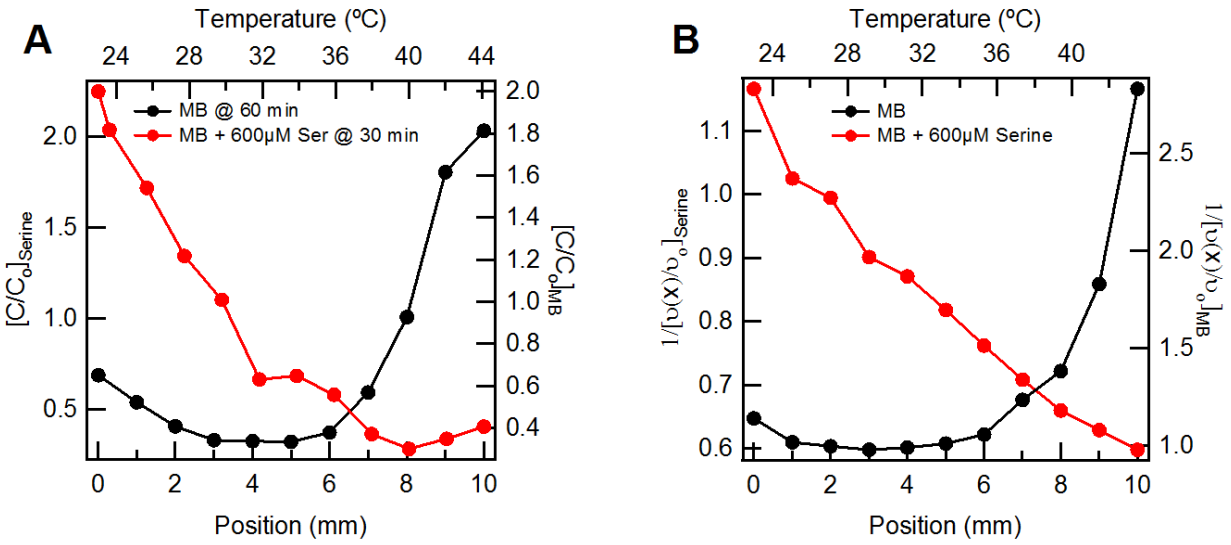

Figure 3.8: Density profile and inverse speed profile comparison

The concentration profiles in motility buffer without serine and with 600µM serine are presented in (A) to compare with the profile of the bacterial reciprocal swimming speed presented in (B). Concentration values are normalized by the initial concentration and speed values are normalized by the speed at room temperature. The linear relation between density profiles shown in A and the inverse speed profiles shown in B is presented in Figure 3.9.

The above described results can explain the observed directional migration of bacteria in shallow temperature gradients, with steepness below the bacterial sensing threshold. However, the question remains: what is the reason for the different temperature dependence of the swimming speed at low and high serine concentrations?

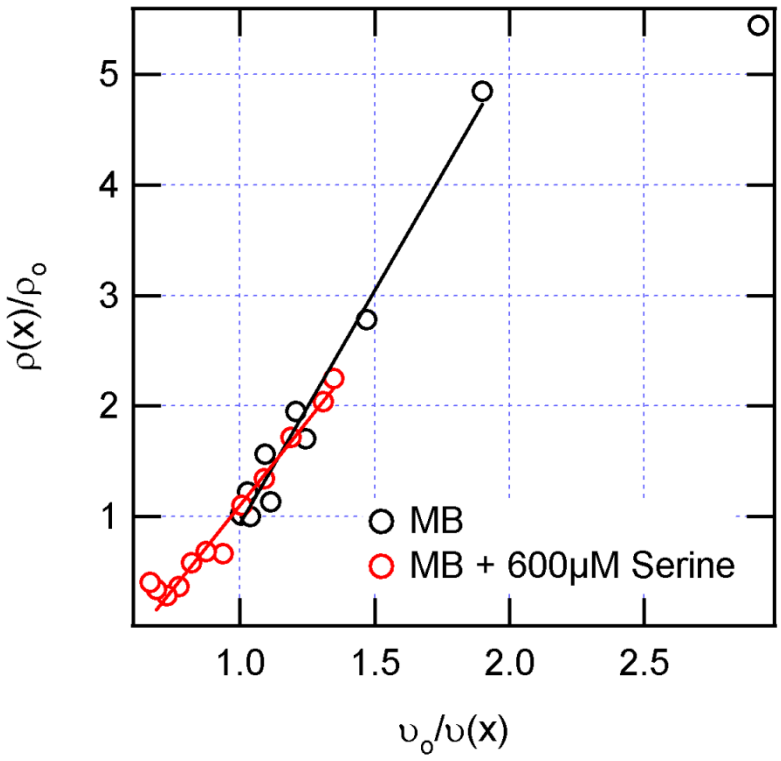

Figure 3.9: Linear relation between density distribution and inverse speed of bacteria

The density of bacteria along the gradient, measured as the total number of cells within a 1mm window, was normalized by the density at 28 ºC and these values are plotted as a function of inverse speed which were normalized by the speed of bacteria at 28 ºC. The linear relation between normalized speed and inverse normalized speed is consistent with the theory presented in Eqn. 7. It is important to note here that our experiments never reach a true steady state, because bacteria those reach temperatures >40°C die and become immobile and therefore are no longer part of the system. This is similar to a situation where the system is actually open at one end and has a very small flux out.

3.2 THE EFFECT OF SERINE AND TEMPERATURE ON THE BACTERIAL MEMBRANE POTENTIAL AND INTRACELLULAR PH

To answer the question presented at the end of the previous subsection, we invoke the fact that the swimming speed of the bacteria is dependent on the rotational speed of the flagellar motor. We also consider that the flagellar motor is driven by the proton motive force (PMF), which is a combination of the membrane potential and the intracellular-extracellular pH difference (165):

$$\Omega = \alpha(f)\left[\Delta\psi - 2.3\left(\frac{RT}{F}\right)\Delta pH\right] \qquad \textbf{Eqn. 9}$$

where Ω is the rotational speed of the motor, $\alpha(f)$ is a constant that depends on the frictional drag coefficient, f, $\Delta\psi$ is the membrane potential, R and F are the gas and Faraday constants, respectively, T is the temperature in °K, and $\Delta\psi - 2.3\left(\frac{RT}{F}\right)\Delta pH$ is the PMF. Therefore, a change in the swimming speed of the bacteria is a result of a change in the membrane potential and/or the intracellular-extracellular pH difference.

To determine what changes in the membrane potential and/or pH, are responsible for the observed change in the swimming speed, we measured both as a function of temperature and serine concentration separately. Figure 3.10 shows that the membrane potential (measured using PROPS as described in Materials and Methods (section 2.0)) changes little when the serine concentration is changed, but it increases with the temperature up to ~35°C and decreases afterwards (see also (120) Fig. 10).

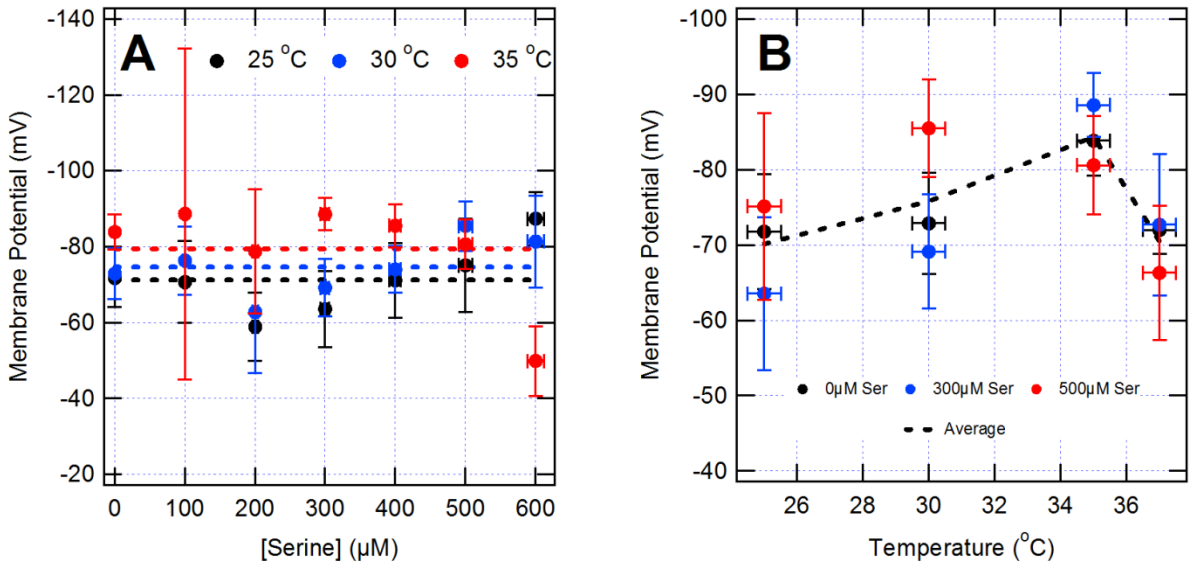

Figure 3.10: The effects of serine on the membrane potential

(A) The membrane potential of bacteria as a function of serine concentration for different temperatures as indicated in the figure legend. Note that the membrane potential is not affected by increase in the serine concentration at different temperatures. Dashed lines are averages of the MP at different temperatures (B) The Membrane potential of bacteria as a function of temperature at different serine concentrations as indicated in the figure legend. The membrane potential increases up to 35 °C and decreases above that temperature for all serine concentrations. Dashed line is the average of the temperature series. All measurements we carried out as described in Materials and Methods (section 2.0).

On the other hand, our measurements of the intracellular and extracellular pH, using YFP and BCECF, respectively, as described in Materials and Methods (section 2.0), show that while the extracellular pH is affected by temperature only, the intracellular pH changes with changing serine amount as well (Figure 3.11).

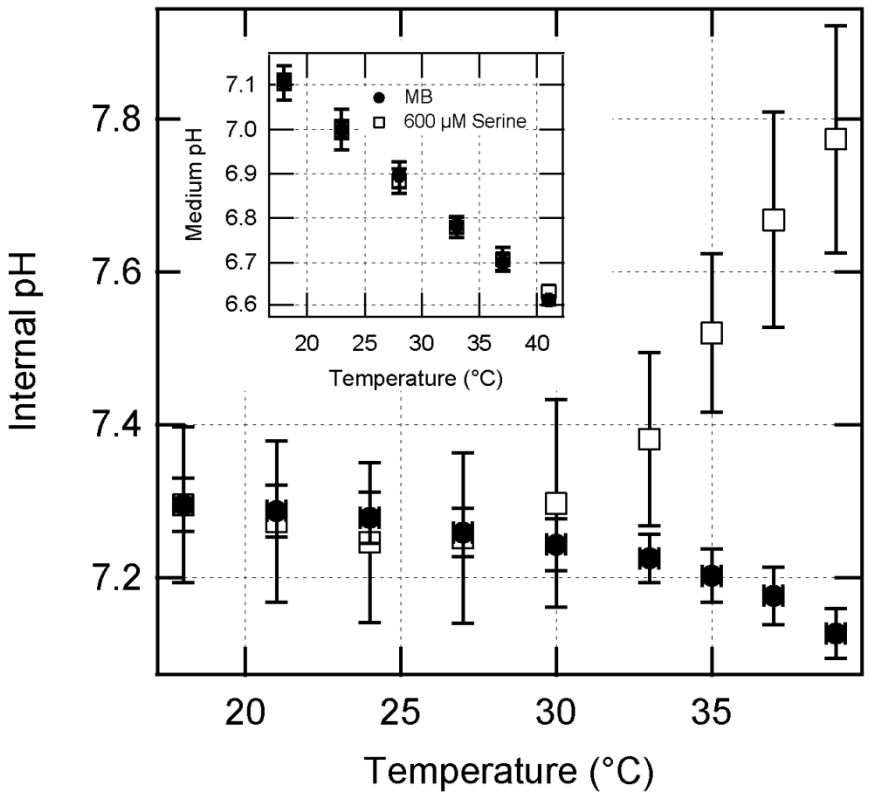

Figure 3.11: The effect of temperature on the internal and external pH

The intracellular pH as a function of temperature with and without 600µM serine. The pH in both cases is almost the same up to 30°C, after which it starts increasing with increasing temperature when serine is present in the medium and decreasing when no nutrients are added. The extracellular pH on the other hand decreases with increasing temperature exactly the same with and without serine as depicted in the inset

Figure 3.12A shows that the intracellular pH exhibits a sigmoid-like behavior as a function of serine concentration similar to the behavior detected in the swimming speed (Figure 3.5). The increase in the intracellular pH occurs around similar values of serine concentration ~250µM, and the difference between the intracellular pH at high and low serine concentrations is also temperature dependent as exhibited by the swimming speed.

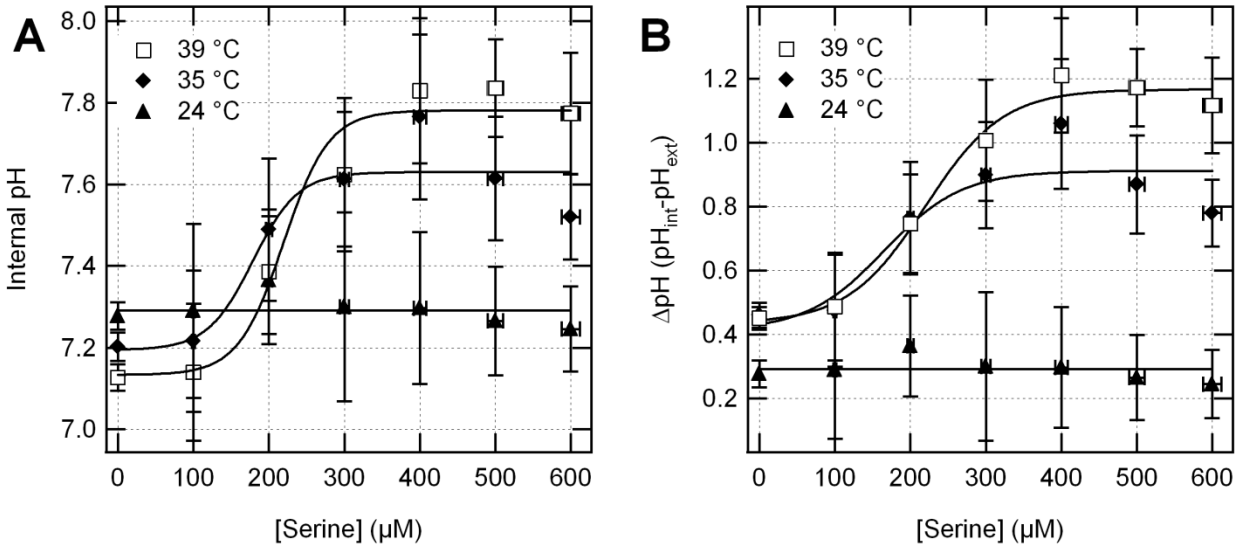

Figure 3.12: The effect of serine on the intracellular pH

(A) The intracellular pH at different temperatures as a function of serine concentration in the medium, measured as described in Materials and Methods (section 2.0). (B) The difference between the intracellular and extracellular pH as a function of serine at different temperatures calculated using the measurements in (A) and Figure 3.11 inset. The lines in the graphs are to guide the reader.

Moreover, the intracellular-extracellular pH difference for low and high serine concentrations are almost the same at low temperature up to ~30°C, but the difference between the two increases for temperatures higher than that (Figure 3.12B).

In addition, the PMF, calculated using the measurements of the membrane potential and pH, shows that at low serine concentration it increases with increasing temperature up to 30°C and decreases afterwards, while for high serine concentration it continuously increases with increasing temperature in good agreement with the measurements of the bacterial swimming speed (Figure 3.13 and Figure 3.6 respectively).

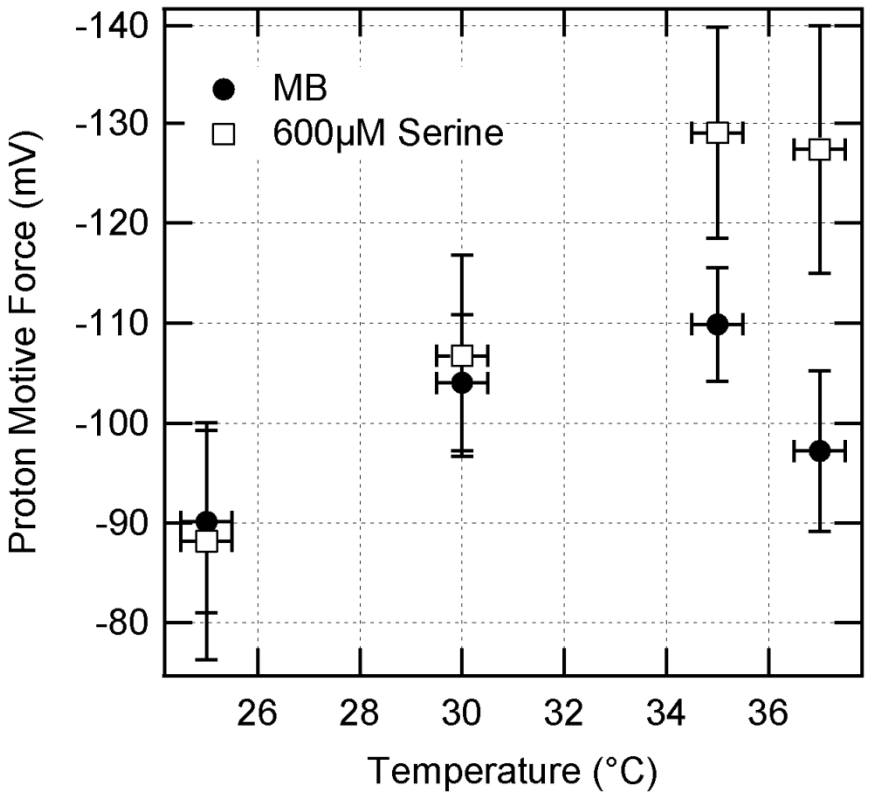

Figure 3.13: The effect of temperature on the PMF

The PMF calculated as defined in Eqn. 1 using the measurements of the membrane potential and the pH described above in Figure 3.10B and Figure 3.12B, respectively.

Finally, the corresponding speed for our measured PMF is calculated by utilizing the data from Gabel et al. (104) and Darnton et al (100). The relationship between the flagellar rotational speed and the proton motive force is obtained from (Fig. 2b in (104)) (Eqn. 10a). This relationship is combined with the linear relation between the motor rotational speed and the bacterial swimming speed obtained from (Fig. 3 in (100)) (Eqn. 10b-c) to get the relation between the swimming speed and proton motive force (Eqn. 10d). Using this relation the PMF data presented in Figure 3.13 is used to calculate the swimming speed of the bacteria presented in Figure 3.14 which is in good agreement with the measured values presented in Figure 3.6.

$$\Omega = (1.5406 \pm 0.003) \times PMF - (1.1329 \pm 0.275) \quad \textbf{Eqn. 10a}$$

$$v = (0.1804 \pm 0.001) \times \omega_{bundle} - (0.048 \pm 0.041) \quad \textbf{Eqn. 10b}$$

$$\omega_{bundle} = (0.8538 \pm 0.001) \times \Omega - (0.0274 \pm 0.055) \quad \textbf{Eqn. 10c}$$

$$v = (0.2373 \pm 0.002) \times PMF - (0.2274 \pm 0.059) \quad \textbf{Eqn. 10d}$$

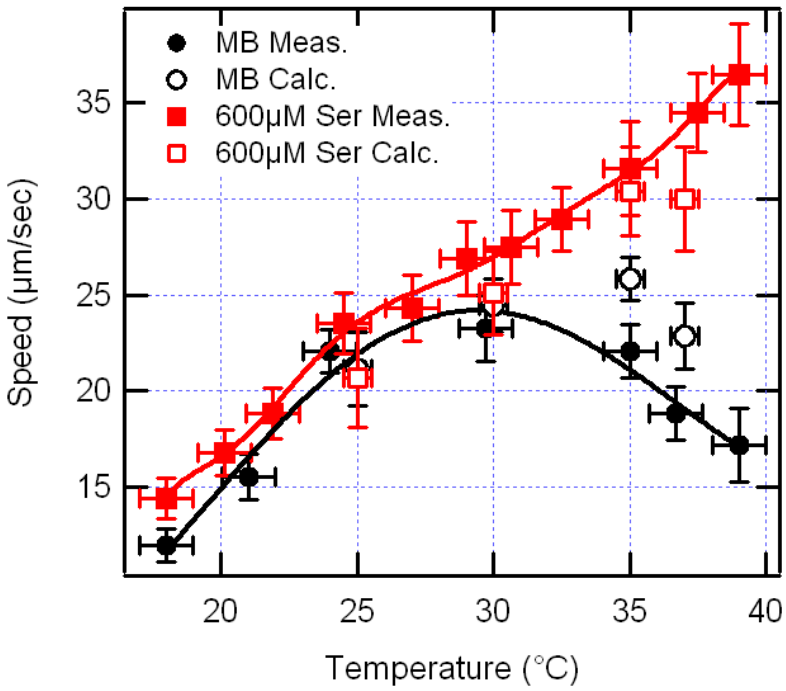

Figure 3.14: Bacterial swimming speed and the PMF

The corresponding speed for our measured PMF is calculated by utilizing the data from Gabel et al. (104) and Darnton et al (100). The relationship between the flagellar rotational speed and the proton motive force is obtained from (Fig. 2b in (104)). This relationship is combined with the linear relation between the motor rotational speed and the bacterial swimming speed obtained from (Fig. 3 in (100)) to get the relation between the swimming speed and proton motive force. Using this relation the PMF data presented in Figure 3.13 is used to calculate the swimming speed of the bacteria presented here. Filled circles are experimental data and empty circles are calculated using PMF measurements from Figure 3.13. Red: MB + 600 μM Serine, Black: MB.

Note that the motility medium used in the experiments whose results are given above is similar to the medium that we used in our experiments. Since the experimental conditions are similar, the relations given in Eqn. 10 are applicable to our results too.

The change in the intracellular pH detected here (Figure 3.11 and Figure 3.12) is very surprising, and it seems contradictory to previous observations of cellular pH homeostasis (166) since bacteria have mechanisms to maintain their intracellular pH at a constant level even when external conditions change abruptly. However, it is important to note that the MB used in all measurements does not contain a carbon source and does not support cellular growth or protein production, and therefore, it is possible that the cell in such environment is not capable also of regulating and maintaining a stable cytoplasmic environment. As a result, in MB the intracellular pH behaves in a similar manner to the extracellular pH and therefore decreases with increasing temperature (Figure 3.11 inset). On the other hand, serine as mentioned earlier is known to be a bacterial source of carbon that can be used to maintain bacterial motility under anaerobic conditions (113, 162). Therefore, when it is added to the medium perhaps the bacteria are able to maintain a stable intracellular environment and increase their pH close to its normal values (i.e. pH=7.8).

This increase however, occurs only for temperatures higher than 24°C (Figure 3.12) possibly because of the reduced rate of metabolism at lower temperature. To further support this hypothesis, we have measured the kinetics of pH increase as a function of time after adding serine to the medium and compared it to the serine consumption kinetics. Our measurements presented in Figure 3.15 show that when serine is added to a bacterial sample, suspended in MB and incubated at 37°C, at a 600 μM concentration the internal pH increases from ~7.25 to ~ 7.8 within minutes and the bacteria are able to maintain the internal pH increase for ~ 2 hours.

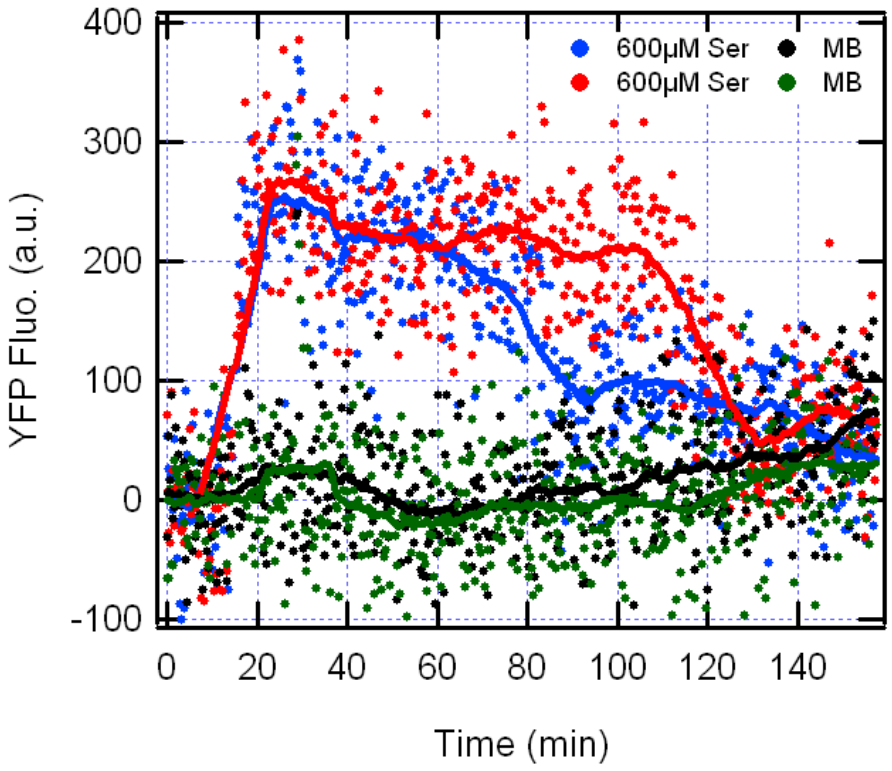

Figure 3.15: Internal pH dynamics upon serine addition

Intracellular pH increase upon serine addition. Intracellular pH increases from initial value, i.e. 7.25, to ~7.8 upon addition of serine at a final concentration of 600 µM. The pH increase happens within minutes. The observed intracellular pH increase persists for ~ 2 hours and decreases back to the MB values. Dots represent measurements at every 20 seconds and lines are the moving average smoothing of the data. The graph represents two different experiments for both MB and 600 µM serine addition. Experiments were performed at 37 °C.

The length of time that bacteria maintain the internal pH increase is consistent with the time required for the bacteria to consume all the serine in the medium (Figure 3.16). The hypothesis that internal pH increase is related to metabolism of serine is also supported by the fact that this effect is not detected when a non-metabolizable form of serine is used. In order to understand the exact mechanism that controls this observed change in the intracellular pH, further investigation is required, but these results provide an important insight that can be also useful for understanding the mechanism bacteria use to regulate their intracellular pH.

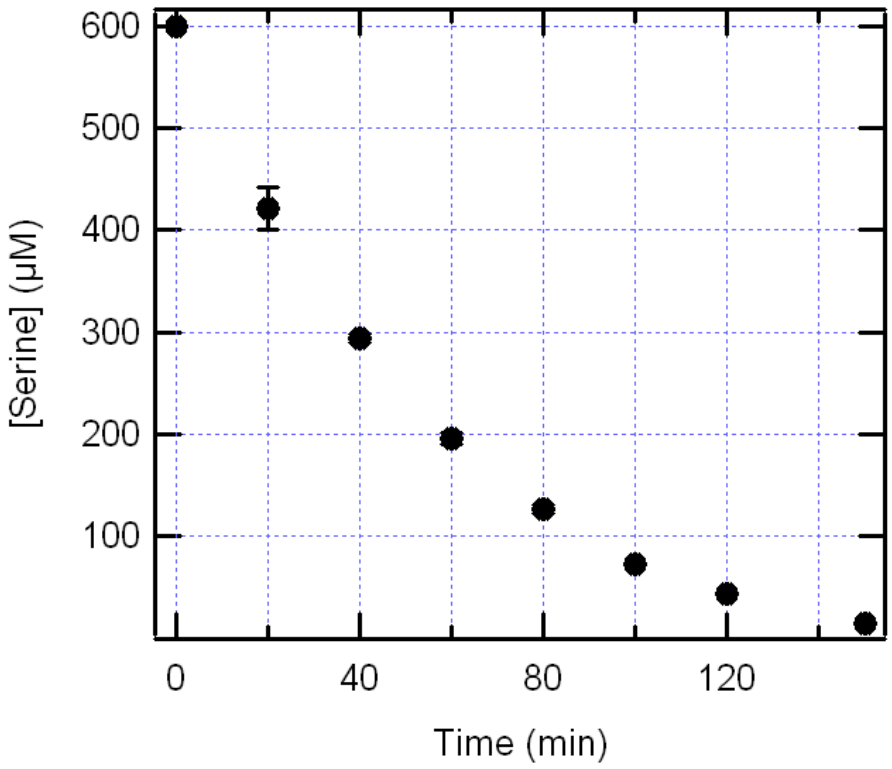

Figure 3.16: Serine uptake by bacteria

Serine uptake by bacteria from medium is measured as described in subsection 2.4.3. Vertical axis represents the amount of serine in the medium.

3.3 STOCHASTIC SIMULATIONS OF BACTERIA IN SHALLOW TEMPERATURE GRADIENTS

To further test our theory, we have performed stochastic simulations (SS) of random walkers in a temperature gradient with temperature dependent speed and step size. The simulations were carried out with the parameters obtained from constant temperature measurements in order to compare the simulations with our experimental results. The main point

here is that the random walk model we used in the simulations does not include directional dependence of tumbling rate which would imply response of the sensory network to the temperature changes along the gradient. Thus, the result of the simulations is due to spatially dependent speed and run time and there is no contribution from the signal transduction system at all.

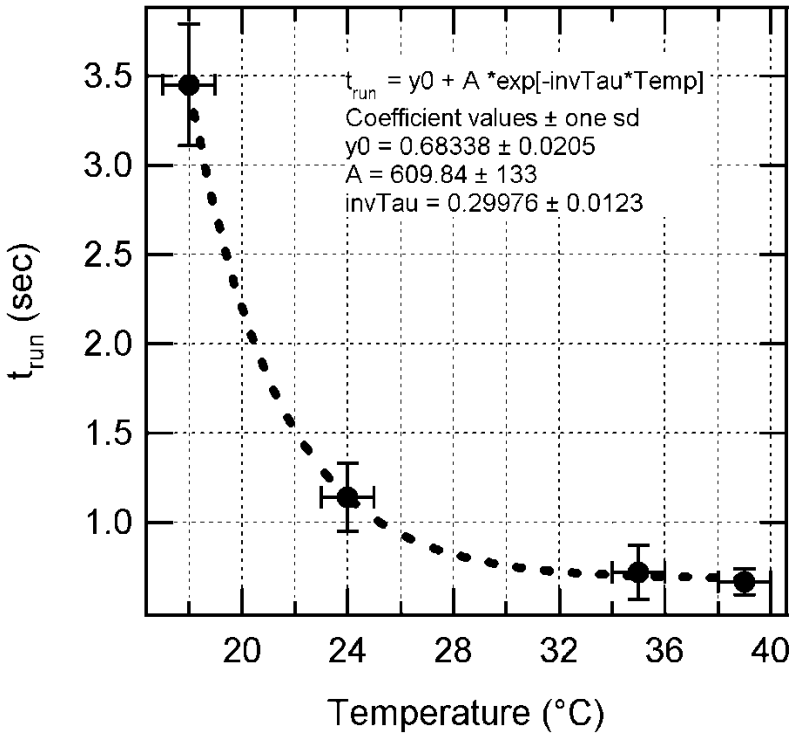

Figure 3.17: Effect of temperature on run time of bacteria

Run time, t_{run}, of bacteria measured by fitting the model $\langle \Delta r^2(t) \rangle = 4Dt\left(1 - exp(-t/t_{run})\right)$ to the mean square displacement calculated from the trajectories of swimming bacteria in MB and MB + 600 µM serine. Values and dependence to the temperature are similar for both medium and average values of both medium are represented.

In each SS, initially 3000 bacteria were distributed randomly along the linear gradient which is 10 mm in length (x axis) and 800 µm in width (y axis) so that the initial density is

uniform. The temperature gradient was one dimensional along the x direction starting at 23 °C and ending at 43 °C. At the beginning of the simulation, each bacterium was assigned to a speed, a run time and a run direction in the 2D space. The run time was randomly drawn from a Poisson distribution (167) whose mean was determined based on our own measurements presented in Figure 3.17. Similarly, the speed was drawn from a lognormal distribution (based on our measurements) whose mean and width were estimated from our data presented in Figure 3.6 and Figure 3.7 respectively.

For simplicity we assumed linear speed dependence on temperature for the case with 600 μM serine, and quadratic dependence for MB. Initially, the run direction, relative to the positive x axis, was selected randomly between 0° and 360°. Each bacterium swam with the given initial speed and direction during the assigned run time and then tumbled.

During the tumble, which lasted for a time step, the speed and run time were adjusted to the new location and a new direction was assigned randomly from a lognormal distribution centered around 62º, with a standard deviation of 26º, relative to the previous run direction (23). The time resolution of the simulation was hundred milliseconds. Since the durations of runs are about one order of magnitude higher than this time step and we are interested in the density profiles of bacteria in time-scales larger than minutes, 100 milliseconds time-step is reasonable for the simulation. The boundaries of the channel were considered reflective such that a bacterium that hit a wall was reflected with the same speed. The MATLAB (The Mathworks, Natick, MA) code for the simulations is included in Appendix B, and the results presented in Figure 3.18 exhibit good agreement with our experimental results.

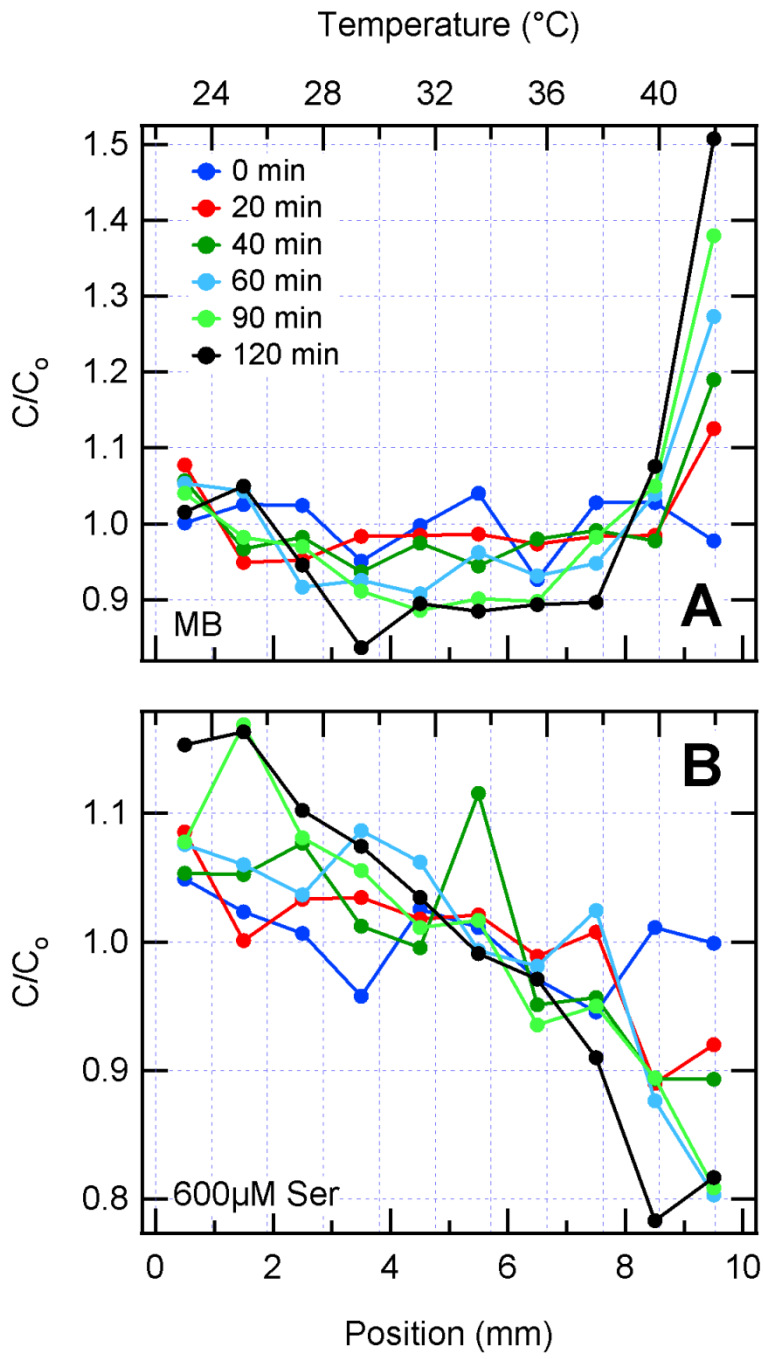

Figure 3.18: Stochastic Simulations of WT accumulation in shallow temperature gradient

The concentration profiles were obtained from stochastic simulations (SS) as explained in the text above. The normalized density profiles of the bacteria, without serine added to the medium (A) and with 600μM serine (B) recorded at different times in SS. All values were normalized by the initial concentration at each location to allow better comparison of different experiments.

The simulation results confirm that the bacteria accumulate at the warmer end of the temperature gradient in motility buffer (Figure 3.18A) and at the colder end in the presence of 600 µM serine in motility buffer (Figure 3.18B), consistent with the experimental observations presented in Figure 3.3. The agreement between the experiment and the simulation in the direction as well as the time courses of the accumulation confirms that the migration of the bacteria in shallow temperature gradients is mainly due to the speed modulation by temperature changes, not through temperature sensing.

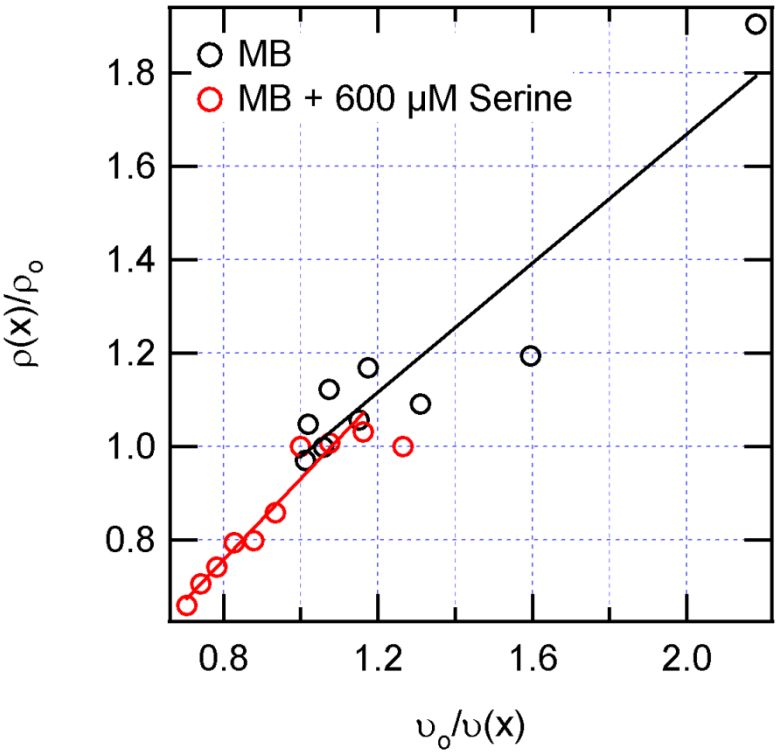

Figure 3.19: SS - Linear relation between density distribution and inverse speed of bacteria

The density of bacteria along the gradient, obtained from SS as the total number of cells within a 1mm window, was normalized by the density at 28 ºC and these values are plotted as a function of inverse speed which was normalized by the speed of bacteria at 28 ºC. The linear relation between normalized density and normalized inverse speed is consistent with the theory presented in Eqn. 7 for both cases of bacteria in MB and MB + 600µM serine under shallow temperature gradients.

In addition, the linear relationship between the density and the inverse speed presented in Figure 3.19 is in good agreement with the theory suggested by Schnitzer et al. in Eqn. 7. However, unlike the experiment (Figure 3.8), the slope and the intercept on the y-axis of the linear relation in Figure 3.19 ($m_{sim} \sim 0.8$, $b_{sim} \sim 0.13$, average of the slopes and y-intercepts of red and black lines) are close to the values predicted by the theory ($m_{model}=1$, $b_{model}=0$). This is to be expected in this case since the stochastic simulations do not include any flux of bacteria into or out of the system, as in the case of experiments.

Allowing bacteria to diffuse in and out of the system (i.e. the 10mm part of the channels with the temperature gradient of interest) at the hot end of the shallow gradient makes the simulations more realistic, because in our experiments both hot and cold ends are open and bacteria are free to swim in both directions. Furthermore, the simulation might become more realistic by introducing a decrease in the number of bacteria via death at temperatures above 40 °C. These two scenarios are simulated using the above described model and code. The differences between closed system, the system with the open hot end, and the one with the open hot end and where bacteria die above 40 °C with a rate of 2 bacteria/mm/min are shown in Figure 3.20. These results indicate that, the decrease in the relative density at the location with the highest temperature (i.e. highest inverse speed for the bacteria in MB) presented in Figure 3.9 can be explained by a flux out of the system, since the simulations in which a flux is introduced at the hot end of the gradient produces the observed discrepancy (Figure 3.20).

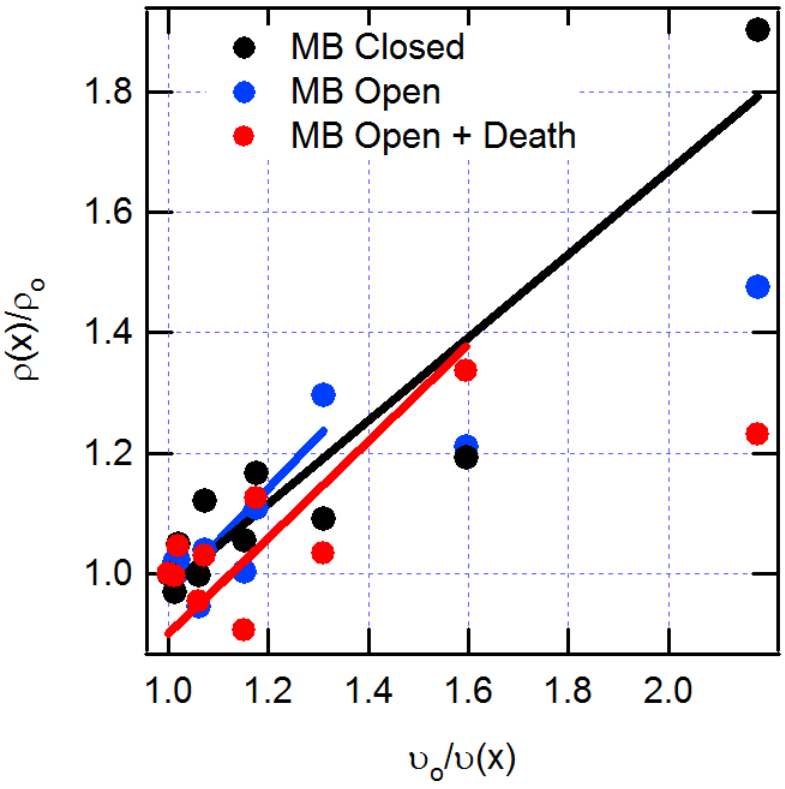

Figure 3.20: Comparison of SS of different scenarios

The density of WT bacteria along the gradient, obtained from SS as the total number of cells within a 1mm window, was normalized by the density at 28 ºC and these values are plotted as a function of inverse speed which was normalized by the speed of the bacteria at 28 ºC. The linear relation between normalized density and normalized inverse speed is consistent with the theory presented in Eqn. 7 (solid lines), however allowing the bacteria to swim in and out of the system at the hot end decreases the density at that location (i.e. the point with the highest inverse speed) compared to the closed system (blue and black markers respectively). An additional flux out of the system by introducing bacterial death at temperatures above 40 ºC decreases the density at the hot end further (red markers).

4.0 THE EFFECT OF TEMPERATURE CHANGE DYNAMICS ON THE FLAGELLAR MOTOR'S SPEED UNDER HEAVY LOAD

In the previous section we have shown that the directional migration of bacteria in a shallow temperature gradient is driven by speed modulation rather than active response to temperature changes sensed by the bacterial sensing receptors. However, in a sharp temperature gradient speed modulation might have a contribution to thermotaxis apart from the signal transduction system. As explained earlier, bacteria respond to thermal changes by extending the period of counter clock-wise rotation (CCW) of their flagellar motors when the temperature changes are favorable (52–58, 60). This allows them to extend their run period in the direction of the temperature of their preference. However, it is important also to understand how thermal changes experienced by bacteria during their excursion in a temperature gradient affect their run speed, and their run speed dynamics.

In addition, the bacterial flagellar motors are small molecular machines which are subject to thermal fluctuations that can affect their rotational speed as well as their switching rate. As a result, thermal changes will introduce additional noise into the output of the signal transduction network that can affect the behavior of the bacteria in a temperature gradient and influence its sensing precision. Therefore, it is important to quantitatively measure these effects. Also, the dynamics of molecular machines in general can help reveal hidden structural features and interactions between the different components that cannot be detected through structural studies

alone. In this section we study the effect of temperature dynamics on the rotational speed of the bacterial flagellar motor. We begin by measuring the response of the bacterial flagellar motor to temporal linear temperature changes applied at different rates and then we study the response of the motor to thermal fluctuations with various frequencies.

The torque generated by the bacterial flagellar motor (BFM) will rotate an attached object at a speed such that the viscous drag on the object balances the generated torque. The viscous drag on the object (cell body, flagellar bundle, latex bead etc.) determines the load under which the motor operates. For a sphere of radius r rotating through its central axis with a speed of Ω in a viscous medium with viscosity η the viscous drag will be $8\pi\eta\Omega r^3$. For large objects ($r\sim1\mu m$) the load is considered heavy, which corresponds to the plateau region in the torque-speed curve of the BFM (Figure 1.4 and Figure 4.5), whereas for relatively small objects ($r<0.3\mu m$) the load is light, which corresponds to the linear decay region. In our experiments with the tethered cells, motors are forced to rotate the cell body. Therefore, our studies were carried out under the heavy load which does not completely represent a free swimming bacterium; however it still reveals important quantitative information about the internal dynamics of the BFM.

4.1 RESPONSE OF THE FLAGELLAR MOTOR TO LINEAR TEMPERATURE CHANGES

Using a focused infrared laser beam (λ=1480nm) as described in material and methods, section 2.4.5 (Figure 2.15), we increased almost linearly the surrounding temperature transiently

(Figure 4.1) of a tethered bacterium and measured its rotational speed as a function of time and temperature.

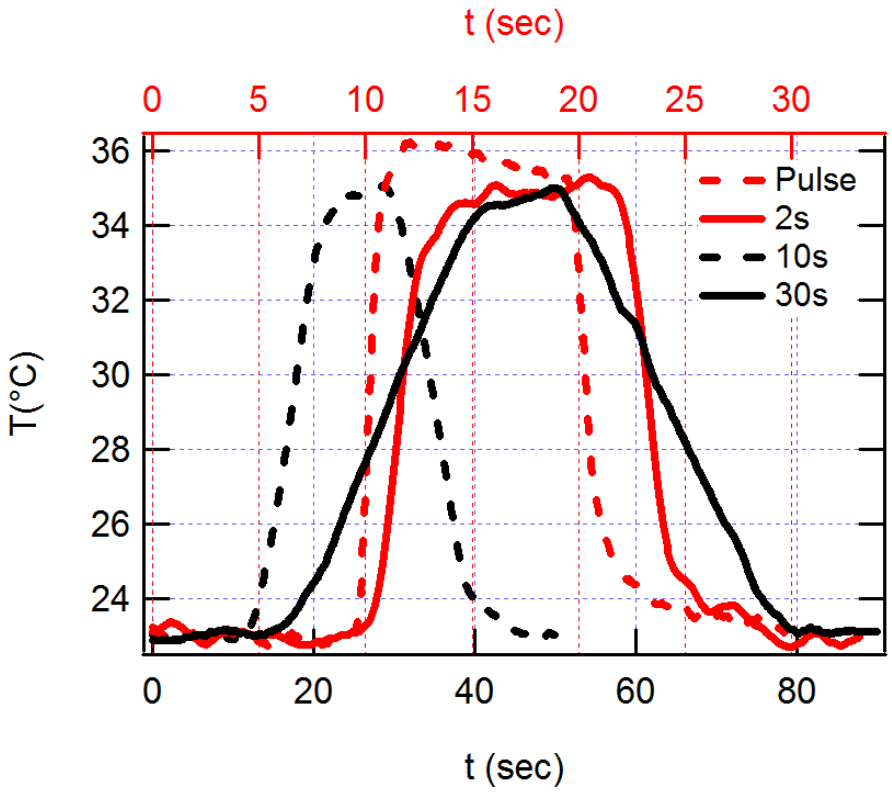

Figure 4.1: Linear temperature increase & decrease

The temperature around the rotating bacteria as a function of time was estimated from the change in the fluorescence intensity of the BCECF at the center of the image and is plotted for all the signals applied in our experiments in (see Figure 2.15). In all experiments, the laser was turned on 10 seconds after the recording of the tethered bacterium started. Its power was increased by changing the applied current from zero to 200mA gradually over 2, 10, or 30 seconds, or applied as a pulse at 225mA. The applied current was then kept constant at 200mA for 10 seconds after which it was decreased back to zero at the same rate of increase. The recording of the bacteria's rotation continued for another 10 seconds after the laser power reached zero. For time axis, use top for pulse and 2s (red), and bottom for 10s and 30s (black).

Our measurements were carried out for several rates of increase and decrease but always starting from an initial steady state at room temperature, and allowing the motor's rotational

speed to reach steady state at the highest temperature applied before starting to decrease the temperature (Figure 4.2). To avoid the effects of changing the rotational direction in response to thermal changes, we used the mutant strain VH1 (123) whose motors rotate continuously in one direction only (see section 2.4.5 for experimental details).

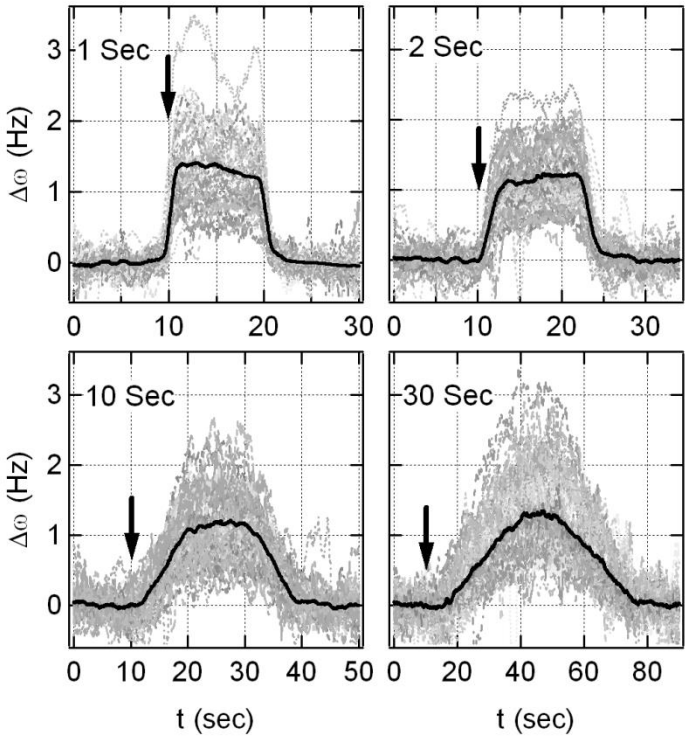

Figure 4.2: The motor's rotational speed as a function of time

Grey dashed lines depict the rotational speed of different bacteria. Black thick lines depict the averages of each set of experiments. The speed at room temperature was subtracted from each curve. The number of bacteria recorded for temperature increases as a pulse and over periods of 2, 10, and 30 seconds are 46, 59, 62, and 54 respectively. Arrows indicate where the laser power started to increase.

Notice that we have used speed increases for analysis rather than relative speed (i.e. speed increase relative to the background). Since the temperature increase and decrease happens within seconds, we assume that the internal pH and membrane potential do not change during the process (see section 3.2). Taking these quantities as constants from Eqn. 9, we can express the

speed of the bacteria as $\Omega(\Delta T) = \Omega_o + c\Delta T$. Here Ω is the angular speed in Hz, ΔT is the temperature difference from room temperature (i.e. $\Delta T = T - T_{Room}$), Ω_o is the angular speed at room temperature, and c is a constant that depends on the viscosity of medium, size of the bacteria, pH difference, and gas and Faraday constants. Since these quantities are the same for all temperature increase and decrease rates one would expect that the increase in the average speed of the population relative to the speed at room temperature should be the same. Indeed, that claim is verified by looking at the distribution of speed increase in Figure 4.2 and Figure 4.3.

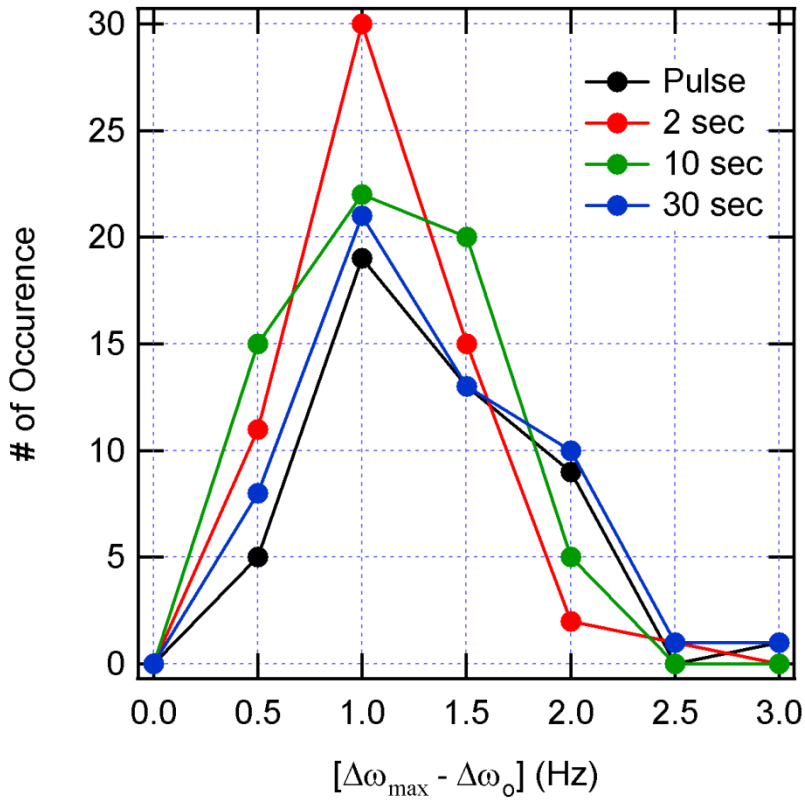

Figure 4.3: Distribution of maximum speed increase with respect to room temperature speed

The initial speed values are subtracted from the ones at the steady state after linear temperature increase for each bacterium, and histograms were calculated for each linear increase rate. Speed increase distributions for pulse, 2, 10, and 30 sec are represented with black, red, green, and blue curves. Using speed increase for statistics and calculations is reasonable since speed histograms are consistent.

Our measurements show that when we increase the surrounding temperature from room temperature (~23°C) to ~34°C and decrease it back to room temperature, the motors' rotational speed changes with temperature during both, its increase and decrease, and the rotational speed of all motors at the beginning and end of all measurements is similar. Moreover, at all rates of the temperature change (~0.3°C/s, ~1°C/s, ~5°C/s, ~10°C/s), the speed decreases with the temperature in almost an identical fashion to its increase and maintains an almost linear dependence on temperature (Figure 4.4).

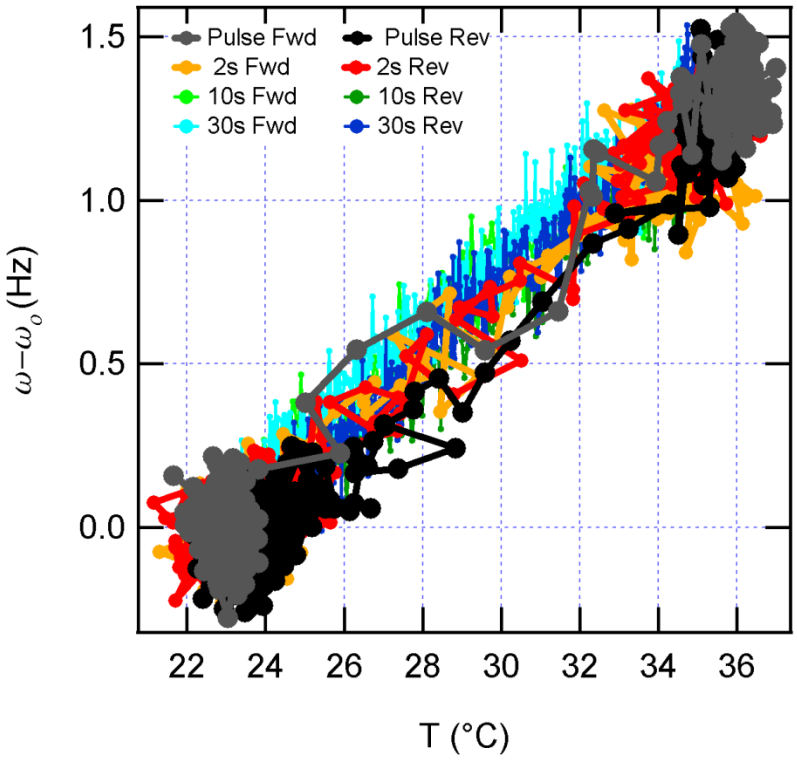

Figure 4.4: The average rotational speed of the flagellar motors as a function of temperature

The gray, orange, light green, and light blue lines depict the speed dynamics as the temperature increases, while the black, red, dark green and dark blue lines depict the speed dynamics as the temperature decreases for the different time periods over which the temperature increase occur, pulse, 2s, 10s, and 30s respectively. Notice that the rotational speed of the flagellar motors appears to be almost linear with temperature in both directions of change.

Amazingly, our results show that, under the heavy load the response of the motor to thermal changes is instantaneous without any delay (Figure 4.4). In other words, the change in the motors' speed in response to changes in temperature does not depend on the rate of temperature increase or decrease within the rates that we have tested. However there might be some phase shift in the response of the BFM to temperature changes, nevertheless we do not observe that due to limitations of our data acquisition and experimental precision. The instantaneous and linear response is not a surprising result, and it is what would be expected from previous studies performed under steady state. Under a heavy load the speed of the motor is limited to the low frequency range, where the torque is almost constant as a function of the motor's speed (104). As a result, the change in the rotational speed of the motor as a function of temperature will be mostly due to the change in the medium's viscosity, which is instantaneous. However, there is a need to extend this study to rotation under light load and higher rotational speed. Under light load and high rotational speed, the torque will change significantly as a function of speed. In addition, the speed-torque relationship is temperature dependent (Figure 4.5) (66).

Therefore, under light load, when changing the temperature, both speed and torque will change and the dynamics of this change will not necessarily follow the steady-state curve. The rotational speed dynamics as a function of temperature under these conditions will reflect the dynamics of the torque generating components of the motor.

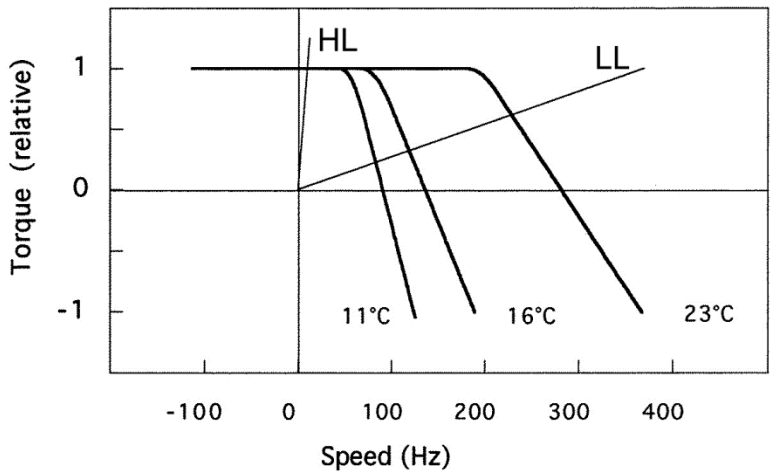

Figure 4.5: Torque-Speed curve

The torque-speed curve for the flagellar motor of E. coli shown at three temperatures (thick lines), together with two load lines (thin lines), one for an object the size of the cell body of wild-type E. coli (effective radius about 1 μm, H. L.), the other for a mini-cell (effective radius about 0.3 μm, L. L.). Figure reproduced from Berg et al. 2003 (66).

The bacterial flagellar motor is a complex machine assembled of many components that interact together in an orchestrated manner to result in the rotation observed. From the curves presented in Figure 4.5, it is obvious that these interactions and their results are temperature dependent (62, 66, 168). However, the transition dynamics from one temperature-dependent state to another is not a priori known, and it could be different in different directions of change. It is very important to study such dynamics as a function of the rate of change of temperature, as the results will allow us to better understand the response of bacteria to different temperature gradients, with different steepness, and as a function of the swimming direction of the bacteria in the gradient. In addition, the results of this study could reveal hidden mechanisms of interactions that are not reflected in the steady-state behavior.

Finally, even though our results in this section do not reveal new features of the motor, the technique used here for the first time has proven to be successful and can be easily used in the future to study the rotation of the flagellar motors under light load.

4.2 SPEED DYNAMICS UNDER OSCILLATING TEMPERATURES

To better understand how the bacterial motor's speed responds to thermal changes and whether its response depends on the rate of change of the temperature, we used the infrared laser setup described earlier in subsection 2.4.5 to apply sinusoidal temperature oscillations to tethered bacteria.

Using the LabVIEW (National Instruments Corporation, Austin TX) software we controlled the laser's input current and changed its output power at the desired frequency. The maximum current applied was carefully adjusted for each frequency such that the maximum temperature of the bacterial surrounding be the same for all frequencies, and the background temperature remains constant at ~30°C (Figure 4.6A). We have carried out these measurements for different temperature amplitudes as can be seen in Figure 4.6B.

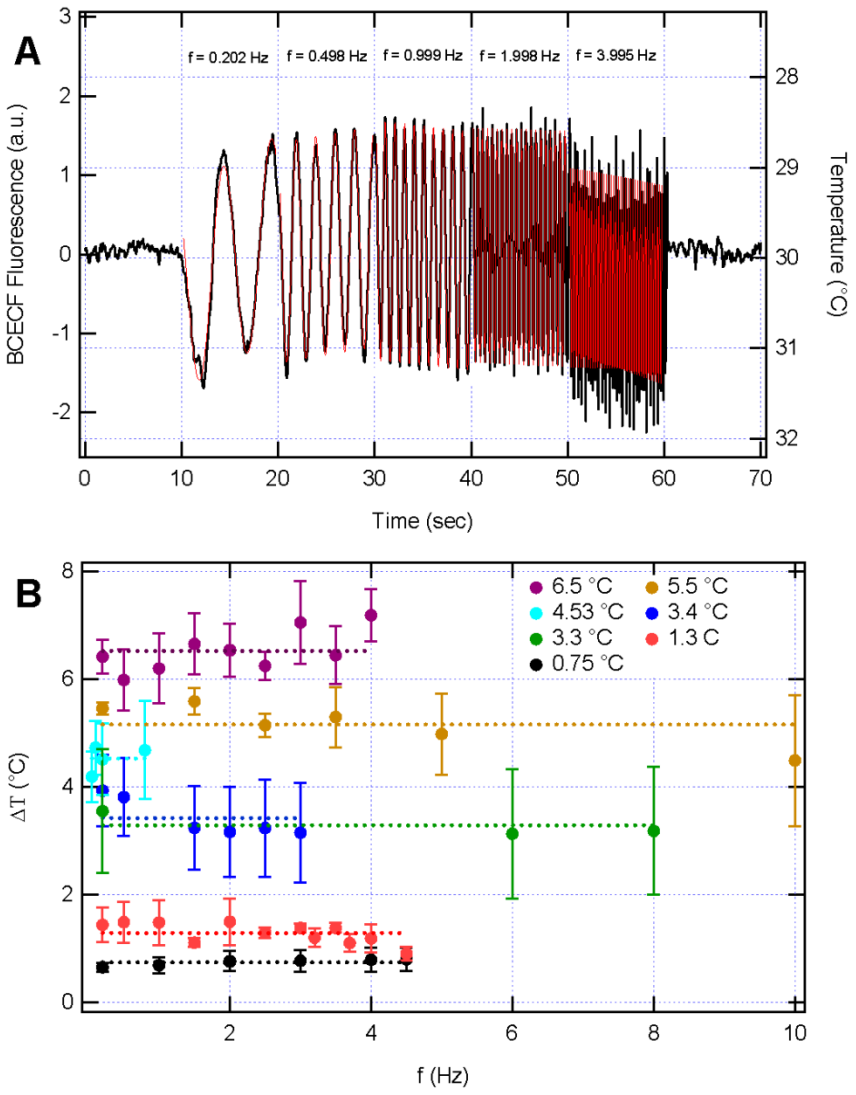

Figure 4.6: Oscillating Temperature Profile and Amplitudes

Fluorescence of the BCECF (see Material and Methods (section 2.0 for details) and amplitudes of temperature oscillations. (A) The fluorescence of temperature sensitive dye BCECF (left axis) and corresponding temperature values (right axis) of the medium at the laser spot as a function of time (black curve). Fluorescence values are w.r.t. the background. Each oscillation was driven for 10 seconds. Background temperature of the laser spot is set to ~30°C. Amplitudes of the temperature oscillations were calculated by fitting sinus functions (red curves) to each 10 second windows. (B) Measurements of A with more datasets. Amplitude of the temperature oscillations were kept fixed for the same experiment and six different temperature amplitudes were tested (i.e. 0.7, 1.3, 3.4, 4.5, 5.5 and 6.5 °C). The dashed lines in (B) are hand-drawn to guide the reader.

The oscillations in temperature were applied after the bacterial rotation was recorded at the background temperature for 10 seconds, and each frequency was applied for 10 seconds while the rotation was continuously recorded. The speed of the motor's rotation was calculated then from these recordings. A typical speed measurement for several frequencies at fixed temperature amplitude is presented in Figure 4.7.

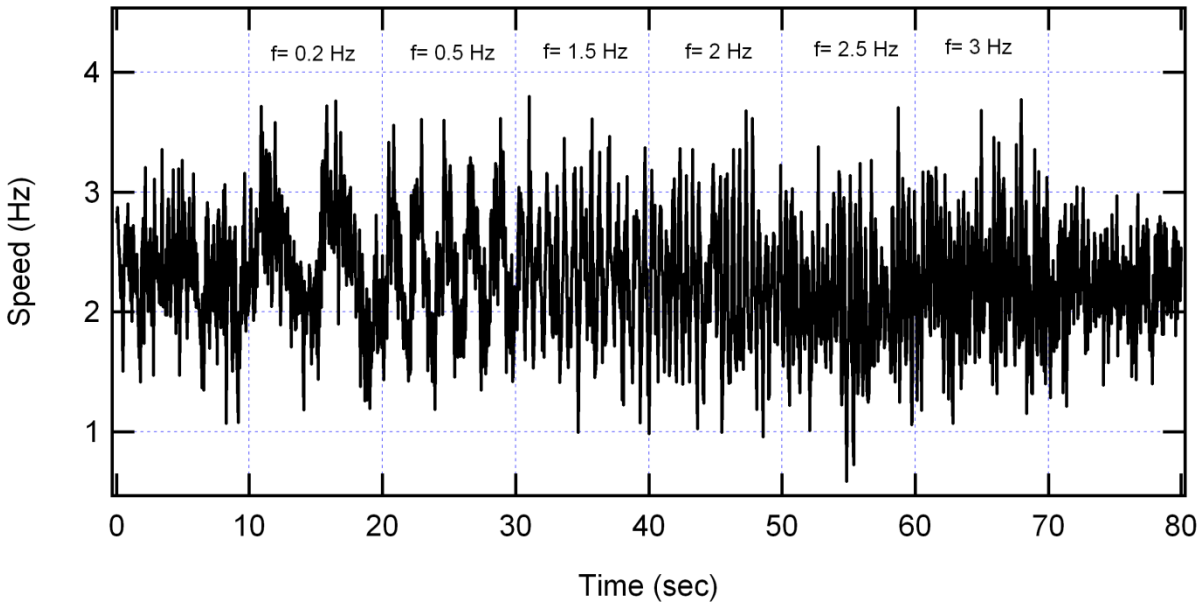

Figure 4.7: BFM Speed in Response to Oscillating Temperature

Speed of bacteria in response to the temperature oscillations. Speed of a single bacterium vs. time in response to the applied temperature change as in Figure 4.6A with frequencies listed in the figure. Amplitude of the temperature oscillations is 3.5 ºC.

We have measured the amplitudes of the speed oscillations by fitting a sinusoidal function to each 10 seconds window of different frequencies. The relative amplitude values with respect to the background speed were calculated by dividing the speed amplitude at one frequency with the average background speed at that frequency, i.e. $\Delta\omega_{rel} = {\Delta\omega}/{\omega_o}$.

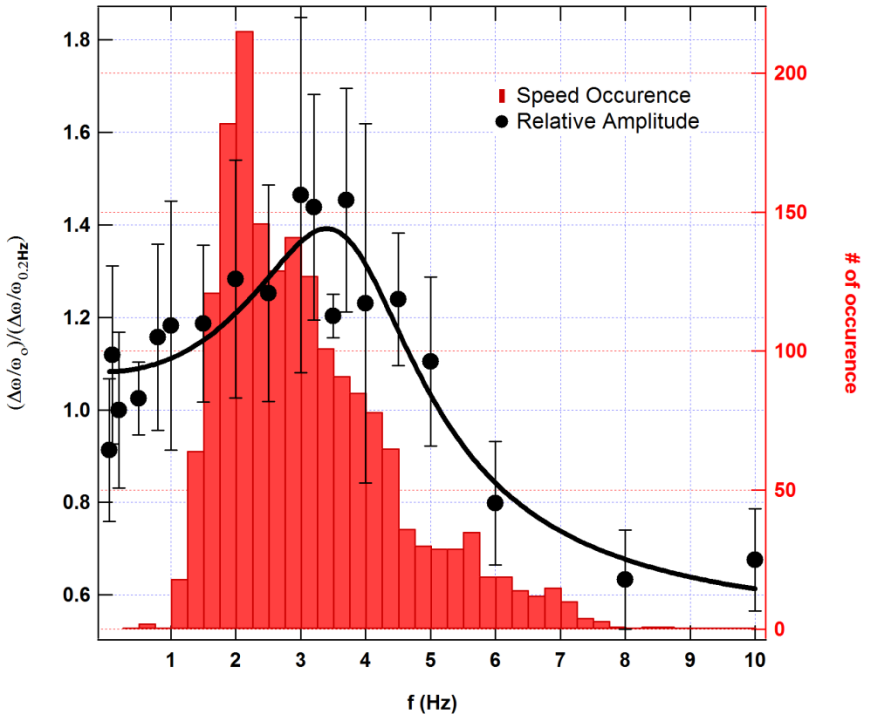

Figure 4.8: BFM speed amplitude response to temperature oscillation frequency

Relative amplitudes ($\Delta\omega_{rel} = {}^{\Delta\omega}/_{\omega_\circ}$) of the speed oscillations are calculated by fitting sinus functions to each 10 second window and dividing the obtained amplitudes with background speed. Relative amplitudes of a single experiment set are normalized with the relative amplitude at 0.2 Hz, and normalized relative amplitudes are averaged for all experiments. Error bars are standard deviation of relative amplitudes of different experiments. Average normalized relative amplitude increases as the oscillation frequency increases up to 3-4 Hz and decreases sharply above a "resonance frequency" (black circles). The black line is the fit of model described in Eqn. 11. Comparison with the speed histogram (red bars) confirms that bacterium-surface hydrodynamic interactions is not the cause of the observed resonance. Use left axis for normalized relative speed amplitudes and right axis for speed histogram.

In order to eliminate the effects of different temperature amplitudes and cell-culture variability on rotational speed, we normalized the relative speed amplitudes of a single measurement set with the relative amplitude at the lowest frequency (0.2 Hz) in the same set, so that we could compare different experiments.

Our measurements show that the amplitude of the speed oscillations in response to temperature exhibits a peak around 3-4 Hz with a sharp decay above 4 Hz (Figure 4.8). It is

important to note here that the observed resonance peak is not due to the interaction of the cells with the glass surface. If for instance, the cell is tethered unevenly to the surface then it is expected to slow down at fixed points when it is rotating. Therefore surface interactions would cause the rotation speed to be modulated with the rotation rate which would make the resonance frequency the same as the rotation rate. To verify this is not the case, we compared the rotational speed histogram with the oscillation amplitudes (Figure 4.8 red bars). As evident there, the majority of the cells tested have a rotation rate different from the resonance peak frequency.

This result was also confirmed by calculating the power spectra of the rotational speed in response to the different frequencies. As can be seen in Figure 4.9 and Figure 4.10, the response is indeed maximal in the same frequency range observed before (3-4 Hz). This behavior is characteristic of forced damped harmonic oscillators, which exhibit resonance when driven at its natural frequency. Indeed, we were able to fit the response amplitude of the rotational speed to the function:

$$Amp(f) = \frac{A}{\sqrt{4\pi^2\left({f_o}^2 - f^2\right)^2 + 4f^2\beta^2}} + B \qquad \textbf{Eqn. 11}$$

This function describes the amplitude dependency of a damped-forced harmonic oscillator to the driving factor. Here, f is the temperature oscillation frequency and it is the independent variable, whereas A, B, f_o, and β are fitting parameters. A (59.001±15.2 Hz^2) is a constant to fit the model to the normalized data, B (0.49±0.09) is a constant to account for background amplitude fluctuations, f_o (4.01±0.21 Hz) is the natural oscillation frequency of the motor and β (8.30±1.37 Hz) is a parameter associated with damping.

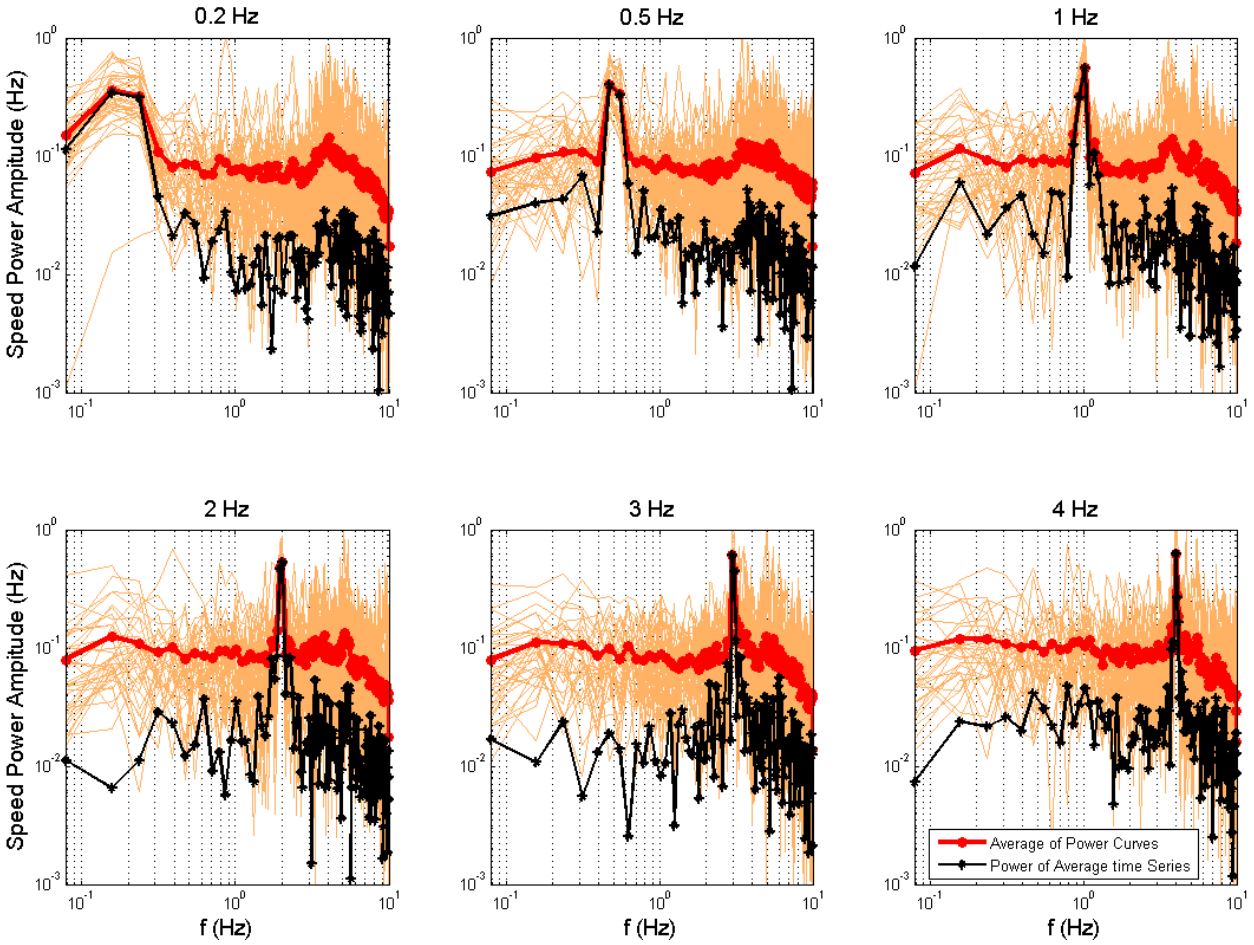

Figure 4.9: Power spectra of rotational speed of bacteria under oscillating temperature

Power spectral analysis of rotational speed of bacteria under oscillating temperature with amplitude of 6.5 ºC. The frequency of the temperature oscillation is shown on top of each graph. Thin orange lines represent the speed power spectra of individual bacteria. Thick red curves with circular markers are the average of all individual power spectra representing the average behavior. In order to eliminate the rotational speed oscillations which are not driven by the temperature oscillations, time series of rotational speed of bacteria are aligned by shifting them to get in phase with respect to the driving frequency and then averaged. The black curve represents the power spectra of the averaged time series of the speed of the bacteria which is aligned with the driving frequency. The resonance peak is evident in individual power spectra and average of all.

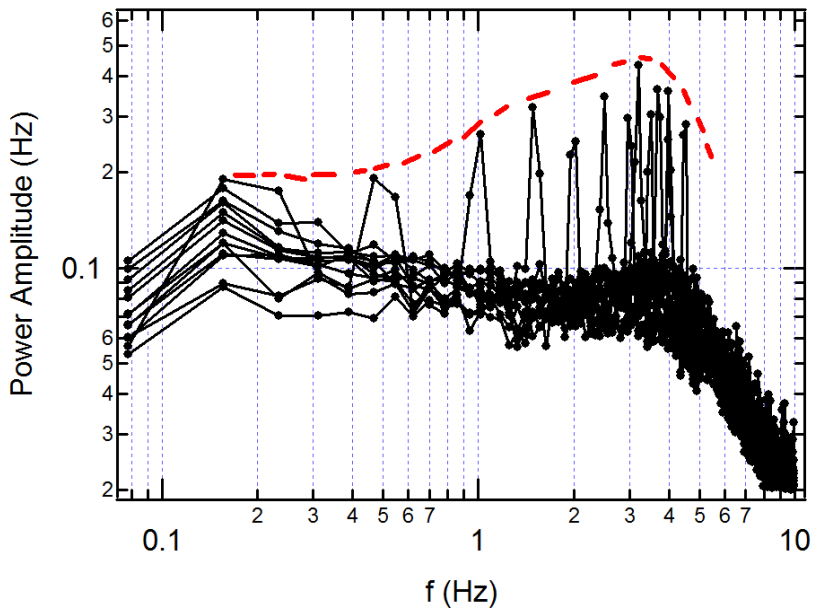

Figure 4.10: Power Spectra Amplitude of BFM rotational speed

Average of power spectra calculated from speed of bacteria as response to oscillating temperature with 1.3 ºC amplitude. Each curve represents average power spectrum of one frequency. The resonance peak around 3-4 Hz is evident in each spectrum and the driving oscillation corresponding to resonance frequencies are amplified. Dashed red line is hand drawn and guide for the reader.

To understand how such a behavior can be observed in the response of the motor's speed to thermal oscillations, let us remember that the bacterial flagellar motor is a complex machine assembled of many components that interact together in an orchestrated manner to result in the rotation observed. Due to the complexity of the motor, the interactions between the different components can exhibit various states, at each of which BFM can have a different rotational speed. Thermal fluctuations can lead to transitions between these states with distinct frequencies. Thus, a possible explanation to this behavior can be the internal kinetics of the BFM which is a result of the collective dynamics of all different parts that compose the motor. Driving the motor's rotation at frequency that corresponds to one of its natural modes will result in a resonant response like behavior as exhibited by our results. It is important to note here that

identifying these frequencies can help reveal the mechanism controlling them and the various states that the motor exhibits.

To further test this hypothesis, we have performed spectral analysis of long and fast recordings (900 frames/second) of bacterial rotational speed at steady state (Figure 4.11A). If indeed the resonant response of the rotational speed to thermal oscillations is due to natural modes of oscillations exhibited by the motor, then these oscillations should be observed in the power spectrum. The result of this analysis, presented in Figure 4.11B, shows that indeed the rotational speed of the flagellar motor exhibits oscillations at a wide range of frequencies. The data presented here was obtained from one bacterium. However, different bacteria exhibit slightly different frequencies, and while their frequency and amplitude can change slightly from cell to cell, their order of magnitude is about the same. The data presented in Figure 4.9 on the other hand is the average response of hundreds of bacteria, which can lead to eliminating oscillations that appear in individual cells and amplify only the ones that appear in most cells.

Similar oscillations to the ones observed here in the rotational speed were reported in the past by other groups as well. Kara-Ivanov et al. reported two ranges of oscillations, slow (0.15-1.2 Hz) and fast (1.7-25 Hz) (169). They speculated that the slow fluctuations might be due to the local mechanical oscillations and incomplete switching of the motor, whereas fast fluctuations they attributed to association-disassociation of torque generating units and fluctuations in the proton occupancy of the force generating units. However, the very fast oscillation (>100 Hz) that we observe here, they did not report, probably due to measurement limitation.

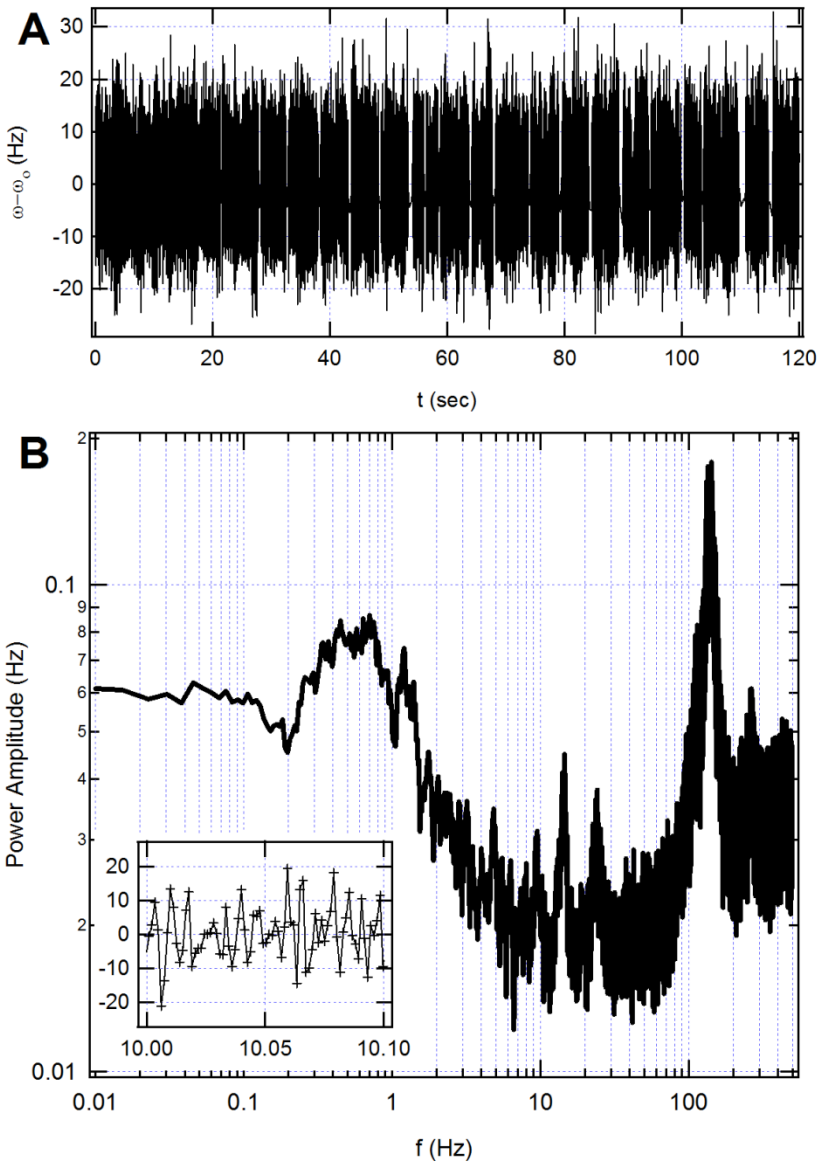

Figure 4.11: Speed oscillations of free rotating tethered bacteria

(A) The speed of free rotating tethered bacterium at room temperature captured at 900 fps. The average speed is subtracted from the data in order to calculate the amplitudes of the oscillations around the background speed using power spectral analysis which is represented in (B). BFM has natural oscillations occurring at low frequencies from 0.01 Hz up to hundreds of Hz. Inset: The magnified view of A between 10 and 10.1 seconds.

As a mechanical motor the BFM has a wide dynamical range that it can respond to environmental changes and driving factors. In addition, it can respond better to and amplify the effect of certain driving frequencies corresponding to its natural frequencies. These natural frequencies may arise due to motor's physical structure and the overall effect of the protein elasticity, coupling strength of torque generating units to rotor, duty ratio of stators, and MP and pH homeostasis capacity of the cell.

Despite the vast knowledge of its physical and biochemical properties, information about the origin of the noise in the rotational speed of the bacterial flagellar motor and the response of the motor to fast environmental changes that can influence its rotational speed is still lacking. Our results presented here, are the first to report resonance in the response of the motor's rotational speed to environmental fluctuations. These results also reveal the importance of understanding the internal kinetics of the motor for characterizing its response to environmental changes, and can be used as a first step for future studies aiming at understanding the nature of mechanical interactions within the motor.

5.0 SUMMARY AND CONCLUSIONS

Temperature is one of the most important factors that influence living organisms. All biochemical reactions are affected by temperature, and therefore, it is important for all living organisms to maintain a stable body temperature optimal for their survival. Multicellular organisms are generally able to regulate their body temperature, and thus are able to thrive in a wide range of temperatures. On the other hand, single-cell microorganisms whose body temperature is set by the environment strive to migrate towards regions where the temperature is optimal for their growth and metabolism. For that purpose, single-cell microorganisms, such as *E. coli* bacteria have developed sensory networks that allow them to sense and respond to thermal cues and direct their migration towards their favored environment. However, active response is not the only mechanism whereby bacteria can migrate in a temperature gradient.

We have shown here that in a shallow temperature gradient, where bacteria are not able to respond to changes in temperature along their run path through the known chemotaxis and thermotaxis signal-transduction pathway, they still exhibit a directed migration along the temperature gradient. This migration we find is due to the effect of temperature on the bacterial swimming speed. Since bacteria spend more time where their speed is lower they tend to accumulate in that region. Moreover, we find that the direction of bacterial migration is affected by the concentration of serine in the environment. Our results show that the bacterial swimming speed increases with the serine concentration following a sigmoidal function with constant

kinetic parameters, S_H and S_0 (Figure 3.5), and a temperature dependent minimum and maximum speeds, $v_{min}(T)$ and $v_{max}(T)$. The temperature dependent nature of $v_{min}(T)$ and $v_{max}(T)$, at high and low serine concentration respectively, is the reason for the change in the direction of bacterial migration. We also find that the difference observed between $v_{min}(T)$ and $v_{max}(T)$ is due to the increase in the bacteria's intracellular pH caused by serine at high temperature.

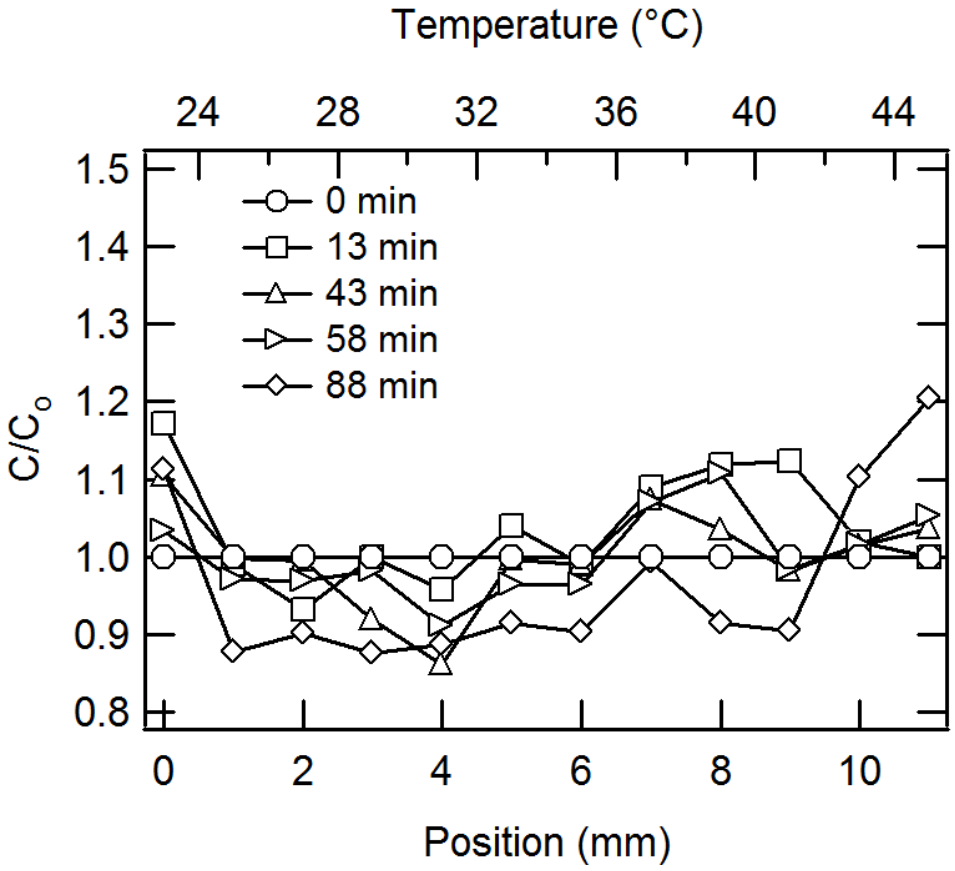

Figure 5.1: Behavior of UU2612 in MB + 600µM Serine under shallow temperature gradient

The concentration profiles of the mutant bacteria UU2612, whose receptors are deleted, in the motility buffer with 600µM serine measured at different times after applying the temperature gradient. See Materials and Methods (section 2.0) for measurement details.

A question that these results immediately raise is whether receptor-less bacteria respond similarly to such temperature gradients under the same chemical conditions. Since the bacteria's temperature sensing ability is negligible under shallow gradients there should not be a difference in terms of accumulation direction between WT bacteria and receptors deleted bacteria. As we stated previously, indeed the mutant strain bacteria UU2612 (136) lacking all chemoreceptors migrate towards high temperature in MB (Figure 3.2). However, when serine is added to the medium, we do not observe a similar migration towards low temperature (Figure 5.1). This could indicate that the observed migration towards low temperature is not a result of the speed dependence on temperature but rather due to direct sensing of the temperature gradient via the chemoreceptors. Yet, measuring the change in the intracellular pH of this mutant strain as a function of temperature and serine, reveal that the intracellular pH does not exhibit a similar behavior. Our results show that in the absence of the all chemoreceptors, the intracellular pH decreases with increasing temperature similarly with and without serine in the medium (Figure 5.2).

Tsr, alongside Tar and Aer, have been shown to respond to changes in the intracellular pH (170–172). However, this is the first observation that suggests that the chemoreceptors might be involved in regulating the intracellular pH, as well. The mechanism underlying the intracellular pH regulation and the role of the receptors in this process are still unclear. Nevertheless, this finding is very important as it suggests that the chemoreceptors could be involved in alternate signal transduction pathways different than the one already known.

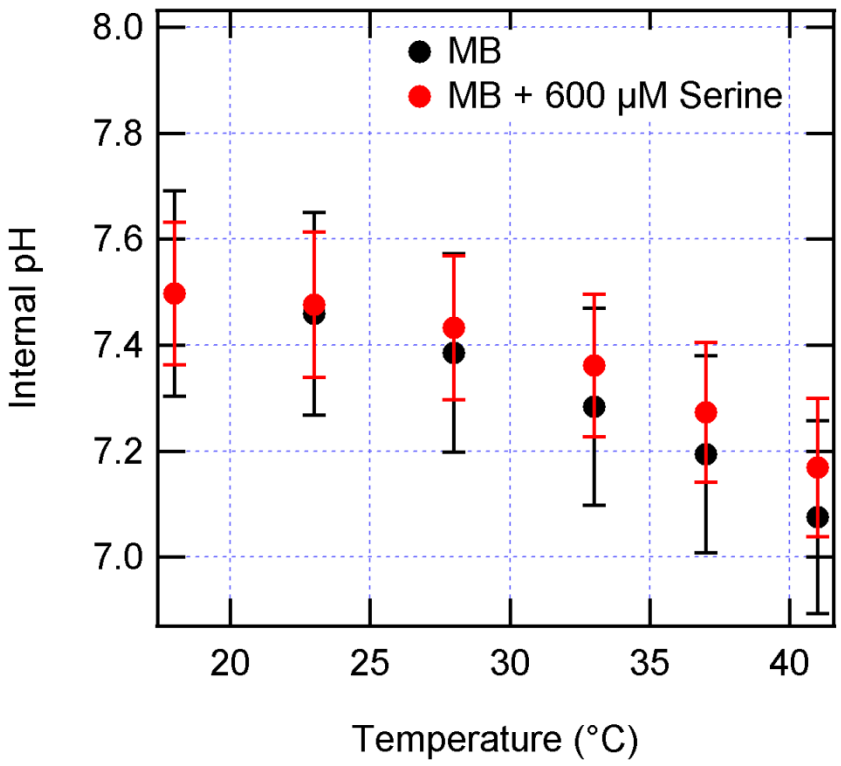

Figure 5.2: The effect of temperature on the internal pH of UU2612

The intracellular pH of all receptors deleted mutant (UU2612) as a function of temperature with and without 600µM serine. The pH in both cases is almost the same which decreases with increasing temperature.

In conclusion, our results show that there is more than one way for bacteria to sense temperature gradients (173). When the temperature gradient is not steep enough to be detected by the classical bacterial signal transduction pathway, the change in the speed (as a result of changes in the intracellular pH, which also seems to be regulated by the chemoreceptors) allows the bacteria to migrate in such environments. This improves the ability of bacteria to respond to thermal gradients.

In addition, we have studied the response of the BFM rotational speed to fast thermal changes. We found that under heavy load, the motor responds to linear thermal changes instantaneously and without any delay. Under heavy load, the change in rotational speed was

shown to be mainly due to changes in the medium's viscosity. Since this change is fast, the speed as well follows the temperature at the same rate. However, when subjected to thermal oscillations, we find that the speed's amplitude depends on the oscillation's frequency. The response of the motor exhibits resonance with the driving factors at frequencies in the range of ~3 – 4 Hz. This result is characteristic of driven damped oscillators, which indicates that the motor has natural oscillations that can be amplified through external driving forces. This was also supported by the spectral analysis of the motor's rotational speed, which reveals that indeed the BFM has several natural frequencies. These frequencies can be due to the complex interactions among the different components forming the motor, which can have different states and corresponding rotational speed.

APPENDIX A

TEMPERATURE APPARATUS DRAWINGS

In this appendix I provide the design details of the apparatuses used for applying shallow and sharp temperature gradients respectively.

A.1 LINEAR SHALLOW GRADIENT APPARATUS

Table 5.1. Linear temperature gradient parts list

Part Name	Material	Quantity	Note
Heat Sink Base	Aluminum	1	Machined
Heat Sink Lid	Aluminum	1	Machined
Plastic Insulation Layer	Plexiglas	1	Machined
Peltier Device	-	2	Custom Thermoelectric
Copper Plate	Copper	2	Machined
Microscope Glass Slide	Glass	1	Fisher Scientific, 25x75x1 mm
Plastic Base	Plexiglas	1	Machined

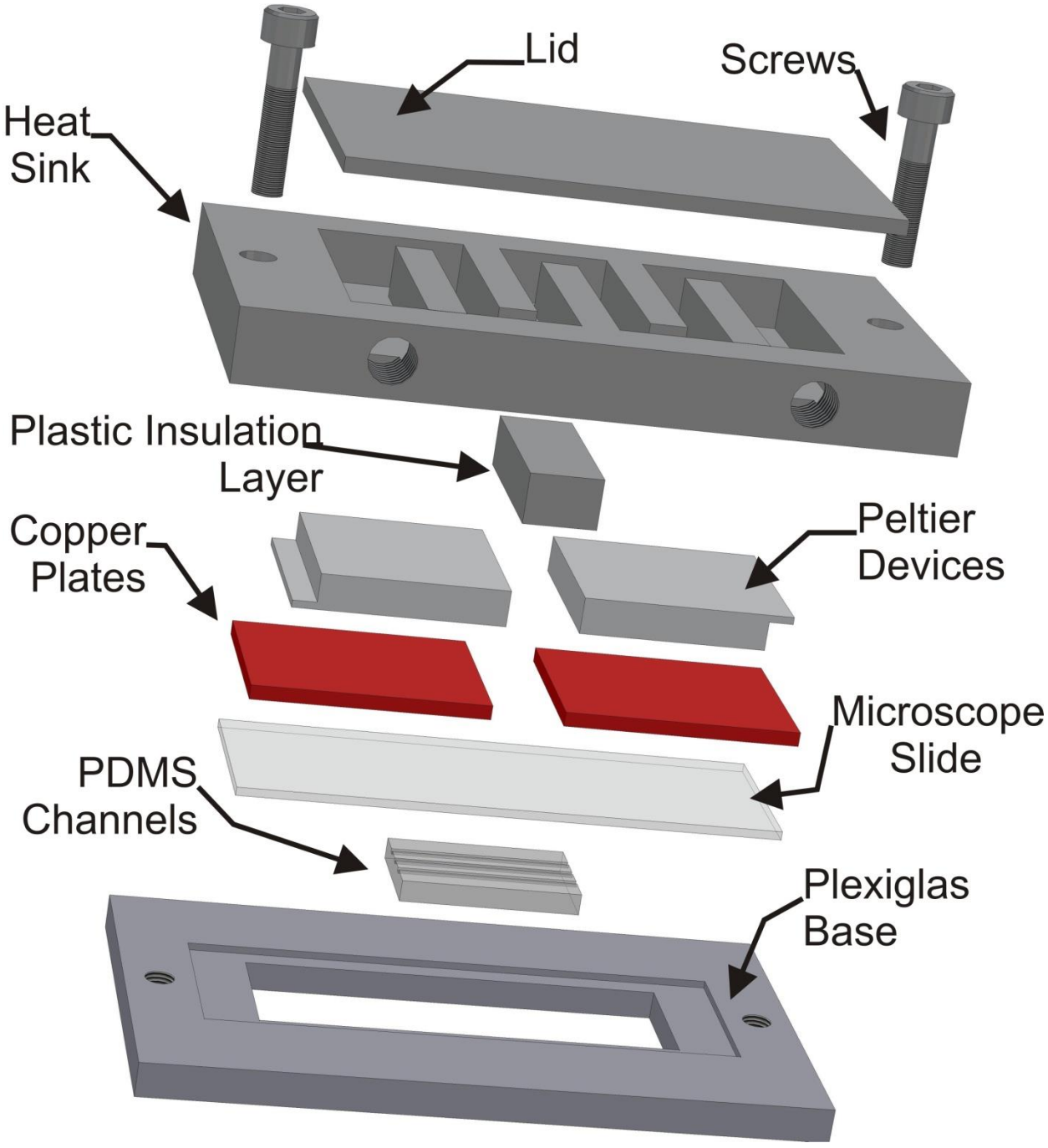

Figure A.1: Linear temperature gradient apparatus - exploded view

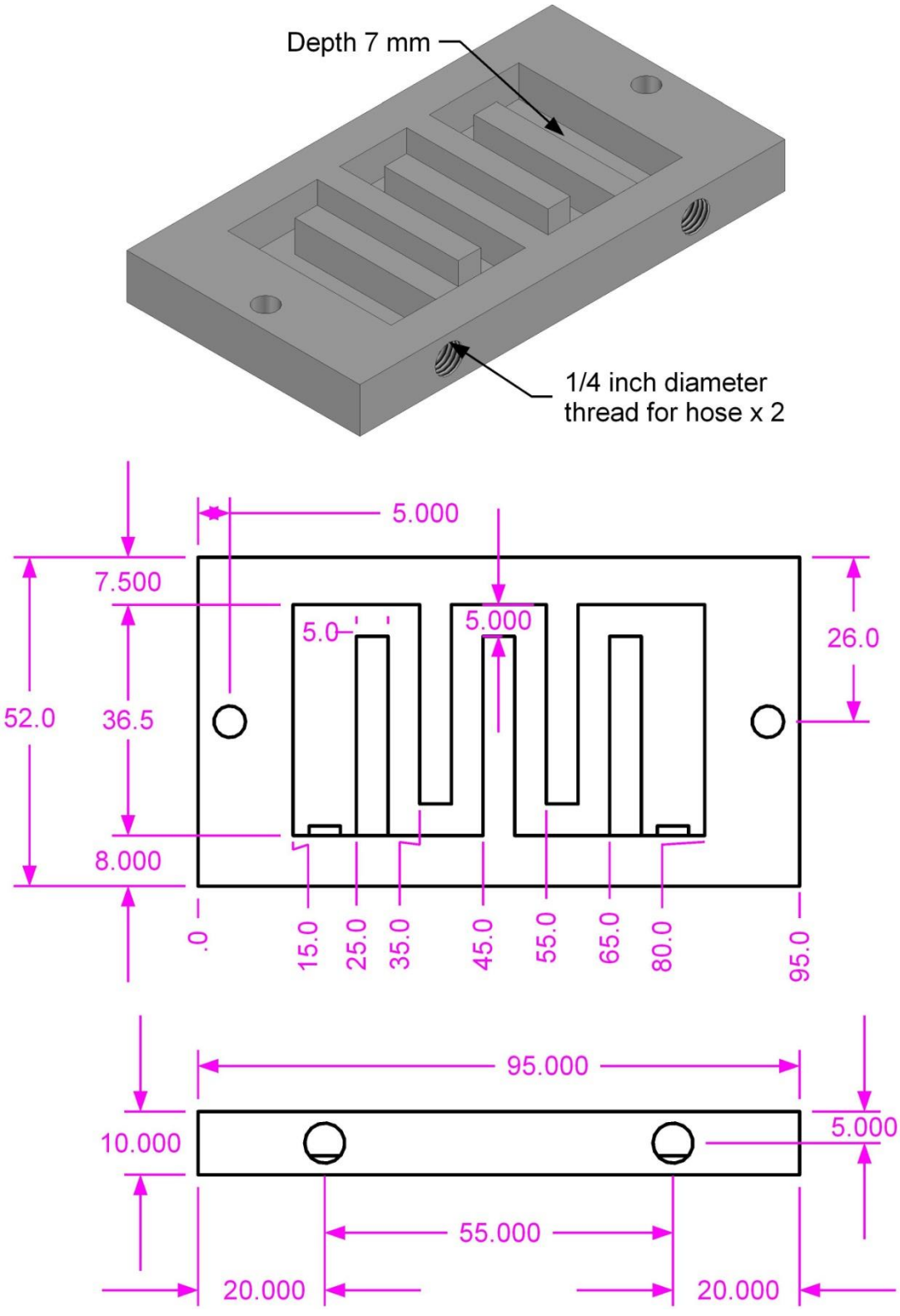

Figure A.2: Linear temperature gradient apparatus - heat sink base

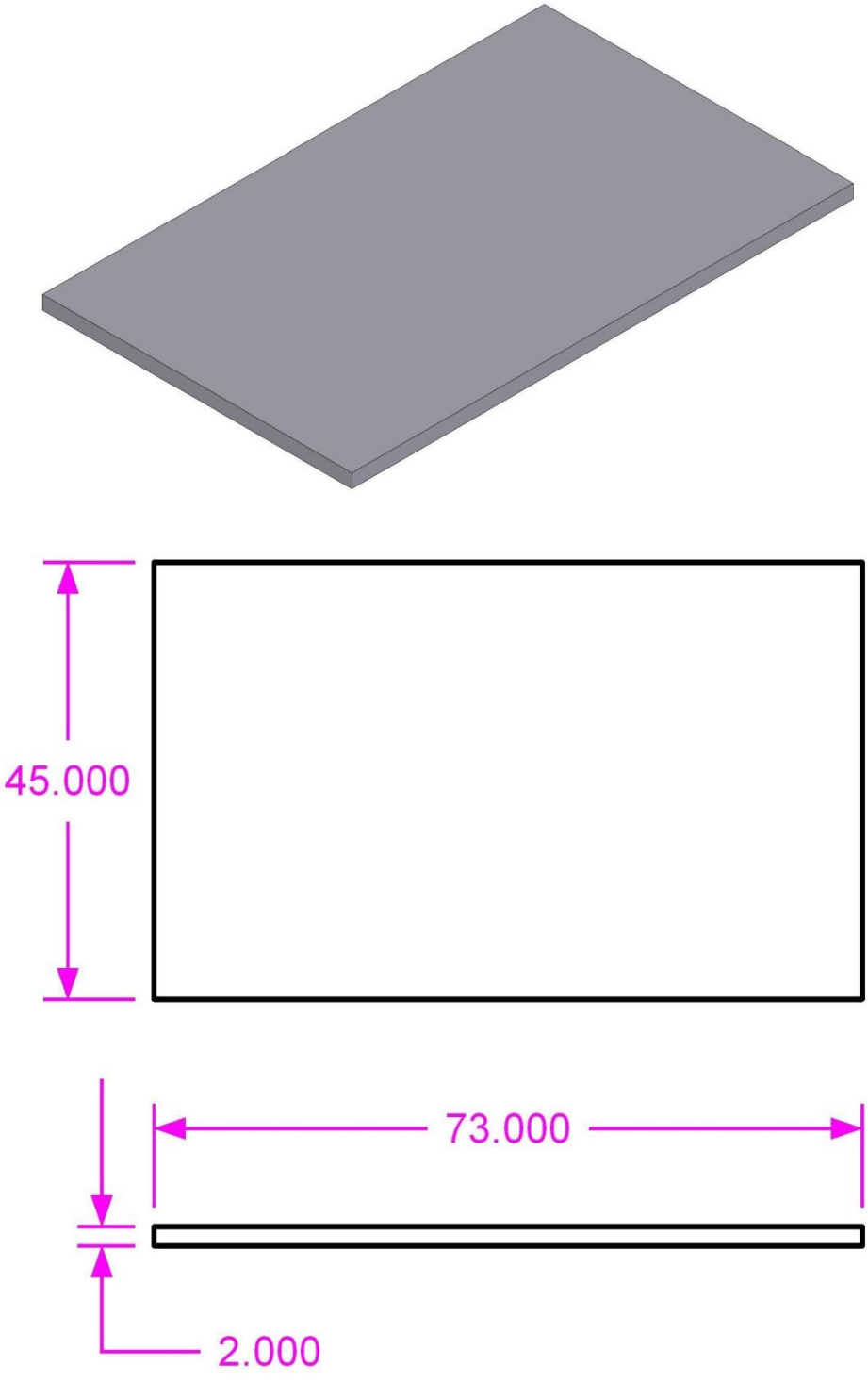

Figure A.3: Linear temperature gradient apparatus - heat sink lid

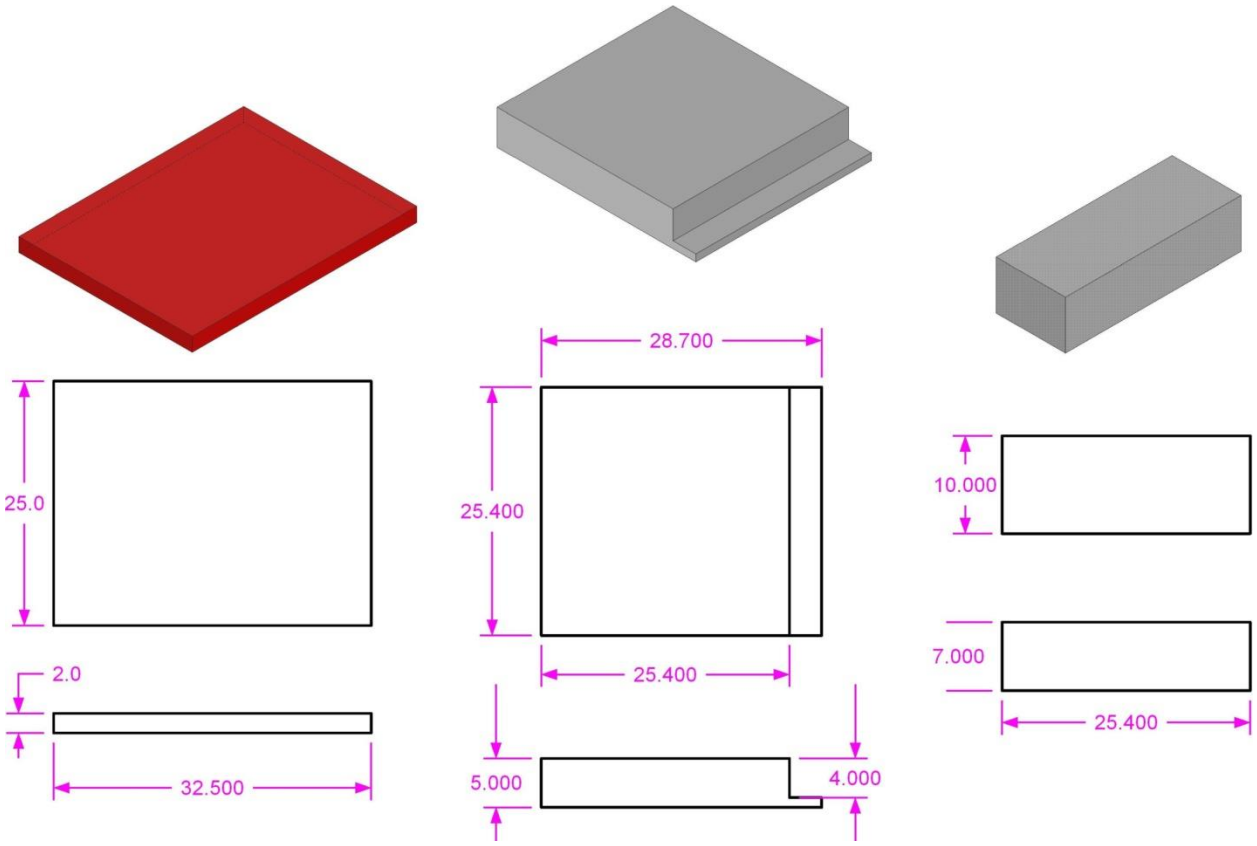

Figure A.4: Linear temperature gradient apparatus - copper plates, peltiers, and plastic insulation layer

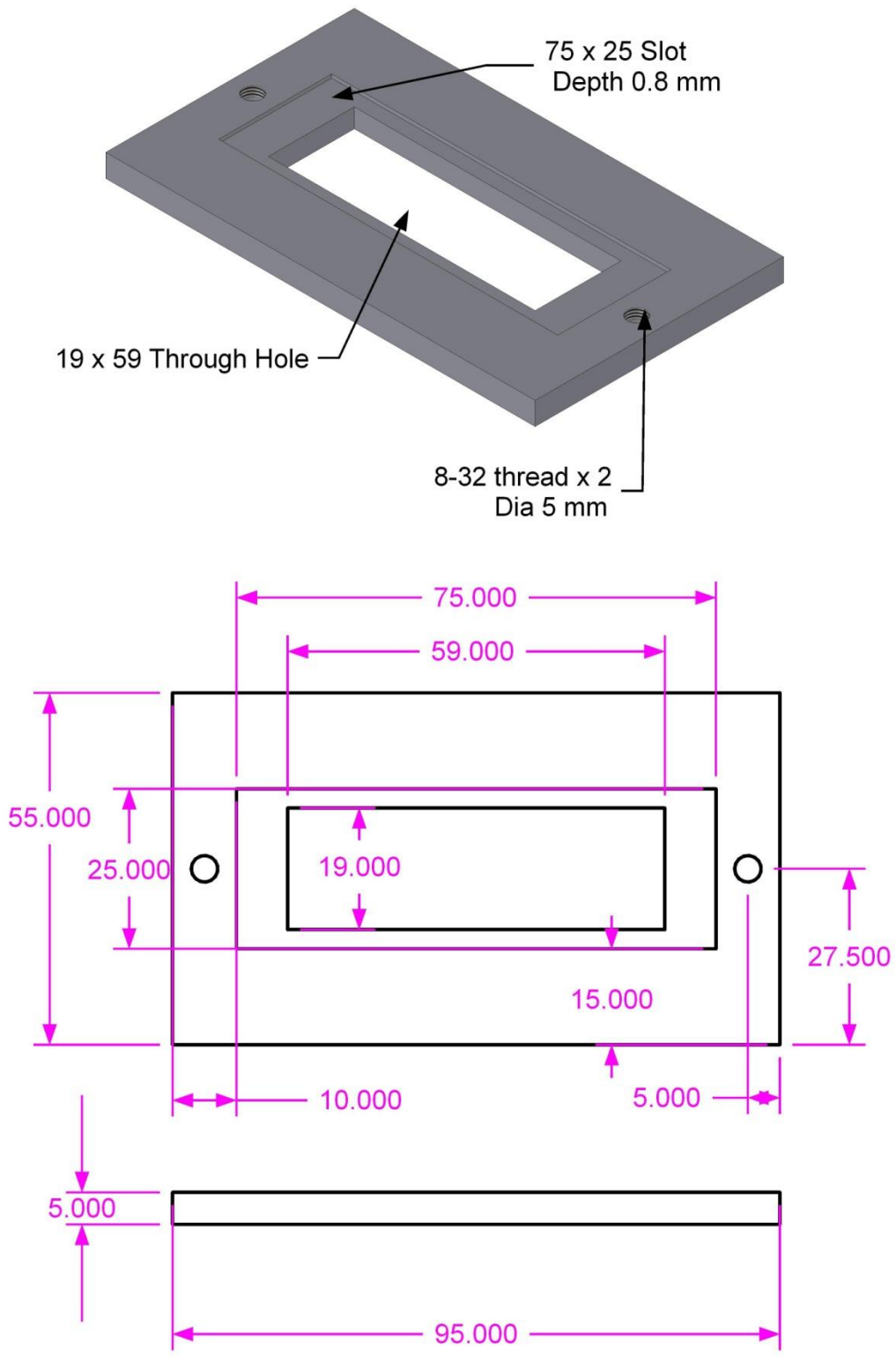

Figure A.5: Temperature gradient apparatuses - plastic base plate

A.2 SHARP TEMPERATURE GRADIENT APPARATUS

Table 5.2. Sharp temperature gradient parts list

Part Name	Material	Quantity	Note
Heat Sink	Aluminum	2	Machined
Peltier Device	-	2	Custom Thermoelectric
Copper Plate	Copper	1	Machined
Microscope Glass Slide	Glass	1	Fisher Scientific, 25x75x1 mm
Plastic Base	Plexiglas	1	Machined

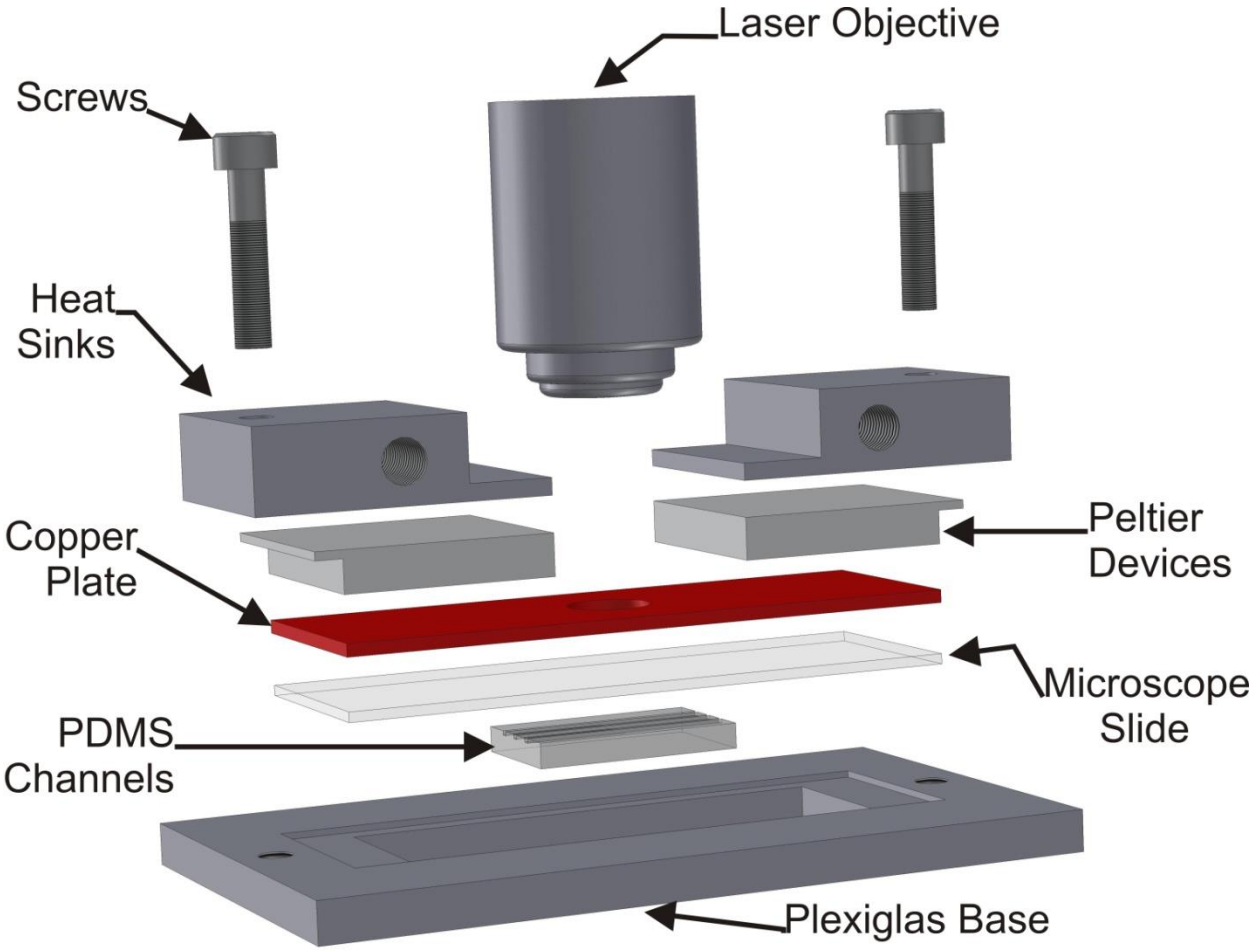

Figure A.6: Sharp temperature gradient apparatus - exploded view

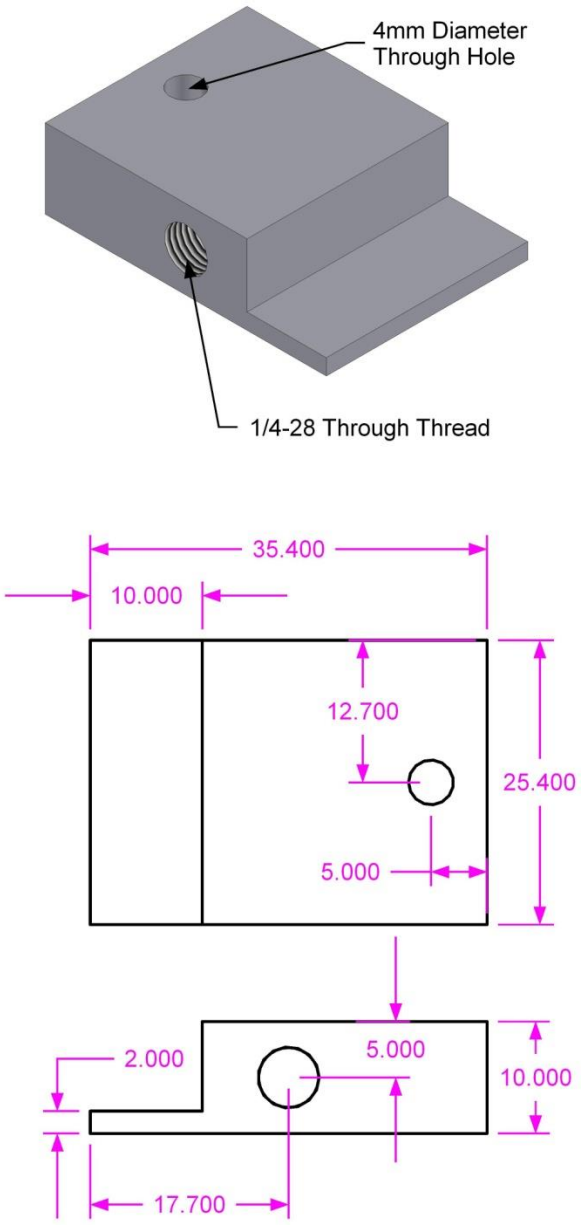

Figure A.7: Sharp temperature gradient apparatus - heat sink

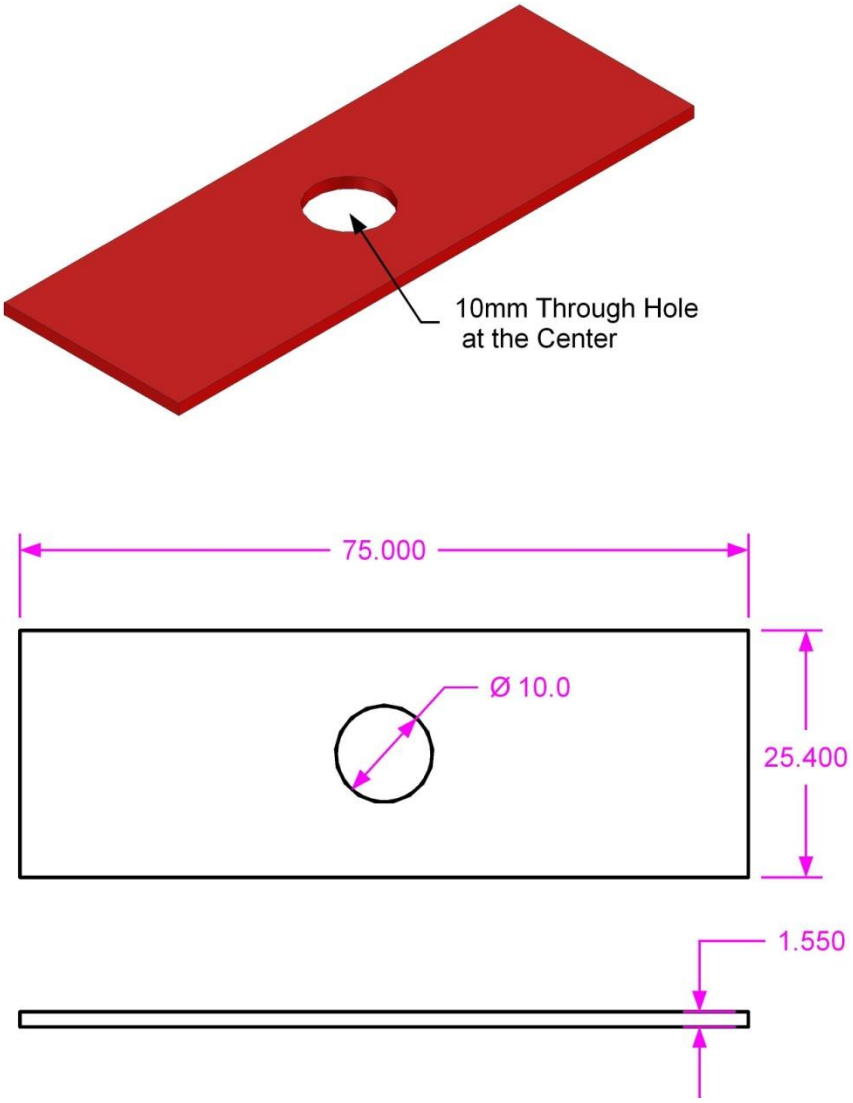

Figure A.8: Sharp temperature gradient apparatus - copper plate

APPENDIX B

STOCHASTIC SIMULATIONS OF THE BACTERIAL BEHAVIOR IN SHALLOW LINEAR TEMPERATURE GRADIENT

The MATLAB (The Mathworks, Natick, MA) code used to simulate the behavior of WT bacteria in shallow temperature gradients is provided below with detailed explanations.

B.1 MAIN CODE

```
% if there is no comment next to the line the one below it is the
% explanation
% MB stands for Motility Buffer and Ser stands for MB + 600 µM Serine
clear;          % clears all the data on the workspace
close all;      % closes all open graphs
clc;            % clears the command window
T = 3;          % (Hour) total time for calculation
N= 3000;        % number of bacteria in the channels
L = 10;         % (mm) the length of the channels
b = .8;         % (mm) the width of the channels
aspectvec = [4 1 1];    % plot box aspect ratio
xmb = L.*rand(N,1);
% (mm) (MB) the vector containing x coordinate of each bacterium.
% Randomly distributed
ymb = b*rand(N,1);
% (mm) (MB) the vector containing y coordinate of each bacterium.
% Randomly distributed
thetamb = 360*rand(N,1);
% (degree) (MB) the vector containing angle value of each bacterium.
% Randomly distributed
xser = L.*rand(N,1);
```

```
% (mm) (Ser) the vector containing x coordinate of each bacterium.
% Randomly distributed
yser = b*rand(N,1);
% (mm) (Ser) the vector containing y coordinate of each bacterium.
% Randomly distributed
thetaser = 360*rand(N,1);
% degree) (Ser) the vector containing angle value of each bacterium.
% Randomly distributed

% initially all bacteria are running
tstep = .1;          % time step (sec)
NT=T*3600/tstep;     % number of calculation steps
xedges=[0:.5:L];     % bin locations for histogram
t= 0;                % initiate the simulation time
rtibacmb = zeros(N,1);
% the vector containing run durations of each bacterium. Memory pre-allocated
rtibacser = zeros(N,1);
% the vector containing run durations of each bacterium. Memory pre-allocated
t2rec = 1*60*1/tstep;          % set recording time steps (min*60*sec/tstep)
datasize = fix(NT/t2rec);      % calculate data recording size for memory
% allocation
xoutmb = zeros(N,datasize);    % (MB) initiate the data matrix for recording x
% coordinates
youtmb = zeros(N,datasize);    % (MB) initiate the data matrix for recording y
% coordinates
tvec = zeros(1,datasize);      % initiate time vector for recording
xoutmb(:,1) = xmb;       % (MB) write the initial x coordinates for time 0
youtmb(:,1) = ymb;       % (MB) write the initial y coordinates for time 0
tvec(1) = 0;             % write time 0
xoutser = zeros(N,datasize);    % (Ser) initiate the data matrix for recording
% x coordinates
youtser = zeros(N,datasize);    % (Ser) initiate the data matrix for recording
% y coordinates
xoutser(:,1) = xser;     % (Ser) write the initial x coordinates for time 0
youtser(:,1) = yser;     % (Ser) write the initial y coordinates for time 0
ind1 = 1;   % initiate recording index

% Now initialize initial running parameters
Tempmb = pos2temp10mmTiTf(xmb,22,43);
% (°C)(MB) calculates the temperatures at each location of the bacteria
Speedmb = Speed_MB(Tempmb)./1000;
% (µm/sec)(MB) calculates the speed values of each bacterium
% (convert to mm/sec)
t2tumblemb = temp2tc_MB(Tempmb);
% (sec)(MB) calculates the run durations of each bacterium
Tempser = pos2temp10mmTiTf(xser,22,43);
% (°C)(Ser) calculates the temperatures at each location of the bacteria
Speedser = Speed_Ser_600(Tempser)./1000;
% (µm/sec)(Ser) calculates the speed values of each bacterium
% (convert to mm/sec)
t2tumbleser = temp2tc_MB(Tempser);
% (sec)(Ser) calculates the run durations of each bacterium

% set lognormal turn angle parameters
mang = 62;      %mean turn angle is 62 degrees
varang = 26;
%variance of the turn angle distribution is 26 degrees, from Berg Nature 1972
```

```
mu = log(mang^2/sqrt(varang+mang^2));   %lognormal parameter
sigma = sqrt(log(varang/mang^2+1));     %lognormal parameter
figure;          % open a graph window
pause(1)         % pause 1 sec to make it full screen manually

for n=1:NT
      rtibacmb = rtibacmb + tstep;
      % (MB) increase the timer of each bacterium by time step
      rtibacser = rtibacser + tstep;
      % (Ser) increase the timer of each bacterium by time step
      for i = 1:N
            % do calculations for MB
            if rtibacmb(i) <= t2tumblemb(i)              % "run" mode
                  % update x and y coordianets
                  xmb(i) = xmb(i) + Speedmb(i)*tstep*cosd(thetamb(i));
                  ymb(i) = ymb(i) + Speedmb(i)*tstep*sind(thetamb(i));
                  % check boundaries and return exiting bacterium
                  if ymb(i) < 0,
                        ymb(i) = abs(ymb(i));
                        thetamb(i) = thetamb(i) + 180;
                  elseif ymb(i) > b,
                        ymb(i) = 2*b - ymb(i);
                        thetamb(i) = thetamb(i) + 180;
                  end
                  if xmb(i) < 0,
                        xmb(i) = abs(xmb(i));
                        thetamb(i) = thetamb(i) + 180;
                  elseif xmb(i) > L,
                        xmb(i) = 2*L - xmb(i);
                        thetamb(i) = thetamb(i) + 180;
                  end
            else              % "tumble" mode
      thetamb(i) = thetamb(i) + getdirbac(randi(2,1,1))*lognrnd(mu,sigma);
      % select another direction
            Tempmb(i) = pos2temp10mmTiTf(xmb(i),22,43);
            % determine the temperature at the new location
            t2tumblemb(i) = poissrnd(tumbf*temp2tc_MB(Tempmb(i)));
            % calculate the run duration for the bacterium, draw from random
            % Poisson ditribution
            rtibacmb(i) = 0;           % reset the timer for the bacterium
            vm = Speed_MB(Tempmb(i));  % calculate the mean speed at that
            % temperature
            mus = log(vm)-0.832^2/2;
            % calculate the mu with sigma = .832 (obtained from experimental
            % data lognormal fit)
            Speedmb(i) = lognrnd(mus,0.832)/1000;
            % calculates the speed value of the bacterium (convert to mm/sec)
            end
            % do the calculations for Serine
            if rtibacser(i) <= t2tumbleser(i)             % "run" mode
            % update x and y coordianets
            xser(i) = xser(i) + Speedser(i)*tstep*cosd(thetaser(i));
            yser(i) = yser(i) + Speedser(i)*tstep*sind(thetaser(i));
            % check boundaries and return exiting bacterium
            if yser(i) < 0,
                  yser(i) = abs(yser(i));
                  thetaser(i) = thetaser(i) + 180;
```

```
      elseif yser(i) > b,
            yser(i) = 2*b - yser(i);
            thetaser(i) = thetaser(i) + 180;
      end
      if xser(i) < 0,
            xser(i) = abs(xser(i));
            thetaser(i) = thetaser(i) + 180;
      elseif xser(i) > L,
            xser(i) = 2*L - xser(i);
            thetaser(i) = thetaser(i) + 180;
      end
      else    % "tumble" mode
 thetaser(i) = thetaser(i) + getdirbac(randi(2,1,1))*lognrnd(mu,sigma);
 % select another direction
      Tempser(i) = pos2temp10mmTiTf(xser(i),22,43);
      % determine the temperature at the new location
      t2tumbleser(i) = poissrnd(tumbf*temp2tc_MB(Tempser(i)));
      % calculate the run duration for the bacterium, draw from random
      % Poisson distribution
      rtibacser(i) = 0;       % reset the timer for the bacterium
      vm = Speed_Ser_600(Tempser(i));     % calculate the mean speed at
      % that temperature
      mus = log(vm)-0.832^2/2;
      % calculate the mu with sigma = .832 (obtained from experimental
      % data lognormal fit)
      Speedser(i) = lognrnd(mus,0.832)/1000;
      % assign the new speed (convert to mm/sec)
      end
end
t = t + tstep;              % update the global timer by time step
numxmb=histc(xmb,xedges);       % estimate the histogram for MB
numxser=histc(xser,xedges);     % estimate the histogram for Ser
if 0    % change to 1 in order to view bacterial motion at each step
      subplot(2,2,1)  % (MB) plot location of bacteria in the channels
      plot(pos2temp10mmTiTf(xmb,22,43),ymb,'k.')
      xlabel('T(C)')
      ylabel('y(mm)')
      title('Motility Buffer')
      axis([22 43 0 b])
      pbaspect(aspectvec)
      subplot(2,2,3)  % (MB) plot the total number of bacteria at each
      % half mm
      bar(xedges,numxmb,'histc')
      xlabel('x(mm)')
      ylabel('number/bin')
      title(t2str(t)) % display time as title
      axis([0 L 0 300])
      subplot(2,2,2)  % (Ser) plot location of bacteria in the channels
      plot(pos2temp10mmTiTf(xser,22,43),yser,'k.')
      xlabel('T(C)')
      ylabel('y(mm)')
      title('MB + 600uM Ser')
      axis([22 43 0 b])
      pbaspect(aspectvec)
      subplot(2,2,4)  % (Ser) plot the total number of bacteria at each
      %half mm
      bar(xedges,numxser,'histc')
```

```
      xlabel('x(mm)')
      ylabel('number/bin')
      title(t2str(t))
      axis([0 L 0 300])
      pause(.0001)        % wait 0.1 ms to let graph refresh
end
% do the data and image recordings at defined times by t2rec
if rem(n,t2rec)==1       %min*60*sec*10
      ind1 = ind1 + 1;
      xoutmb(:,ind1) = xmb;   % (MB) record x coordinates
      youtmb(:,ind1) = ymb;   % (MB) record y coordinates
      xoutser(:,ind1) = xser; % (Ser) record x coordinates
      youtser(:,ind1) = yser; % (Ser) record y coordinates
      tvec(ind1) = t; % record time point
      %generate the current plot in order save it as an image
      subplot(2,2,1)
      plot(pos2temp10mmTiTf(xmb,22,43),ymb,'k.')
      xlabel('T(C)')
      ylabel('y(mm)')
      title('Motility Buffer')
      axis([22 43 0 b])
      pbaspect(aspectvec)
      subplot(2,2,3)
      bar(xedges,numxmb,'histc')
      xlabel('x(mm)')
      ylabel('number/bin')
      title(t2str(t))
      axis([0 L 0 300])
      subplot(2,2,2)
      plot(pos2temp10mmTiTf(xser,22,43),yser,'k.')
      xlabel('T(C)')
      ylabel('y(mm)')
      title('MB + 600uM Ser')
      axis([22 43 0 b])
      pbaspect(aspectvec)
      subplot(2,2,4)
      bar(xedges,numxser,'histc')
      xlabel('x(mm)')
      ylabel('number/bin')
      title(t2str(t))
      axis([0 L 0 300])
      name = strcat('Sim_WT_030713_poissontc_3k_62degree_lognv',…
      num2str (int64(t/60)),'.jpeg');
      % generate the image name
      saveas(gcf,name)    % save the image
      pause(.3)
      close all       % close all the active graphs
      pause(.2)
      data_out = vertcat(tvec,xoutmb,youtmb,xoutser,youtser);
      % combine time and coordinate data (x,y) for MB and Serine
      fname = 'Sim_WT_030713_poissontc_3k_62degree_lognv.txt';
      % define the file name for data recording
      csvwrite(fname,data_out)
      % save the data as a text file
      save('Sim_WT_030713_poissontc_3k_62degree_lognv.mat');
      % save the data in matlab format
end
```

```
end
```

B.2 FUNCTIONS

```
function T = pos2temp10mmTiTf(x,Tmin,Tmax)
% function pos2temp10mmTiTf(x,Tmin,Tmax)
%     calculates the temperature value at the position x in the linear
%     gradient where the linear gradient in the channel starts at Tmin(C)
%     and ends at Tmax(C).
%     The Length of the channel is 10 mm. x can be a point or a vector.
[m,n] = size(x);            % determine the size of the input vector
T = zeros(m,n);          % allocate memory for the output and initiate to zero
c_fac = (Tmax -Tmin)./10;   % calculate the gradient steepness
      % estimate the Temperature
for i = 1:m
    for j = 1:n
        T(i,j) = (x(i,j)).*c_fac+Tmin;
    end
end

function Speed = Speed_MB(T)
% Speed(µm/sec) = Speed_MB(T(°C))
%     calculates the speed of the bacteria which is swimming at a location
%     having temperature T. Values are generated for Motility buffer.
%     The quadratic curve used to generate speed is obtained from
%     experimental values
Speed = -51.732 + 5.1931 * T -.08788 * T.^2;

function Speed = Speed_Ser_600(T)
% Speed(µm/sec)  = Speed_Ser_600(T(°C))
%     calculates the speed of the bacteria which is swimming at a location
%     having temperature T. Values are generated for Motility buffer + 600 µM
%     Serine. The linear curve used to generate speed is obtained from
%     experimental values
Speed = .6848 + .88837 .* T ;

function tc = temp2tc_MB(Temp)
% tc(sec) = temp2tc_MB(Temp(°C))
%     calculates the characteristic time tc, run duration, from the
%     temperature of the bacteria. The exponential curve used to generate
%     values is obtained from experiments
tc = .68329 + 600.78 .* exp(-Temp*.29912);

function bdirec = getdirbac(int)
%function bdirec = getdirbac(int)
%     function bdirec = getdirbac(int)
%     This function generates direction for bacteria such that if int is 1
%     than direction is to the right : bdirec = 1, whereas if int is 2 than
```

```
%     direction is to the left : bdriec = -1
if int ==1
    bdirec = 1;
elseif int==2
    bdirec = -1;
else
    bdirec = 0;
end
```

BIBLIOGRAPHY

1. Griffiths, R.B. 1969. Nonanalytic Behavior Above the Critical Point in a Random Ising Ferromagnet. Physical Review Letters. 23: 17–19.

2. Ziegler, P.A. 1992. Plate tectonics, plate moving mechanisms and rifting. Tectonophysics. 215: 9–34.

3. McKenzie, D.P. 1969. Speculations on the Consequences and Causes of Plate Motions. Geophysical Journal International. 18: 1–32.

4. Bickle, M.J. 1978. Heat loss from the earth: A constraint on Archaean tectonics from the relation between geothermal gradients and the rate of plate production. Earth and Planetary Science Letters. 40: 301–315.

5. Tackley, P.J. 2000. Mantle Convection and Plate Tectonics: Toward an Integrated Physical and Chemical Theory. Science. 288: 2002–2007.

6. Ratkowsky, D.A., J. Olley, T.A. McMeekin, and A. Ball. 1982. Relationship between temperature and growth rate of bacterial cultures. J. Bacteriol. 149: 1–5.

7. Craig Heller, H., G.W. Colliver, and J. Beard. 1977. Thermoregulation during entrance into hibernation. Pflugers Archiv European Journal of Physiology. 369: 55–59.

8. Van Breukelen, F., and S.L. Martin. 2001. Translational initiation is uncoupled from elongation at 18{degrees}C during mammalian hibernation. Am J Physiol Regulatory Integrative Comp Physiol. 281: R1374–1379.

9. Berthold, P. 1996. Control of bird migration. London: Chapman & Hall.

10. Rosenzweig, M., K.M. Brennan, T.D. Tayler, P.O. Phelps, A. Patapoutian, et al. 2005. The Drosophila ortholog of vertebrate TRPA1 regulates thermotaxis. Genes & development. 19: 419–24.

11. Mori, I., and Y. Ohshima. 1995. Neural regulation of thermotaxis in Caenorhabditis elegans. Nature. 376: 344–8.

12. Kessler, J.O., L.F. Jarvik, T.K. Fu, and S.S. Matsuyama. 1979. Thermotaxis, chemotaxis and age. AGE. 2: 5–11.

13. Bahat, A., and M. Eisenbach. 2006. Sperm thermotaxis. Molecular and cellular endocrinology. 252: 115–9.

14. Maeda, K., Y. Imae, J.I. Shioi, and F. Oosawa. 1976. Effect of temperature on motility and chemotaxis of Escherichia coli. Journal of bacteriology. 127: 1039–46.

15. Salman, H., A. Zilman, C. Loverdo, M. Jeffroy, and A. Libchaber. 2006. Solitary Modes of Bacterial Culture in a Temperature Gradient. Physical Review Letters. 97: 118101.

16. Shulman, S.T., H.C. Friedmann, and R.H. Sims. 2007. Theodor Escherich: the first pediatric infectious diseases physician? Clinical infectious diseases : an official publication of the Infectious Diseases Society of America. 45: 1025–9.

17. Ishihara, A., J.E. Segall, S.M. Block, and H.C. Berg. 1983. Coordination of flagella on filamentous cells of Escherichia coli. J. Bacteriol. 155: 228–237.

18. Berg, H.C., and R.A. Anderson. 1973. Bacteria Swim by Rotating their Flagellar Filaments. Nature. 245: 380–382.

19. Silverman, M., and M. Simon. 1974. Flagellar rotation and the mechanism of bacterial motility. Nature. 249: 73–74.

20. Purcell, E.M. 1997. The efficiency of propulsion by a rotating flagellum. Proceedings of the National Academy of Sciences. 94: 11307–11311.

21. Turner, L., W.S. Ryu, and H.C. Berg. 2000. Real-Time Imaging of Fluorescent Flagellar Filaments. Journal of Bacteriology. 182: 2793–2801.

22. Berg, H.C. 2003. E. coli in motion. 2004th ed. New York: Springer.

23. Berg, H.C., and D.A. Brown. 1972. Chemotaxis in Escherichia coli analyzed by Three-dimensional Tracking. Nature. 239: 500–504.

24. Clarke, S., and D.E. Koshland. 1979. Membrane receptors for aspartate and serine in bacterial chemotaxis. J. Biol. Chem. 254: 9695–9702.

25. Wolff, C., and J.S. Parkinson. 1988. Aspartate taxis mutants of the Escherichia coli tar chemoreceptor. J. Bacteriol. 170: 4509–4515.

26. Manson, M.D., V. Blank, G. Brade, and C.F. Higgins. 1986. Peptide chemotaxis in E. coli involves the Tap signal transducer and the dipeptide permease. Nature. 321: 253–6.

27. Bollinger, J. 1984. Structure of the Trg Protein: Homologies with and Differences from Other Sensory Transducers of Escherichia coli. Proceedings of the National Academy of Sciences. 81: 3287–3291.

28. Bibikov, S.I., R. Biran, K.E. Rudd, and J.S. Parkinson. 1997. A signal transducer for aerotaxis in Escherichia coli. Journal of bacteriology. 179: 4075–9.

29. Grebe, T.W., and J. Stock. 1998. Bacterial chemotaxis: The five sensors of a bacterium. Current Biology. 8: R154–R157.

30. Li, M., and G.L. Hazelbauer. 2004. Cellular stoichiometry of the components of the chemotaxis signaling complex. Journal of bacteriology. 186: 3687–94.

31. Maddock, J.R., and L. Shapiro. 1993. Polar location of the chemoreceptor complex in the Escherichia coli cell. Science. 259: 1717–1723.

32. Sourjik, V., and H.C. Berg. 2000. Localization of components of the chemotaxis machinery of Escherichia coli using fluorescent protein fusions. Molecular Microbiology. 37: 740–751.

33. Shiomi, D., I.B. Zhulin, M. Homma, and I. Kawagishi. 2002. Dual recognition of the bacterial chemoreceptor by chemotaxis-specific domains of the CheR methyltransferase. The Journal of biological chemistry. 277: 42325–33.

34. Cantwell, B.J., R.R. Draheim, R.B. Weart, C. Nguyen, R.C. Stewart, et al. 2003. CheZ Phosphatase Localizes to Chemoreceptor Patches via CheA-Short. Journal of Bacteriology. 185: 2354–2361.

35. Banno, S., D. Shiomi, M. Homma, and I. Kawagishi. 2004. Targeting of the chemotaxis methylesterase/deamidase CheB to the polar receptor-kinase cluster in an Escherichia coli cell. Molecular microbiology. 53: 1051–63.

36. Gegner, J.A., D.R. Graham, A.F. Roth, and F.W. Dahlquist. 1992. Assembly of an MCP receptor, CheW, and kinase CheA complex in the bacterial chemotaxis signal transduction pathway. Cell. 70: 975–982.

37. Boukhvalova, M.S., F.W. Dahlquist, and R.C. Stewart. 2002. CheW binding interactions with CheA and Tar. Importance for chemotaxis signaling in Escherichia coli. The Journal of biological chemistry. 277: 22251–9.

38. Bourret, R.B., J. Davagnino, and M.I. Simon. 1993. The carboxy-terminal portion of the CheA kinase mediates regulation of autophosphorylation by transducer and CheW. J. Bacteriol. 175: 2097–2101.

39. Tawa, P., and R.C. Stewart. 1994. Kinetics of CheA Autophosphorylation and Dephosphorylation Reactions. Biochemistry. 33: 7917–7924.

40. Li, J., R. V. Swanson, M.I. Simon, and R.M. Weis. 1995. Response Regulators CheB and CheY Exhibit Competitive Binding to the Kinase CheA. Biochemistry. 34: 14626–14636.

41. Shukla, D. 1998. Flagellar Motor-switch Binding Face of CheY and the Biochemical Basis of Suppression by CheY Mutants That Compensate for Motor-switch Defects in Escherichia coli. Journal of Biological Chemistry. 273: 23993–23999.

42. Kuo, S.C., and D.E. Koshland. 1987. Roles of cheY and cheZ gene products in controlling flagellar rotation in bacterial chemotaxis of Escherichia coli. J. Bacteriol. 169: 1307–1314.

43. McEvoy, M.M., A. Bren, M. Eisenbach, and F.W. Dahlquist. 1999. Identification of the binding interfaces on CheY for two of its targets, the phosphatase CheZ and the flagellar switch protein fliM. Journal of molecular biology. 289: 1423–33.

44. Sourjik, V. 2004. Receptor clustering and signal processing in E. coli chemotaxis. Trends in microbiology. 12: 569–76.

45. Levin, M.D., T.S. Shimizu, and D. Bray. 2002. Binding and diffusion of CheR molecules within a cluster of membrane receptors. Biophysical journal. 82: 1809–17.

46. Djordjevic, S., and A.M. Stock. 1998. Chemotaxis receptor recognition by protein methyltransferase CheR. Nature Structural Biology. 5: 446–450.

47. Hayashi, H., O. Koiwai, and M. Kozuka. 1979. Studies on Bacterial Chemotaxis: II. Effect of cheB and cheZ Mutations on the Methylation of Methyl-Accepting Ghemotaxis Protein of Escherichia coli. J. Biochem. 85: 1213–1223.

48. Kehry, M.R. 1983. Enzymatic Deamidation of Methyl-Accepting Chemotaxis Proteins in Escherichia coli Catalyzed by the cheB Gene Product. Proceedings of the National Academy of Sciences. 80: 3599–3603.

49. Ottemann, K.M. 1999. A Piston Model for Transmembrane Signaling of the Aspartate Receptor. Science. 285: 1751–1754.

50. Berg, H.C., and E.M. Purcell. 1977. Physics of chemoreception. Biophysical journal. 20: 193–219.

51. Maeda, K., and Y. Imae. 1979. Thermosensory transduction in Escherichia coli: inhibition of the thermoresponse by L-serine. Proceedings of the National Academy of Sciences of the United States of America. 76: 91–5.

52. Nishiyama, S., S. Ohno, N. Ohta, Y. Inoue, H. Fukuoka, et al. 2010. Thermosensing Function of the Escherichia coli Redox Sensor Aer. Journal of bacteriology. 192: 1740–1743.

53. Mizuno, T., and Y. Imae. 1984. Conditional inversion of the thermoresponse in Escherichia coli. Journal of bacteriology. 159: 360–7.

54. Lee, L., T. Mizuno, and Y. Imae. 1988. Thermosensing properties of Escherichia coli tsr mutants defective in serine chemoreception. Journal of Bacteriology. 170: 4769–74.

55. Nara, T., L. Lee, and Y. Imae. 1991. Thermosensing ability of Trg and Tap chemoreceptors in Escherichia coli. Journal of Bacteriology. 173: 1120–4.

56. Nara, T., I. Kawagishi, S. Nishiyama, M. Homma, and Y. Imae. 1996. Modulation of the thermosensing profile of the Escherichia coli aspartate receptor tar by covalent modification of its methyl-accepting sites. The Journal of biological chemistry. 271: 17932–6.

57. Nishiyama, S., T. Nara, M. Homma, Y. Imae, and I. Kawagishi. 1997. Thermosensing properties of mutant aspartate chemoreceptors with methyl-accepting sites replaced singly or multiply by alanine. Journal of bacteriology. 179: 6573–80.

58. Nishiyama, S.I., T. Umemura, T. Nara, M. Homma, and I. Kawagishi. 1999. Conversion of a bacterial warm sensor to a cold sensor by methylation of a single residue in the presence of an attractant. Molecular microbiology. 32: 357–65.

59. Nishiyama, S., I.N. Maruyama, M. Homma, and I. Kawagishi. 1999. Inversion of thermosensing property of the bacterial receptor Tar by mutations in the second transmembrane region. Journal of molecular biology. 286: 1275–84.

60. Paster, E., and W.S. Ryu. 2008. The thermal impulse response of Escherichia coli. Proceedings of the National Academy of Sciences of the United States of America. 105: 5373–7.

61. Salman, H., and A. Libchaber. 2007. A concentration-dependent switch in the bacterial response to temperature. Nature cell biology. 9: 1098–100.

62. Sowa, Y., and R.M. Berry. 2008. Bacterial flagellar motor. Quarterly Reviews of Biophysics. 41: 103–132.

63. DePamphilis, M.L., and J. Adler. 1971. Attachment of Flagellar Basal Bodies to the Cell Envelope: Specific Attachment to the Outer, Lipopolysaccharide Membrane and the Cytoplasmic Membrane. J. Bacteriol. 105: 396–407.

64. Namba, K., and F. Vonderviszt. 1997. Molecular architecture of bacterial flagellum. Quarterly Reviews of Biophysics. 30: 1–65.

65. Berry, R.M., and J.P. Armitage. 1999. The bacterial flagella motor. Advances in microbial physiology. 41: 291–337.

66. Berg, H.C. 2003. The rotary motor of bacterial flagella. Annual review of biochemistry. 72: 19–54.

67. Kojima, S., and D.F. Blair. 2004. The bacterial flagellar motor: structure and function of a complex molecular machine. International review of cytology. 233: 93–134.

68. Asakura, S. 1970. Polymerization of flagellin and polymorphism of flagella. Advances in biophysics. 1: 99–155.

69. Calladine, C.R. 1975. Construction of bacterial flagella. Nature. 255: 121–124.

70. Hasegawa, K., I. Yamashita, and K. Namba. 1998. Quasi- and nonequivalence in the structure of bacterial flagellar filament. Biophysical journal. 74: 569–75.

71. Francis, N.R., G.E. Sosinsky, D. Thomas, and D.J. DeRosier. 1994. Isolation, characterization and structure of bacterial flagellar motors containing the switch complex. Journal of molecular biology. 235: 1261–70.

72. Thomas, D.R., D.G. Morgan, and D.J. DeRosier. 1999. Rotational symmetry of the C ring and a mechanism for the flagellar rotary motor. Proceedings of the National Academy of Sciences of the United States of America. 96: 10134–9.

73. Thomas, D.R., N.R. Francis, C. Xu, and D.J. DeRosier. 2006. The three-dimensional structure of the flagellar rotor from a clockwise-locked mutant of Salmonella enterica serovar Typhimurium. Journal of bacteriology. 188: 7039–48.

74. Aizawa, S.-I. 1996. Flagellar assembly in Salmonella typhimurium. Molecular Microbiology. 19: 1–5.

75. Macnab, R.M. 2003. How bacteria assemble flagella. Annual review of microbiology. 57: 77–100.

76. Ueno, T., K. Oosawa, and S.-I. Aizawa. 1992. M ring, S ring and proximal rod of the flagellar basal body of Salmonella typhimurium are composed of subunits of a single protein, FliF. Journal of Molecular Biology. 227: 672–677.

77. Ueno, T., K. Oosawa, and S.-I. Aizawa. 1994. Domain Structures of the MS Ring Component Protein (FliF) of the Flagellar Basal Body of Salmonella typhimurium. Journal of Molecular Biology. 236: 546–555.

78. Suzuki, H., K. Yonekura, and K. Namba. 2004. Structure of the rotor of the bacterial flagellar motor revealed by electron cryomicroscopy and single-particle image analysis. Journal of molecular biology. 337: 105–13.

79. Khan, S., I.H. Khan, and T.S. Reese. 1991. New structural features of the flagellar base in Salmonella typhimurium revealed by rapid-freeze electron microscopy. J. Bacteriol. 173: 2888–2896.

80. Katayama, E., T. Shiraishi, K. Oosawa, N. Baba, and S.-I. Aizawa. 1996. Geometry of the Flagellar Motor in the Cytoplasmic Membrane ofSalmonella typhimuriumas Determined by Stereo-photogrammetry of Quick-freeze Deep-etch Replica Images. Journal of Molecular Biology. 255: 458–475.

81. Minamino, T., and K. Namba. 2004. Self-Assembly and Type III Protein Export of the Bacterial Flagellum. Journal of Molecular Microbiology and Biotechnology. 7: 5–17.

82. Asai, Y., S. Kojima, H. Kato, N. Nishioka, I. Kawagishi, et al. 1997. Putative channel components for the fast-rotating sodium-driven flagellar motor of a marine bacterium. J. Bacteriol. 179: 5104–5110.

83. Blair, D.F., and H.C. Berg. 1990. The MotA protein of E. coli is a proton-conducting component of the flagellar motor. Cell. 60: 439–449.

84. Mot, R., and J. Vanderleyden. 1994. The C-terminal sequence conservation between OmpA-related outer membrane proteins and MotB suggests a common function in both Gram-positive and Gram-negative bacteria, possibly in the interaction of these domains with peptidoglycan. Molecular Microbiology. 12: 333–334.

85. Sato, K. 2000. Functional Reconstitution of the Na+-driven Polar Flagellar Motor Component of Vibrio alginolyticus. Journal of Biological Chemistry. 275: 5718–5722.

86. Garza, A.G. 1995. Motility Protein Interactions in the Bacterial Flagellar Motor. Proceedings of the National Academy of Sciences. 92: 1970–1974.

87. Lloyd, S., H. Tang, X. Wang, S. Billings, and D. Blair. 1996. Torque generation in the flagellar motor of Escherichia coli: evidence of a direct role for FliG but not for FliM or FliN. J. Bacteriol. 178: 223–231.

88. Zhou, J., S.A. Lloyd, and D.F. Blair. 1998. Electrostatic interactions between rotor and stator in the bacterial flagellar motor. Proceedings of the National Academy of Sciences. 95: 6436–6441.

89. Zhou, J., and D.F. Blair. 1997. Residues of the cytoplasmic domain of MotA essential for torque generation in the bacterial flagellar motor. Journal of molecular biology. 273: 428–39.

90. Leake, M.C., J.H. Chandler, G.H. Wadhams, F. Bai, R.M. Berry, et al. 2006. Stoichiometry and turnover in single, functioning membrane protein complexes. Nature. 443: 355–8.

91. Berry, R.M., and H.C. Berg. 1997. Absence of a barrier to backwards rotation of the bacterial flagellar motor demonstrated with optical tweezers. Proceedings of the National Academy of Sciences of the United States of America. 94: 14433–7.

92. Lowe, G., M. Meister, and H.C. Berg. 1987. Rapid Rotation of flagellar bundles in swimming bacteria. Nature. 325: 637–640.

93. Chen, X., and H.C. Berg. 2000. Solvent-isotope and pH effects on flagellar rotation in Escherichia coli. Biophysical journal. 78: 2280–4.

94. Ryu, W.S., R.M. Berry, and H.C. Berg. 2000. Torque-generating units of the flagellar motor of Escherichia coli have a high duty ratio. Nature. 403: 444–7.

95. Sowa, Y., H. Hotta, M. Homma, and A. Ishijima. 2003. Torque–speed Relationship of the Na+-driven Flagellar Motor of Vibrio alginolyticus. Journal of Molecular Biology. 327: 1043–1051.

96. Sowa, Y., A.D. Rowe, M.C. Leake, T. Yakushi, M. Homma, et al. 2005. Direct observation of steps in rotation of the bacterial flagellar motor. Nature. 437: 916–9.

97. Lo, C.-J., M.C. Leake, and R.M. Berry. 2006. Fluorescence measurement of intracellular sodium concentration in single Escherichia coli cells. Biophysical journal. 90: 357–65.

98. Lo, C.-J., M.C. Leake, T. Pilizota, and R.M. Berry. 2007. Nonequivalence of membrane voltage and ion-gradient as driving forces for the bacterial flagellar motor at low load. Biophysical journal. 93: 294–302.

99. Reid, S.W., M.C. Leake, J.H. Chandler, C.-J. Lo, J.P. Armitage, et al. 2006. The maximum number of torque-generating units in the flagellar motor of Escherichia coli is at least 11. Proceedings of the National Academy of Sciences of the United States of America. 103: 8066–71.

100. Darnton, N.C., L. Turner, S. Rojevsky, and H.C. Berg. 2007. On torque and tumbling in swimming Escherichia coli. Journal of bacteriology. 189: 1756–64.

101. White, D. 1995. The Physiology and Biochemistry of Prokaryotes. 1st ed. New York: Oxford University Press.

102. Nichols, D., and S. Ferguson. 1992. Bioenergetics 2. 2nd ed. San Diego: Academic Press.

103. Asai, Y., T. Yakushi, I. Kawagishi, and M. Homma. 2003. Ion-coupling Determinants of Na+-driven and H+-driven Flagellar Motors. Journal of Molecular Biology. 327: 453–463.

104. Gabel, C. V, and H.C. Berg. 2003. The speed of the flagellar rotary motor of Escherichia coli varies linearly with protonmotive force. Proceedings of the National Academy of Sciences of the United States of America. 100: 8748–51.

105. Purcell, E.M. 1977. Life at low Reynolds number. American Journal of Physics. 45: 3–11.

106. Chen, X., and H.C. Berg. 2000. Torque-speed relationship of the flagellar rotary motor of Escherichia coli. Biophysical journal. 78: 1036–41.

107. Berg, H.C., and L. Turner. 1993. Torque Generated by the Flagellar Motor of Escherichia coil. Biophysical journal. 65: 2201–2216.

108. Charati, S.G., and S.A. Stern. 1998. Diffusion of Gases in Silicone Polymers: Molecular Dynamics Simulations. Macromolecules. 31: 5529–5535.

109. Leclerc, E., Y. Sakai, and T. Fujii. 2003. Cell Culture in 3-Dimensional Microfluidic Structure of PDMS (polydimethylsiloxane). Biomedical Microdevices. 5: 109–114.

110. Chang, W.-J., D. Akin, M. Sedlak, M.R. Ladisch, and R. Bashir. 2003. Poly(dimethylsiloxane) (PDMS) and Silicon Hybrid Biochip for Bacterial Culture. Biomedical Microdevices. 5: 281–290.

111. Demir, M., C. Douarche, A. Yoney, A. Libchaber, and H. Salman. 2011. Effects of population density and chemical environment on the behavior of Escherichia coli in shallow temperature gradients. Physical Biology. 8: 063001.

112. Sbalzarini, I.F., and P. Koumoutsakos. 2005. Feature point tracking and trajectory analysis for video imaging in cell biology. Journal of Structural Biology. 151: 182–95.

113. Douarche, C., A. Buguin, H. Salman, and A. Libchaber. 2009. E. Coli and Oxygen: A Motility Transition. Physical Review Letters. 102: 198101.

114. Wilks, J.C., and J.L. Slonczewski. 2007. pH of the cytoplasm and periplasm of Escherichia coli: rapid measurement by green fluorescent protein fluorimetry. Journal of Bacteriology. 189: 5601–7.

115. Udenfriend, S., S. Stein, P. Bohlen, W. Dairman, W. Leimgruber, et al. 1972. Fluorescamine: A Reagent for Assay of Amino Acids, Peptides, Proteins, and Primary Amines in the Picomole Range. Science. 178: 871–872.

116. Stein, S., P. Böhlen, J. Stone, W. Dairman, and S. Udenfriend. 1973. Amino acid analysis with fluorescamine at the picomole level. Archives of Biochemistry and Biophysics. 155: 203–212.

117. Kralj, J.M., D.R. Hochbaum, A.D. Douglass, and A.E. Cohen. 2011. Electrical Spiking in Escherichia coli Probed with a Fluorescent Voltage-Indicating Protein. Science. 333: 345–348.

118. Breeuwer, P., and T. Abee. 2004. Assessment of the membrane potential , intracellular pH and respiration of bacteria employing fluorescence techniques. Molecular Microbial Ecology Manual. 8.01: 1563–1579.

119. Toll, L., and B.D. Howard. 1978. Role of Mg2+-ATPase and a pH gradient in the storage of catecholamines in synaptic vesicles. Biochemistry. 17: 2517–23.

120. Jiao, N., Y. Yang, and T. Luo. 2004. Membrane potential based characterization by flow cytometry of physiological states in an aerobic anoxygenic phototrophic bacterium. Aquatic Microbial Ecology. 37: 149–158.

121. Novo, D., N.G. Perlmutter, R.H. Hunt, and H.M. Shapiro. 1999. Accurate flow cytometric membrane potential measurement in bacteria using diethyloxacarbocyanine and a ratiometric technique. Cytometry. 35: 55–63.

122. Shapiro, H.M. 1994. Cell membrane Potential Analysis. Methods in Cell Biology. 41: 121–133.

123. Endres, R.G., O. Oleksiuk, C.H. Hansen, Y. Meir, V. Sourjik, et al. 2008. Variable sizes of Escherichia coli chemoreceptor signaling teams. Molecular Systems Biology. 4: 211.

124. Hedblom, M.L., and J. Adler. 1983. Chemotactic response of Escherichia coli to chemically synthesized Amino Acids. Journal of Bacteriology. 155: 1463–1466.

125. Baker, M.D., P.M. Wolanin, and J.B. Stock. 2006. Signal transduction in bacterial chemotaxis. BioEssays : news and reviews in molecular, cellular and developmental biology. 28: 9–22.

126. Sourjik, V., and H.C. Berg. 2002. Receptor sensitivity in bacterial chemotaxis. Proceedings of the National Academy of Sciences of the United States of America. 99: 123–7.

127. Kentner, D., and V. Sourjik. 2009. Dynamic map of protein interactions in the Escherichia coli chemotaxis pathway. Molecular systems biology. 5: 238.

128. Alexandre, G., and I.B. Zhulin. 2001. More Than One Way To Sense Chemicals. Journal of Bacteriology. 183: 4681–4686.

129. Alon, U., M.G. Surette, N. Barkai, and S. Leibler. 1999. Robustness in bacterial chemotaxis. Nature. 397: 168–71.

130. Imae, Y., T. Mizuno, and K. Maeda. 1984. Chemosensory and thermosensory excitation in adaptation-deficient mutants of Escherichia coli. Journal of bacteriology. 159: 368–74.

131. Jiang, L., Q. Ouyang, and Y. Tu. 2009. A mechanism for precision-sensing via a gradient-sensing pathway: a model of Escherichia coli thermotaxis. Biophysical journal. 97: 74–82.

132. Spudich, J.L., and D.E. Koshland. 1975. Quantitation of the sensory response in bacterial chemotaxis. Proceedings of the National Academy of Sciences of the United States of America. 72: 710–3.

133. Macnab, R.M., and D.E. Koshland. 1972. The gradient-sensing mechanism in bacterial chemotaxis. Proceedings of the National Academy of Sciences of the United States of America. 69: 2509–12.

134. Khan, S., S. Jain, G.P. Reid, and D.R. Trentham. 2004. The fast tumble signal in bacterial chemotaxis. Biophysical journal. 86: 4049–58.

135. Endres, R.G., and N.S. Wingreen. 2006. Precise adaptation in bacterial chemotaxis through "assistance neighborhoods". Proceedings of the National Academy of Sciences of the United States of America. 103: 13040–4.

136. Parkinson, J.S. 1978. Complementation analysis and deletion mapping of Escherichia coli mutants defective in chemotaxis. Journal of Bacteriology. 135: 45–53.

137. Size, I.W., F.F. Nord, and C.H. Werkman. 2006. Effects of Temperature on Enzyme Kinetics. In: Nord FF, C. Werkman, editors. Advances in Enzymology and Related Areas of Molecular Biology. Hoboken, NJ, USA: John Wiley & Sons, Inc.

138. Somero, G.N. 1978. Temperature Adaptation of Enzymes: Biological Optimization Through Structure-Function Compromises. Annual Review of Ecology and Systematics. 9: 1–29.

139. Boon, M.., A.E.. Janssen, and K. van 't Riet. 2000. Effect of temperature and enzyme origin on the enzymatic synthesis of oligosaccharides. Enzyme and Microbial Technology. 26: 271–281.

140. Haight, R.D., and R.Y. Morita. 1962. Interaction between the parameters of hydrostatic pressure and temperature on aspartase of Escherichia coli. J. Bacteriol. 83: 112–120.

141. Sinensky, M. 1974. Homeoviscous Adaptation-A Homeostatic Process that Regulates the Viscosity of Membrane Lipids in Escherichia coli. Proceedings of the National Academy of Sciences. 71: 522–525.

142. Lemaux, P.G., S.L. Herendeen, P.L. Bloch, and F.C. Neidhardt. 1978. Transient rates of synthesis of individual polypeptides in E. coli following temperature shifts. Cell. 13: 427–434.

143. Magnuson, K., S. Jackowski, C.O. Rock, and J.E. Cronan. 1993. Regulation of fatty acid biosynthesis in Escherichia coli. Microbiol. Mol. Biol. Rev. 57: 522–542.

144. Gillooly, J.F., J.H. Brown, G.B. West, V.M. Savage, and E.L. Charnov. 2001. Effects of size and temperature on metabolic rate. Science (New York, N.Y.). 293: 2248–51.

145. Drew, H.R., and A.A. Travers. 1984. DNA structural variations in the E. coli tyrT promoter. Cell. 37: 491–502.

146. Roe, J.-H., R.R. Burgess, and M.T. Record. 1985. Temperature dependence of the rate constants of the Escherichia coli RNA polymerase-λPR promoter interaction. Journal of Molecular Biology. 184: 441–453.

147. Pelham, H. 1988. Heat-shock proteins. Coming in from the cold. Nature. 332: 776–7.

148. Lohman, T.M., and M.E. Ferrari. 1994. Escherichia coli single-stranded DNA-binding protein: multiple DNA-binding modes and cooperativities. Annual review of biochemistry. 63: 527–70.

149. Zavodszky, P. 1998. Adjustment of conformational flexibility is a key event in the thermal adaptation of proteins. Proceedings of the National Academy of Sciences. 95: 7406–7411.

150. Revzin, A., and P.H. Von Hippel. 1977. Direct measurement of association constants for the binding of Escherichia coli lac repressor to non-operator DNA. Biochemistry. 16: 4769–4776.

151. Snider, M.J., S. Gaunitz, C. Ridgway, S.A. Short, and R. Wolfenden. 2000. Temperature Effects on the Catalytic Efficiency, Rate Enhancement, and Transition State Affinity of Cytidine Deaminase, and the Thermodynamic Consequences for Catalysis of Removing a Substrate "Anchor."Biochemistry. 39: 9746–9753.

152. Whelan, J.A., P.R. Dunbar, D.A. Price, M.A. Purbhoo, F. Lechner, et al. 1999. Specificity of CTL Interactions with Peptide-MHC Class I Tetrameric Complexes Is Temperature Dependent. J. Immunol. 163: 4342–4348.

153. Bett, K.E., and J.B. Cappi. 1965. Effect of Pressure on the Viscosity of Water. Nature. 207: 620–621.

154. Korson, L., W. Drost-hansen, and F.J. Millero. 1968. Viscosity of Water at Various Temperatures. The Journal of Physical Chemistry. 73: 34–39.

155. Yancey, P.H., and G.N. Somero. 1978. Temperature dependence of intracellular pH: Its role in the conservation of pyruvate apparentK m values of vertebrate lactate dehydrogenases. Journal of Comparative Physiology B. 125: 129–134.

156. Franck, P. 1996. Measurement of intracellular pH in cultured cells by flow cytometry with BCECF-AM. Journal of Biotechnology. 46: 187–195.

157. Glagolev, A.N., and V.P. Skulachev. 1978. The proton pump is a molecular engine of motile bacteria. Nature. 272: 280–282.

158. Manson, M.D., P.M. Tedesco, and H.C. Berg. 1980. Energetics of flagellar rotation in bacteria. Journal of Molecular Biology. 138: 541–561.

159. Ravid, S., and M. Eisenbach. 1984. Minimal requirements for rotation of bacterial flagella. J. Bacteriol. 158: 1208–1210.

160. Schnitzer, M.J., S.M. Block, H.C. Berg, and E.M. Purcell. 1990. Strategies for chemotaxis. Symposium of the Society for General Microbiology. 46: 15–34.

161. Schnitzer, M.J. 1993. Theory of continuum random walks and application to chemotaxis. Physical Review E. 48: 2553–2568.

162. Adler, J. 1966. Effect of Amino Acids and Oxygen on Chemotaxis in Escherichia coli. J. Bacteriol. 92: 121–129.

163. Vuppula, R.R., M.S. Tirumkudulu, and K. V Venkatesh. 2010. Chemotaxis of Escherichia coli to L-serine. Physical biology. 7: 026007.

164. Lovely, P.S., and F.W. Dahlquist. 1975. Statistical measures of bacterial motility and chemotaxis. Journal of Theoretical Biology. 50: 477–496.

165. Manson, M.D. 1977. A Protonmotive Force Drives Bacterial Flagella. Proceedings of the National Academy of Sciences. 74: 3060–3064.

166. Booth, I.R. 1985. Regulation of cytoplasmic pH in bacteria. Microbiological reviews. 49: 359–78.

167. Korobkova, E., T. Emonet, H. Park, and P. Cluzel. 2006. Hidden Stochastic Nature of a Single Bacterial Motor. Physical Review Letters. 96: 058105.

168. Meacci, G., G. Lan, and Y. Tu. 2011. Dynamics of the bacterial flagellar motor: the effects of stator compliance, back steps, temperature, and rotational asymmetry. Biophysical journal. 100: 1986–95.

169. Kara-Ivanov, M., M. Eisenbach, and S.R. Caplan. 1995. Fluctuations in rotation rate of the flagellar motor of Escherichia coli. Biophysical journal. 69: 250–63.

170. Repaske, D.R., and J. Adler. 1981. Change in intracellular pH of Escherichia coli mediates the chemotactic response to certain attractants and repellents. Journal of bacteriology. 145: 1196–1208.

171. Krikos, a, M.P. Conley, a Boyd, H.C. Berg, and M.I. Simon. 1985. Chimeric chemosensory transducers of Escherichia coli. Proceedings of the National Academy of Sciences of the United States of America. 82: 1326–30.

172. Umemura, T., Y. Matsumoto, K. Ohnishi, M. Homma, and I. Kawagishi. 2002. Sensing of cytoplasmic pH by bacterial chemoreceptors involves the linker region that connects the membrane-spanning and the signal-modulating helices. The Journal of biological chemistry. 277: 1593–8.

173. Demir, M., and H. Salman. 2012. Bacterial thermotaxis by speed modulation. Biophysical journal. 103: 1683–90.